ORNL/TM-2015/722-R3

Preparation of Simulated LBL Defects for Round Robin Experiment

Tyler J. Gerczak
Charles A. Baldwin
Grant Helmreich
John D. Hunn
Fred C. Montgomery

Approved for public release.
Distribution is unlimited.

Revision 3
September 2022

OAK RIDGE National Laboratory

ORNL IS MANAGED BY UT-BATTELLE LLC FOR THE US DEPARTMENT OF ENERGY

ORNL/TM-2015/722-R3

Fusion and Materials for Nuclear Systems Division

PREPARATION OF SIMULATED LBL DEFECTS FOR ROUND ROBIN EXPERIMENT

Tyler J. Gerczak
Charles A. Baldwin
Grant Helmreich
John D. Hunn
Fred C. Montgomery

Revision 3
September 2022

Work sponsored by
US DEPARTMENT OF ENERGY
Office of Nuclear Energy - Advanced Reactor Technologies
under the
Advanced Gas Reactor Fuel Development and Qualification Program

Prepared by
OAK RIDGE NATIONAL LABORATORY
Oak Ridge, TN 37831
managed by
UT-BATTELLE, LLC
for the
US DEPARTMENT OF ENERGY
under contract DE-AC05-00OR22725

CONTENTS

LIST OF FIGURES

LIST OF TABLES

ACRONYMS

AGR	Advanced Gas Reactor Fuel Development and Qualification Program
AGR-1	First AGR program irradiation experiment
AGR-2	Second AGR program irradiation experiment
CVD	chemical vapor deposition
DUO_2	depleted uranium oxide
FIB	focused-ion beam milling system
GIF	Generation IV International Forum
HTGR	high-temperature gas-cooled reactor
INET	Institute of Nuclear and New Energy Technology (Tsinghua University, China)
IPyC	inner pyrolytic carbon (layer)
KAERI	Korea Atomic Energy Research Institute
LBL	leach-burn-leach
MTS	methyltrichlorosilane
NA	not applicable
NIST	National Institute of Standards and Technology
OPyC	outer pyrolytic carbon (layer)
ORNL	Oak Ridge National Laboratory
SEM	scanning electron microscope
SiC	silicon carbide (layer)
SRM	standard reference material
TBD	to be determined
TRISO	tristructural-isotropic (coated particles)
UCO	uranium carbide/uranium oxide (kernels)
UO_2	uranium oxide (kernels)
VHTR	very-high temperature reactor

ACKNOWLEDGMENTS

This work was sponsored by the US Department of Energy Office of Nuclear Energy through the Idaho National Laboratory Advanced Reactor Technologies Technology Development Office as part of the Advanced Gas Reactor Fuel Development and Qualification Program. Analysis of leach solutions was provided by the Oak Ridge National Laboratory Nuclear Analytical Chemistry & Isotopics Laboratory.

1. BACKGROUND

Tristructural-isotropic (TRISO) coated particle fuel development and qualification is a current focus for advancing the deployment of select Generation IV reactor concepts, particularly for high-temperature gas-cooled reactor (HTGR) and very high temperature reactor (VHTR) applications [Petti et al. 2010]. TRISO fuel and HTGR development programs are ongoing in many Generation IV International Forum (GIF) member states. A cooperative round robin experiment to benchmark the leach-burn-leach (LBL) process has been undertaken by the GIF VHTR Fuel and Fuel Cycle Project Management Board. Primary participants in this LBL round robin are China, South Korea, and the United States.

The TRISO-coated particle fuel design for most contemporary HTGRs comprises a uranium-bearing kernel containing either uranium oxide (UO_2) or a blend of uranium oxide and uranium carbide (UCO), surrounded by a porous carbon buffer layer, and successive isotropic layers of inner pyrolytic carbon (IPyC), chemical vapor–deposited silicon carbide (SiC), and outer pyrolytic carbon (OPyC). Figure 1a shows a TRISO particle cross section identifying the general construction of the particle. Depending on the reactor design, individual TRISO particles are compacted into either a cylindrical shape for the prismatic-core reactor or a spherical shape for the pebble-bed reactor. The compacting is completed by first overcoating the particles in a resinated graphite powder, followed by pressing of the overcoated particles into a final shape and firing them at elevated temperature to carbonize the resin. This yields a fully refractory fuel form with individual TRISO particles dispersed throughout. The distribution of TRISO particles in a prismatic fuel compact from the AGR-2 irradiation campaign is shown in Figure 1b.

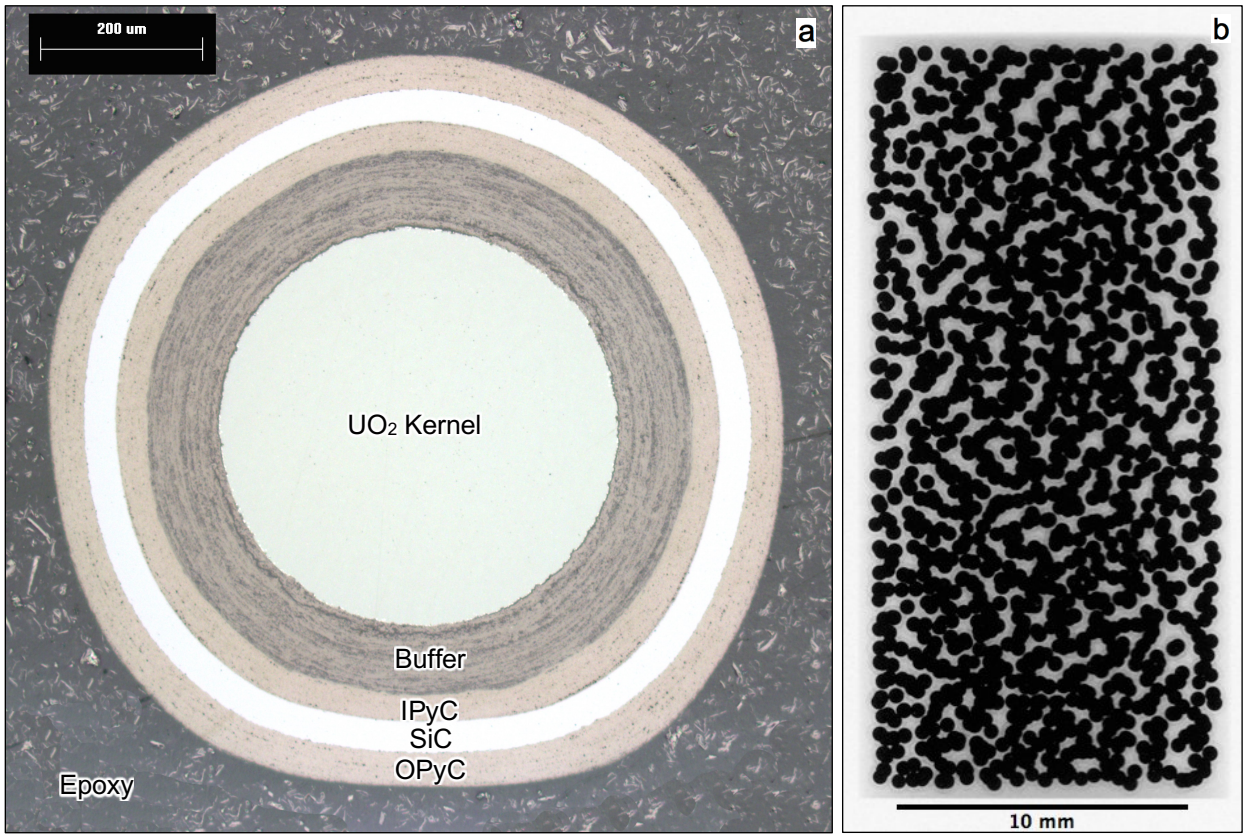

Figure 1. Overview of the AGR-2 TRISO fuel form: (a) cross-section of as-fabricated AGR-2 UO_2 TRISO particle showing particle construction, and (b) x-ray radiograph of as-fabricated AGR-2 UO_2 fuel compact showing particle distribution in the graphite matrix (black circles indicate projections of kernels).

A critical characteristic of the TRISO fuel design is its ability to retain fission products. During reactor operation, the TRISO layers act as barriers to release of fission products not stabilized in the kernel. Each

component of the TRISO particle and compact construction plays a unique role in retaining select fission products, and layer performance is often interrelated. The IPyC, SiC, and OPyC layers are barriers to the release of fission product gases such as Kr and Xe. The SiC layer provides the primary barrier to release of metallic fission products not retained in the kernel, as transport across the SiC layer is rate limiting as a result of the greater permeability of the IPyC and OPyC layers to many metallic fission products. These attributes allow intact TRISO coatings to successfully retain most fission products released from the kernel, with the majority of released fission products during operation being from defective, damaged, or failed coatings. This dominant release of fission products from compromised particles contributes to the overall source term for reactor accidents, causing safety and maintenance concerns and limiting the lifetime of the fuel. Under these considerations, an understanding of the nature and frequency of compromised particles is an important part of predicting the expected fission product release and ensuring safe and efficient operation.

2. OVERVIEW OF LEACH-BURN-LEACH ROUND ROBIN

Leach-burn-leach is an analysis method used to determine several properties of TRISO-coated particles and fuel compacts. The two key defect populations measured by LBL are the number of exposed kernels (i.e., kernels not contained within any intact retentive layer, sometimes referred to as particles with defective or failed TRISO) and the number of particles with defective or failed SiC (i.e., particles for which SiC is not intact but that still have intact pyrocarbon containing the kernels). These two defects lead to fission product release in reactor. The concentrations of impurities outside of intact SiC layers, especially the dispersed uranium (sometimes called *uranium contamination*), are additional variable properties measured by LBL. A related method—burn-crush-burn-leach—which includes intentional destruction of the SiC and other coating layers, is used to measure uranium content in the particles or compacts.

The general LBL process at Oak Ridge National Laboratory (ORNL) includes three or four stages: (1) electrolytic compact deconsolidation (unless analysis is performed on particles before compacting), (2) preburn acid leaching, (3) burning in air to remove exposed carbon, and (4) postburn acid leaching. A flow chart of the LBL process is presented in Figure 2. In the leaching stages, any particles and matrix debris that are present are leached in concentrated nitric acid. Leaching before or after the 750°C burn is performed with two separate 24 h leaches, and the leachates are measured to determine the quantity of uranium and various impurities that were leached. Exposed uranium detected at quantities below one-half of an average kernel's inventory is assumed to be related to uranium contamination outside of intact SiC, whereas higher values are used to enumerate leached kernels. Uranium from exposed kernel defects is detected in the preburn leach; an example of an exposed kernel defect is a particle with an impact fracture that propagated from the OPyC through to the kernel area. Uranium from particles with a defective SiC layer is detected in the postburn leach; an example of this type of defect is a TRISO fuel particle with a porous SiC layer with at least one intact pyrocarbon layer (IPyC or OPyC), such that the kernel is not exposed to acid leaching until after the intact pyrocarbon layer is burned away. SiC defects without a protective pyrocarbon layer are counted as exposed kernel defects. Figure 3 shows examples of particles with preburn and postburn leach defects. Additional detail on the ORNL LBL process can be found in the literature [Hunn 2013, Hunn et al. 2013, Baldwin et al. 2014].

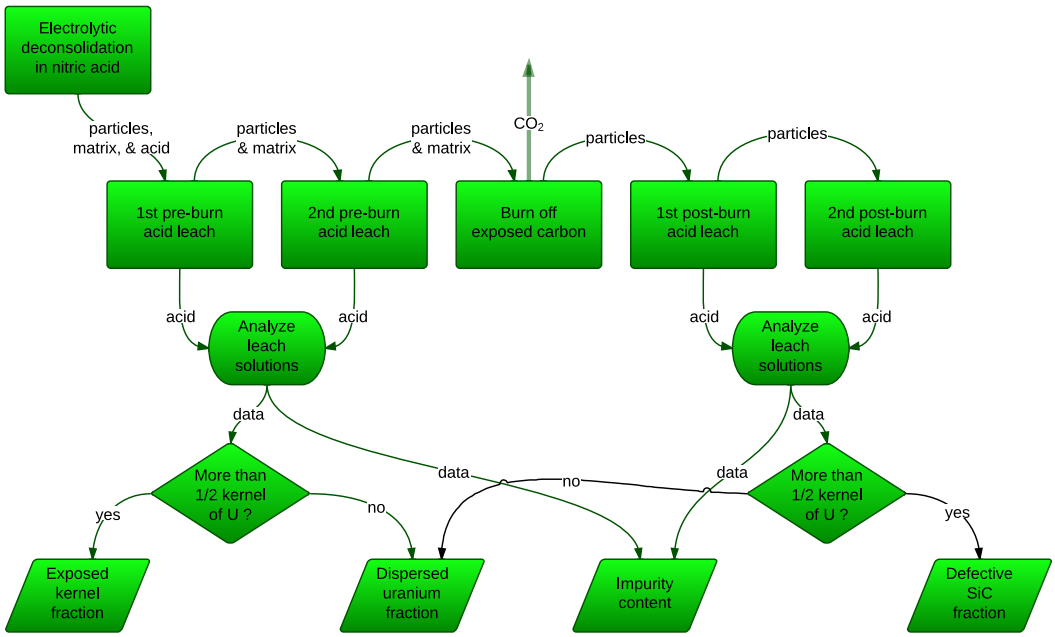

Figure 2. Flow chart of the LBL process, which demonstrates the individual steps in the analysis and determination of particle defect properties.

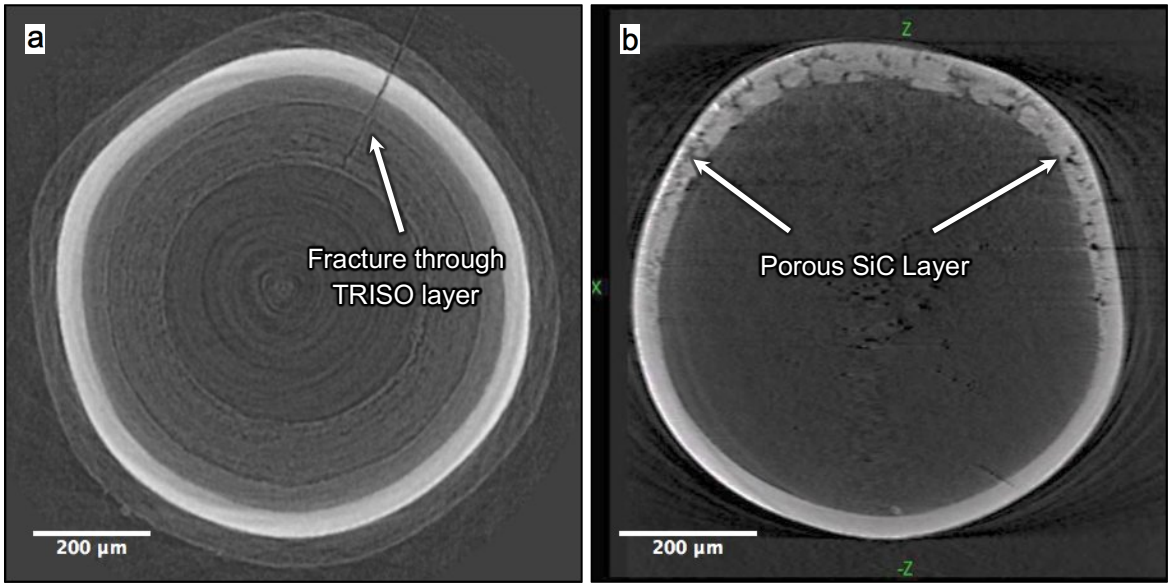

Figure 3. High-resolution x-ray tomographs showing defective TRISO particles: (a) example of a preburn leach defect with an exposed kernel caused by a fracture propagating from the OPyC through to the kernel, and (b) example of a postburn leach defect with a defective SiC layer caused by a large soot inclusion that allowed the IPyC and buffer to be burned out. Kernels in both particles were removed during LBL.

The motivation of the GIF LBL benchmarking round robin experiment is to show consistency in LBL analysis results among the participating members and to potentially understand the influence of LBL process variations on accurate determination of measured fuel properties (LBL defect fractions, uranium contamination, and impurity content). This will be accomplished through a systematic study of two sets of round robin test samples. The first set of test samples will be representative TRISO particles provided by the Chinese Institute of Nuclear and New Energy Technology (INET). Samples of representative TRISO particles will consist of riffled sublots of TRISO-coated particles with depleted uranium oxide (DUO_2) kernels from a single, large (~3 million particle) parent lot. Samples will be distributed by INET to the other two participating organizations: ORNL and the Korean Atomic Energy Research Institute (KAERI). Each participating organization (INET, KAERI, and ORNL) will perform LBL analysis on the DUO_2 TRISO samples and report their measurements. The large random samples involved in this part of the round robin experiment will support a statistically significant comparison of the results obtained.

A second set of round robin test samples has been prepared by ORNL and will be distributed to each participant for LBL analysis. Each of these samples has a known number of simulated LBL defect particles containing DUO_2 kernels (0, 1, 2 or, 4 particles) mixed in with nonuranium surrogate particles containing ZrO_2 kernels to hide the actual number of LBL defect particles. Test samples contain particles with either preburn leach or postburn leach simulated defects that have been fabricated as described in the following sections of this report. Combination of both types of defects into a single sample, as originally conceived when planning the round robin experiment, was not implemented because of the possible data analysis confusion that would occur if postburn leach defects were prematurely leached before the burn. The simulated LBL defect particles contain DUO_2 kernels, so that they can be detected by the same LBL analysis that is used to measure the presence of real LBL defects. In addition to these simulated LBL defect particles, a variable but known amount of a coal impurity standard obtained from the National Institute of Standards and Technology (NIST SRM 1632d) was also mixed into each sample to provide a round robin comparison of the impurity analysis performed during LBL. The NIST SRM 1632d standard reference material contains known quantities of key impurities found in the graphite materials used to fabricate HTGR fuel elements (compacts and pebbles), including Al, Ca, and many of the transition metals (e.g., Ti, V, Cr, Mn, Fe, Co, and Ni). Transition metal contamination in fuel compacts or pebbles is a concern, and impurity limits are included in HTGR fuel specifications because certain metals may react with the SiC layer during irradiation.

The samples with known numbers of simulated LBL defect particles and known impurity content were prepared as follows. Labels were laser-etched into each sample vial, and then the vials were thoroughly cleaned, dried, and weighed. Approximately 0.50 g of NIST SRM 1632d material was added to each vial following the NIST procedure for homogenization before use, and the vials were weighed again to determine the mass of powder in each sample. Data for correcting to dry powder mass were also obtained and used for accurate determination of the impurity content in each powder sample; these data were recorded and will be made available after each organization has completed its LBL analysis. Simulated LBL defect particles were then added according to the summary in Table 1 and the detailed distribution list in Appendix A. Finally, the nonuranium surrogate particles were added, and the bottles were sealed, weighed, and prepared for shipment. The surrogate particles (ZrO-GIF) were spherical ZrO_2 kernels coated with a carbon buffer layer, a carbon inner pyrocarbon layer, and a SiC layer. The ZrO-GIF surrogate particles were cleaned in hot nitric acid and rinsed thoroughly to remove any surface impurities prior to mixing in with the NIST SRM 1632d powder and simulated LBL defect particles. The vials for each sample set were labeled A–G. The correspondence between these labels and the numeric labels in Table 1 and Appendix A were recorded and not provided to participants, with the intent that the information would be made available after the LBL measurements were complete, along with the masses of the impurities from the dried NIST SRM 1632d standard material. This version of ORNL/TM-2015/722 has been revised and reissued after the completion of the blind LBL study to include the assignment between the 1–7 labels to the A–G labels (Appendix A) to serve as a reference to the round robin study, and an additional appendix was added to communicate the mass of each impurity contained in the standard reference material (SRM 1632d) that was mixed into each sample (Appendix B). Images of each simulated LBL defect particle listed in Appendix A were acquired to verify and document the defect; these can be found in Appendix D, Appendix E, and Appendix F.

Table 1. Description of GIF LBL round robin test samples with simulated defects and impurities

Test sample	Number of simulated preburn leach defect DUO_2 TRISO particles	Number of simulated postburn leach defect DUO_2 TRISO particles	Number of ZrO-GIF surrogate particles	Weight of SRM 1632d
1	0	0	~9,000	~0.5 g
2	1	0	~9,000	~0.5 g
3	2	0	~9,000	~0.5 g
4	4	0	~9,000	~0.5 g
5	0	1	~9,000	~0.5 g
6	0	2	~9,000	~0.5 g
7	0	4	~9,000	~0.5 g

Each participant will perform LBL analysis on their respective seven round robin test samples. Participants careful ensure that the material in each vial is completely transferred to the LBL leaching vessel so that the entirety of the NIST SRM 1632d powder is included in the analysis. Results can be reported in an Excel data report form that will be distributed to all participants prior to the initiation of the LBL testing. The form will clearly identify the information required for completion of the LBL analysis. An example of the Excel data report form is shown in Appendix C. A summary report is also requested from each participating institution to describe their unique analysis procedures and results.

3. ORNL DUO_2 TRISO PARTICLES USED TO MAKE SIMULATED DEFECTS

The particles used for preburn and postburn leach simulated defect fabrication came from coating batch DUN500S-10A. These are DUO_2 kernels that were coated at ORNL with TRISO layers somewhat similar to those tested in the Advanced Gas Reactor Fuel Development and Qualification (AGR) Program's first irradiation experiment (AGR-1). The kernels were fabricated at ORNL by the internal gelation technique and have an average diameter of 519±12 μm and an average density of 10.7±0.3 g/cm^3. The deposition of the TRISO layers was carried out as an uninterrupted process using a laboratory-scale, fluidized bed chemical vapor deposition (CVD) furnace with a 50 mm inner diameter conical chamber. The layer properties and select deposition parameters are listed in Table 2 [Lowden and McLaughlin 2004].

Table 2. Fluidized-bed CVD coating conditions and TRISO layer thicknesses of DUN500S-10A

Layer	Precursor gas	Deposition temperature (°C)	Layer thickness (μm)	Density (g/cm^3)
Buffer	Ar + C_2H_2	1,300	101 ± 9	-
IPyC	Ar + C_2H_2 + C_3H_6	1,300	49 ± 4	-
SiC	H_2 + MTS	1,510	35.5 ± 1.4	3.205±0.001
OPyC	Ar + C_2H_2 + C_3H_6	1,300	46 ± 3	1.898±0.009

MTS = methyltrichlorosilane
Note that the deposition temperatures and layer thicknesses of DUN500S-10A differ from the process conditions and layer thicknesses of particles irradiation tested under the AGR program.

Particles were randomly selected for the simulated defect fabrication to limit bias. The following sections describe the development of the simulated defect fabrication process and the analysis of the simulated defect particles to confirm the nature of the defects. The value for average total uranium per DUO_2 TRISO particle is required to calculate the number of defects from the measurement of exposed uranium during the LBL analysis. This value and the ^{235}U weight fraction were determined by burn-crush-burn-leach on three separate 5 g fuel batches. The average total uranium per DUO_2 TRISO particle was 7.003×10^{-4} g with a standard deviation of 1.7×10^{-6} g, and the average measured ^{235}U content was 2.17×10^{-3} g^{235}U/gU with a standard deviation of 3×10^{-5} g^{235}U/gU. These values are included as input in the data form shown in Appendix C.

4. FABRICATION OF SIMULATED PREBURN LEACH DEFECTS

Simulated preburn leach defects were sought which mimicked exposed kernel defects similar to that shown in Figure 3. Defects of this type have been observed in as-fabricated fuel lots as a result of impact-induced brittle fracture of the TRISO layers during handling. As such, an effort was developed to manually fracture TRISO particles in a controlled manner to generate particles with an exposed kernel that could be used as simulated preburn leach defects. Through-layer cracks through all TRISO layers were successfully produced by subjecting particles to single-point impact.

The impact fracture apparatus used to fabricate the simulated preburn leach defects is shown in Figure 4. A small weight was dropped to strike a flat-tipped ram which moved along a track vertically and was normally positioned with respect to the particle holder plate. The particles to be fractured were secured on the aluminum plate with Crystalbond 509 mounting adhesive such that a small area of each particle remained exposed. The Crystalbond held the particle in position and provided additional support during the impact event. The mass and drop height of the small weight were adjusted to control the impact force.

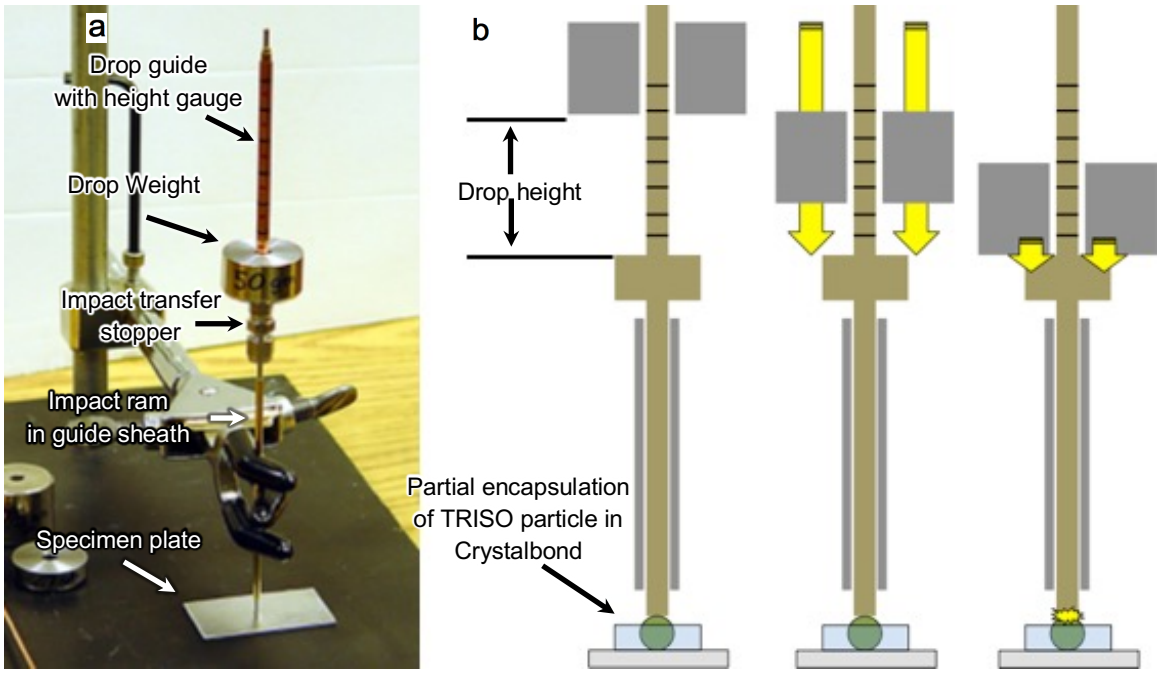

Figure 4. Impact fracture apparatus showing (a) system overview with markings for drop height in 1 cm increments, and (b) schematic of the impact process identifying how the ram is in contact with TRISO particles partially encapsulated in Crystalbond and showing the process of dropping the weight at a defined height and transferring the impact force to the particle through the ram.

A series of validation tests were performed on surrogate TRISO particles with ZrO_2 kernels to identify the impact conditions necessary to achieve fine-scale, complete TRISO layer fracture and to identify the indicators of a successfully fractured particle. Initial testing focused on a 75 g weight dropped from heights of 1–3 cm. Varied responses were observed ranging from faint cracks moving radially out from the impact site to catastrophic failure; examples of the varied responses are shown in Figure 5.

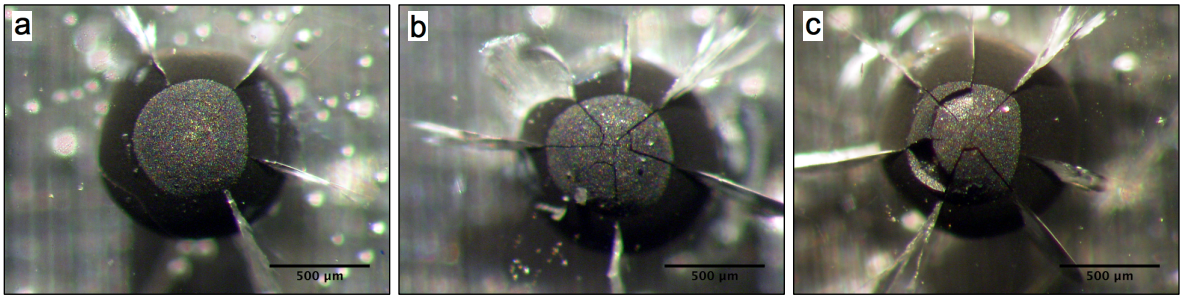

Figure 5. Optical images of impact-fractured particles embedded in Crystalbond after dropping a 75 g weight 1 cm: (a) particle with radial fractures extending into Crystalbond, (b) particle with large visible fractures in OPyC layer, and (c) particle with catastrophic failure of TRISO layers.

The particles with excessive visible fractures did not meet the fine-scale fracture criteria; however, particles with faint radial fractures radiating out into the Crystalbond were observed to correlate to fine-scale, complete TRISO layer failure; this correlation is shown in Figure 6 for a particle fractured with a 75 g weight dropped from 1 cm. Particles with excessive fracturing typically exhibited more visible damage to the OPyC and more extensive cracking in the Crystalbond. Therefore, the presence of faint radial fractures propagating into the Crystalbond layer was used as an initial selection criterion for identifying appropriately fractured particles.

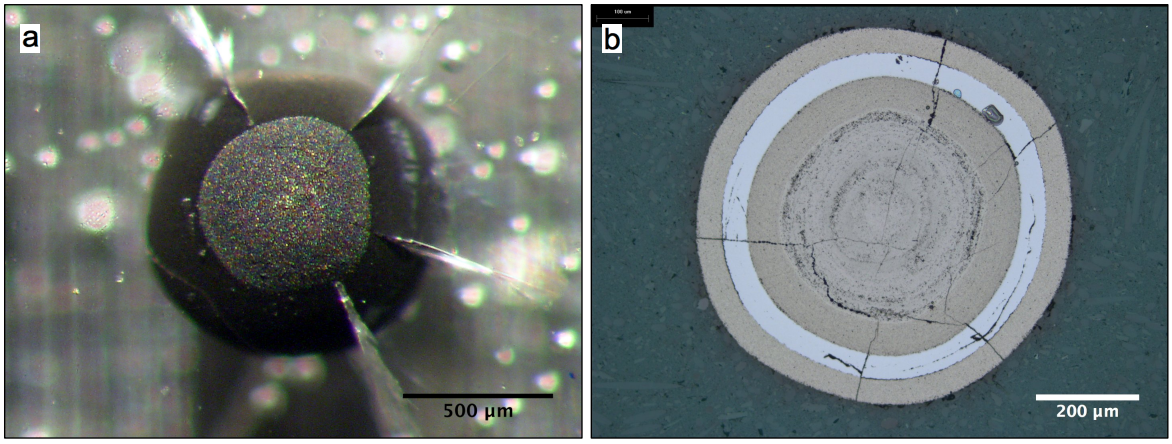

Figure 6. Optical images of impact-fractured particle after dropping a 75 g weight 1 cm: (a) particle embedded in Crystalbond with radial fractures extending into Crystalbond, and (b) polished cross section approximately normal to the impact site showing radial fracture traversing the TRISO layers.

The variable fracture response using the 75 g weight did not provide acceptable fracture behavior yields. To achieve a more repeatable fracture behavior, a lighter, 4.9 g impact weight was utilized and dropped from a greater height (2.5–4 cm). This procedural change was able to produce consistent faint radial fractures in the OPyC and Crystalbond. X-ray imaging was used as a nondestructive technique to confirm that each impact-fractured particle in the round robin test was cracked all the way through the TRISO layers. Figure 7 shows the correlation of TRISO layer cracks observed in x-ray analysis to the radial fractures observed after impact. Note that the tangential fracturing of the SiC layer seen in the polished cross section optical image in Figure 6b was not observed in the lower weight impact fracture tests.

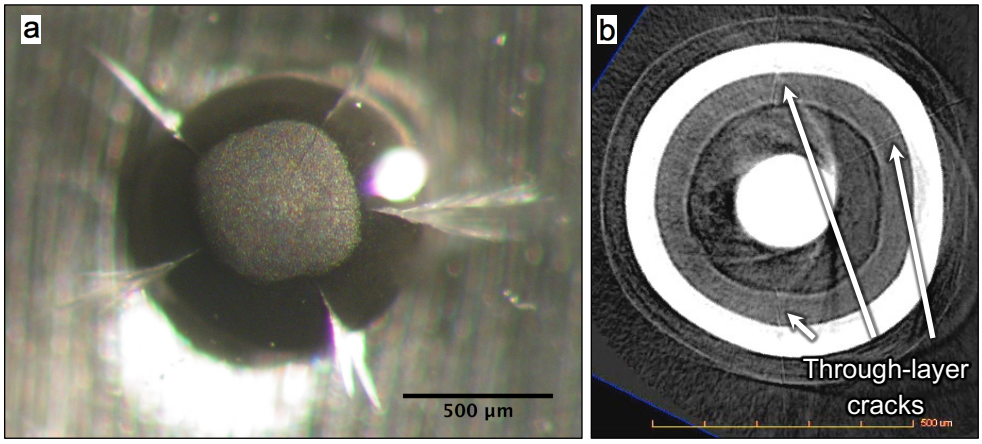

Figure 7. Example of results from a 4.90 g weight dropped 2.5 cm: (a) optical image showing faint radial fractures in OPyC and Crystalbond, and (b) x-ray tomograph normal to impact direction showing cracks in TRISO layers.

3D renderings of the SiC surface were investigated for select particles to gain further insight on the nature of the SiC fracture behavior. The 3D renderings of the SiC surfaces demonstrate the nature of the fracture propagation. In the example presented in Figure 8, faint fracturing can be observed extending radially out from the impact site, similar to the fractures propagating in the Crystalbond. The radial fractures ultimately terminate and do not extend around the entire circumference of the particle. This provides confidence that the particles will remain intact during handling.

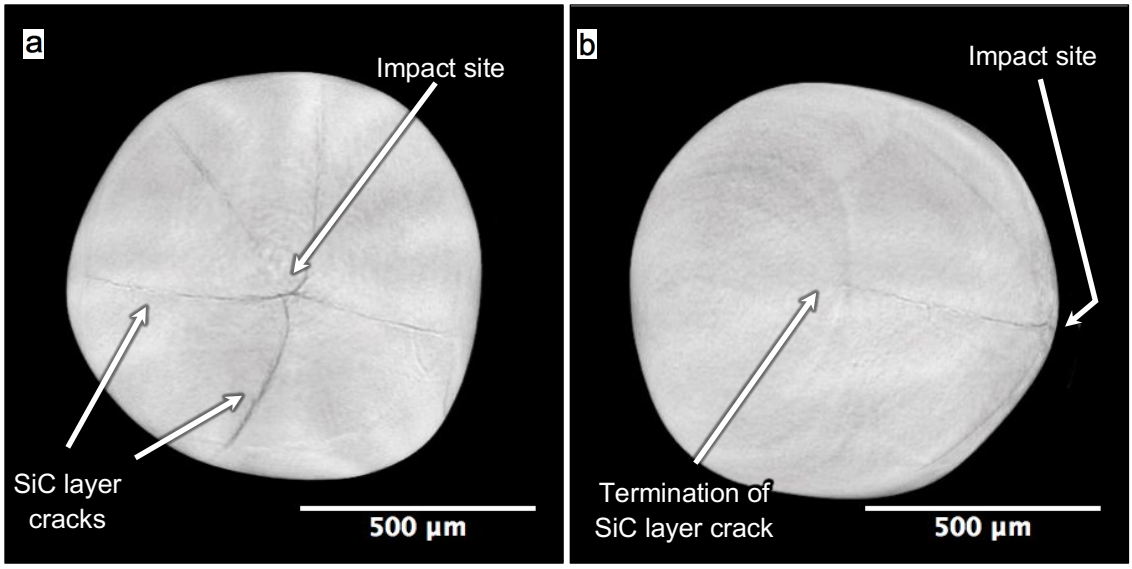

Figure 8. 3D x-ray tomography visualization of a particle's SiC surface after impact fracturing with a 4.90 g weight dropped 2.5 cm: (a) view normal to the impact fracture showing radial fracture pattern, and (b) view rotated approximately 90 degrees to the impact fracture site showing termination of one of the radial fractures.

Particles from DUN500S-10A were randomly selected for impact-fracture preburn leach simulated defect fabrication. The prefix "GIF" and a sequential number (GIF-#) were used to identify each impact-fractured particle. Fifty particles were fractured, and particles with the appropriate visible fracture behavior in the OPyC and Crystalbond were analyzed with x-ray tomography to examine the nature of the fracture behavior. Appendix D shows the optical images of all 50 particles subjected to impact fracturing. If a complete TRISO fracture were confirmed with x-ray analysis, then the particle was considered to be acceptable for inclusion in the round robin test. Figure 9 shows example optical and x-ray images of a

particle that exhibited acceptable impact fracture in which a fracture can be seen extending from the outside surface of the OPyC to the kernel, whereas the overall fracture damage is minimal. Appendix E shows x-ray tomographs of all particles confirmed for inclusion in the GIF LBL round robin experiment.

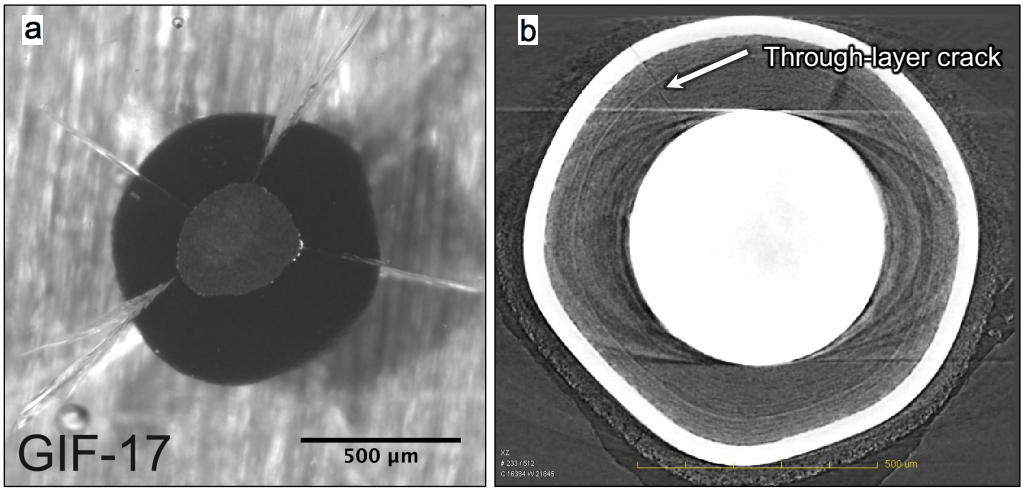

Figure 9. (a) Optical image of GIF-17 showing the OPyC and Crystalbond fracture after impact, and (b) x-ray tomograph showing the fracture propagating through the TRISO layers.

Particle GIF-48 was subjected to a preburn leach test to ensure that the kernel was exposed by the impact fracturing process and the simulated defect performed as expected. The leachate solutions were analyzed to measure the uranium content; the uranium content in the first leachate was equivalent to 120±10% of the uranium in an average kernel, whereas <0.1% was observed in the second leachate solution. This indicated that the entire kernel content was leached in the first 24 h leach step. X-ray radiography of the particle after the preburn leach indicated that no kernel remained (Figure 10), corroborating the uranium analysis results, and confirming that the impact-fractured particle acted properly as a simulated preburn leach (exposed kernel) defect.

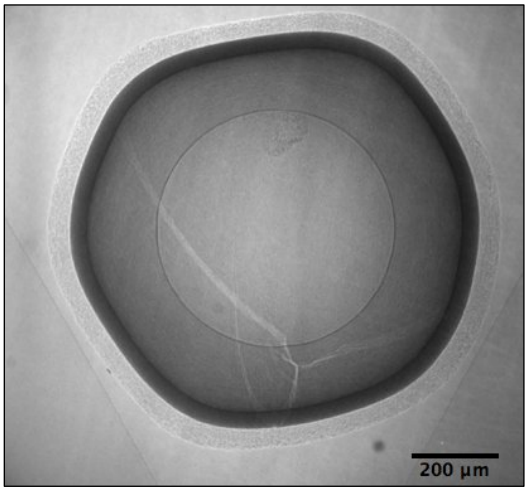

Figure 10. X-ray radiograph of GIF-48 showing complete absence of the DUO_2 kernel after preburn leach.

Table 3 summarizes the observations made regarding the 50 particles involved in this study. Particles to be included in the round robin experiment are highlighted, and Appendix A identifies the sample assignment for each of these particles. The seven particles identified in Table 3 as “spare” are extra particles for use if assigned particles are lost or damaged.

Table 3. Status of 50 particles from DUN500S-10A fabricated for inclusion in round robin experiment as simulated preburn leach defects using impact fracture method

Particle ID	Imaging status	TRISO layer failure	Number of radial cracks	Included in round robin
GIF-01	Optical/x-ray	None confirmed	1	No
GIF-02	Optical/x-ray	Confirmed	4	Yes
GIF-03	Optical/x-ray	Confirmed	3	Yes
GIF-04	Optical/x-ray	Confirmed	4	Yes
GIF-05	Optical	-	6	-
GIF-06	Optical/x-ray	Confirmed	4	Yes
GIF-07	Optical/x-ray	Confirmed	5	Yes
GIF-08	Optical	-	5	-
GIF-09	Optical/x-ray	Confirmed	5	Yes
GIF-10	Optical	-	5	-
GIF-11	Optical	-	5	-
GIF-12	Optical/x-ray	Confirmed	3	Spare
GIF-13	Optical	-	4	-
GIF-14	Optical/x-ray	Confirmed	5	Yes
GIF-15	Optical/x-ray	Confirmed	4	Yes
GIF-16	Optical	-	5	-
GIF-17	Optical/x-ray	Confirmed	4	Yes
GIF-18	Optical	-	6	-
GIF-19	Optical/x-ray	Confirmed	3	Yes
GIF-20	Optical	-	6	-
GIF-21	Optical/x-ray	None confirmed	4	No
GIF-22	Optical	-	5	-
GIF-23	Optical	-	4	-
GIF-24	Optical	-	6	-
GIF-25	Optical	-	6	-
GIF-26	Optical	-	5	-
GIF-27	Optical/x-ray	Confirmed	3	Yes
GIF-28	Optical/x-ray	Confirmed	3	Yes
GIF-29	Optical/x-ray	Confirmed	4	Yes
GIF-30	Optical/x-ray	Confirmed	3	Yes
GIF-31	Optical	-	3	-
GIF-32	Optical	-	3	-
GIF-33	Optical/x-ray	Confirmed	4	Spare
GIF-34	Optical/x-ray	Confirmed	3	Spare
GIF-35	Optical/x-ray	Confirmed	3	Spare
GIF-36	Optical/x-ray	Confirmed	4	Spare
GIF-37	Optical/x-ray	Confirmed	4	Spare
GIF-38	Optical/x-ray	Confirmed	3	Yes
GIF-39	Optical/x-ray	Confirmed	3	Yes
GIF-40	Optical	-	2	-
GIF-41	Optical/x-ray	Confirmed	4	Yes
GIF-42	Optical/x-ray	Confirmed	4	Yes
GIF-43	Optical/x-ray	Confirmed	3	Yes
GIF-44	Optical/x-ray	Confirmed	3	Yes
GIF-45	Optical	-	3	-
GIF-46	Optical	-	2	-
GIF-47	Optical	-	2	-
GIF-48	Optical/x-ray	Confirmed	3	used for LBL
GIF-49	Optical/x-ray	Confirmed	2	Yes
GIF-50	Optical/x-ray	Confirmed	4	Spare

5. FABRICATION OF SIMULATED POSTBURN LEACH DEFECTS

The aim of simulated postburn leach defect fabrication was to fabricate TRISO particles with a single penetration through the SiC layer and at least one intact pyrocarbon layer to protect the kernel from acid leaching prior to the burn stage of the LBL analysis. A dual-beam focused ion beam (FIB) milling system attached to a scanning electron microscope (SEM) was identified as an optimal instrument for production of controlled, micron-scale, local defects with a defined geometry in which a hole could be milled in the outer layers such that the SiC was penetrated while some portion of the IPyC remained intact.

The FIB utilized a 30 kV gallium (Ga^+) ion beam that was raster-scanned in predefined patterns to selectively sputter material from the target area. As part of initial development of a process to fabricate the simulated defect particles, multiple approaches were investigated to achieve fine-scale SiC defects in ZrO_2 kernel surrogate TRISO particles. A circular, 10 µm diameter raster pattern with a 30 kV, 30 nA Ga^+ ion beam produced the smallest hole through the SiC that displayed repeatable removal of the inner carbon layers during the burn stage. However, LBL analysis of DUN500S-10A particles with simulated postburn leach defects produced inconsistent results that needed to be addressed before including these particles in the GIF LBL round robin experiment. The inconsistent results were presumed to be the result of variable milling behavior related to redeposition of the milled PyC and SiC material, possible ion beam instabilities and specimen drift during milling, and the difficulty adjusting to the different ultimate simulated defect depths required to optimally penetrate the different layer thicknesses in each particle. Polishing off a section of the OPyC layer to expose the SiC reduced the minimum depth for the simulated defects required for breakthrough into the IPyC layer, thus mitigating issues related to the deeper holes; however, LBL inconsistencies remained. This implied that milling variables and redeposition strongly influence the LBL behavior.

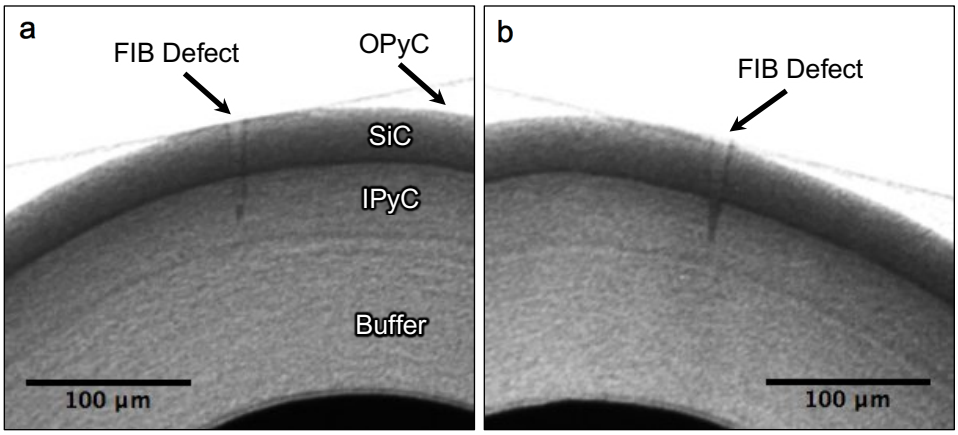

Figure 11. X-ray radiographs of DUN500S-10A particles with differing LBL behaviors showing a closeup of the FIB-fabricated through-layer defects: (a) particle with a simulated defect penetrating 23 µm deep into the IPyC layer, where the equivalent of 97% of an average kernel's total uranium content was dissolved in the postburn leach, and (b) particle with a simulated defect penetrating 28 µm deep into the IPyC layer, where only 7% of an average kernel's total uranium content was dissolved in the postburn leach.

Figure 11 shows x-ray radiographs of two particles with FIB-produced holes extending greater than 20 µm into the IPyC layer. Both particles were subjected to LBL. Prior to subjecting the particles to LBL, a thin layer of epoxy was applied to the surface of the particles to help protect them from premature leaching during the preburn leaching phase. These particles clearly had through-layer SiC defects; however, two different results were observed. Postburn leaching yielded approximately a single kernel's inventory of uranium from one particle, but the other yielded only ~7%. The low uranium recovery observed in the second particle was not expected. During FIB milling, an amorphous phase of Ga, Si, and C was redeposited at the bottom of the simulated defect and on the simulated defect walls. One hypothesis for the inconsistent behavior was that the redeposited material may have oxidized during the burn stage

and clogged the hole that was milled through the SiC. The influence of redeposition in the particles presented in Figure 11 was not clear, because the hole could not be imaged along its length. This inconsistent behavior did not provide the confidence that the 10 µm diameter simulated defects would behave as expected during the round robin testing, so a new approach was developed to produce simulated postburn leach defects in the DUN500S-10A particles more consistently.

Two key changes in the simulated postburn leach defect fabrication process were (1) to completely remove the OPyC layer from the DUN500S-10A particles by heating them in air at 750°C, and (2) to program the FIB raster patterns to produce larger diameter holes in the SiC layer. These changes ensured higher confidence in the through-layer nature of the simulated defects. The larger diameter holes and shallower ultimate hole depth allowed for direct confirmation with SEM imaging that the IPyC layer was exposed while also minimizing the risk of penetrating too deeply into the IPyC. In addition, the large hole size mitigated the possibility of redeposition on the crater walls influencing the LBL process.

The indicators for successful fabrication of a FIB-produced simulated postburn defect were determined by stepwise milling of a large-diameter hole. Multiple circular craters were produced with increasing milling times, and the bottoms of the craters were analyzed by SEM imaging. With increased milling time, a transition in the visual appearance of the crater bottom was observed (Figure 12). For shorter milling times, the crater bottoms were smooth and featureless, whereas a mottled surface appeared at the bottom of the craters milled for a longer time. This transition to a mottled surface indicated that the IPyC layer had been exposed, which was confirmed by additional analysis discussed below.

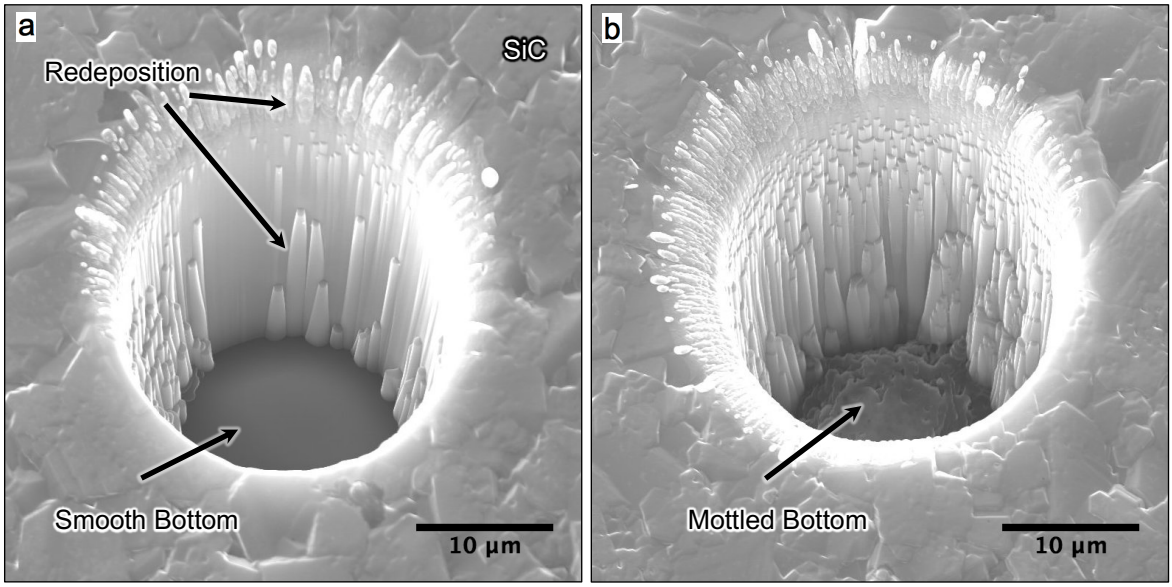

Figure 12. Secondary -electron SEM micrographs of craters produced with a 25 µm diameter raster pattern showing the initial SiC surface, the sidewall, and the bottom of the craters. Both features were produced with a two-step milling process utilizing a 30 kV, 50 nA Ga^+ ion beam followed by a 30 kV, 15 nA Ga^+ ion beam: (a) 33 min at 50 nA followed by 10 min at 15 nA, and (b) 38 min at 50 nA followed by 10 min at 15 nA.

Imaging of the crater sidewalls was pursued to confirm that the craters extended beyond the IPyC/SiC interface. The sidewalls had significant redeposition buildup, so direct imaging of the SiC/IPyC interface was not possible after primary milling. Therefore, on select particles, additional milling was performed to remove redeposited material from a localized area on the sidewall and allow better imaging. After cleaning the sidewalls, SEM imaging confirmed that the IPyC layer had been penetrated on samples with crater bottoms with a mottled appearance (Figure 13). However, sidewall cleaning resulted in redeposition on the crater bottom, so this method for confirming the ultimate depth of the simulated defect was not used for the round robin specimens because of the uncertainty associated with the influence of this secondary redeposition on the LBL behavior.

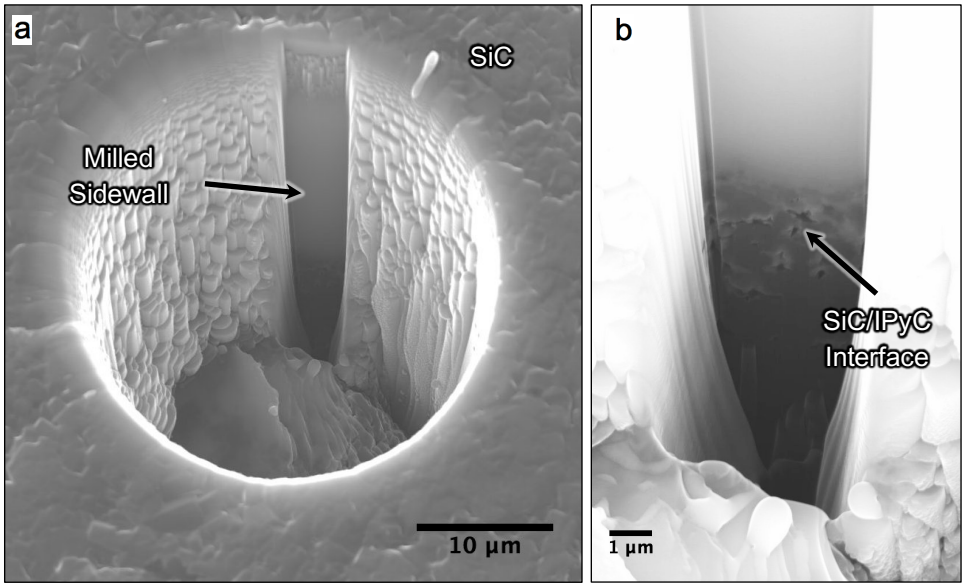

Figure 13. Secondary-electron SEM micrographs of a crater showing (a) the section of cleaned sidewall, and (b) a closeup of the transition from SiC to IPyC confirming breakthrough into the IPyC layer.

X-ray radiographs were taken to determine the ultimate depth of each simulated defect. This analysis was complementary to the SEM imaging of the crater bottoms in verifying that the crater depths were optimized. SEM imaging confirmed that the SiC was penetrated and the IPyC was exposed, whereas the x-ray radiographs confirmed that the milled holes did not penetrate into the IPyC layer to excessive depths. Confining the milling to the first few microns of the IPyC layer helps to ensure consistent behavior of the simulated postburn leach defects and prevent premature leaching prior to the burn phase. Figure 14 shows two examples of the cross section images obtained by x-ray radiography. These radiographs indicate that the crater bottoms terminate near the IPyC/SiC interface for both particles, whereas Figure 12 shows that only the particle shown on the right in both figures has the mottled appearing crater bottom indicative of penetration into the IPyC. This highlights that confident determination of the through-layer nature of these simulated defects is not provided by the x-ray radiographs alone.

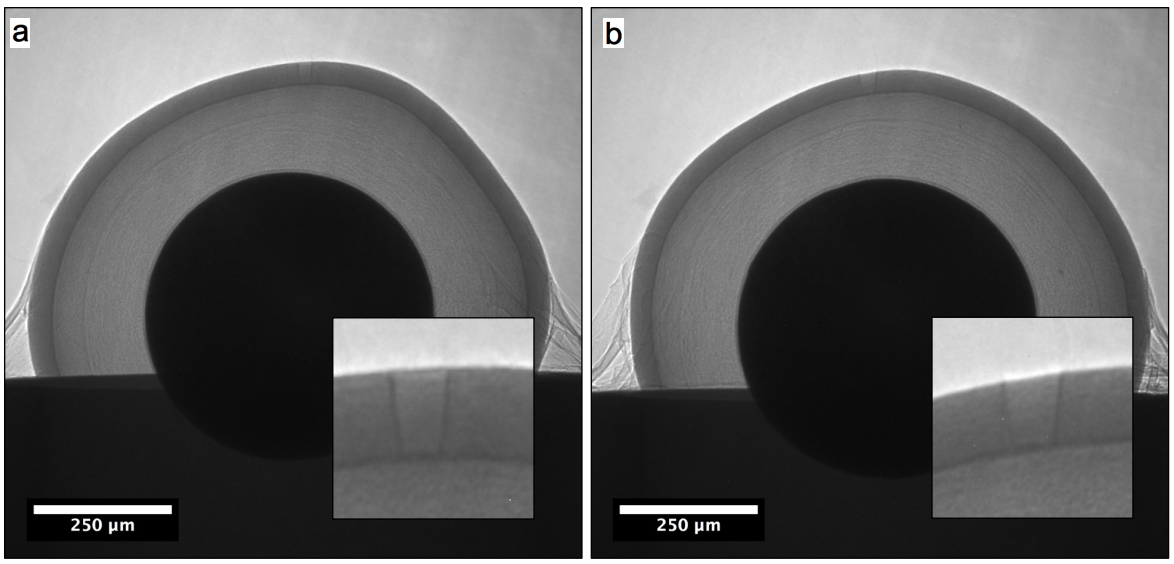

Figure 14. X-ray radiographs showing cross sections of the FIB-milled craters produced in the two particles shown in Figure 12: (a) particle with smooth crater bottom and (b) particle with mottled crater bottom (inset shows a close up of each feature).

The SEM imaging provided confirmation that the IPyC layer had been reached through the milling process; however, the IPyC/buffer burn behavior required confirmation to ensure that the particles would behave as expected when using the mottled appearance at the bottom of the FIB-milled crater as an acceptance criterion. A total of fourteen particles with simulated postburn leach defects milled to various depths were subjected to a 750°C 60 h burn to confirm the IPyC/buffer burn response. After the burn step, x-ray radiographs were obtained of each particle to detemine whether or not the buffer and IPyC layers were burned out. All particles with the mottled-appearing crater bottom exhibited complete oxidation and removal of the buffer and IPyC layers, confirming that this SEM selection criteria were sufficient to ensure that this process would occur as expected. Figure 15 shows the two particles that were imaged with SEM (Figure 12) and with x-ray (Figure 14) prior to the burn step. The particle on the left did not exhibit any sign of oxidation, confirming that the smooth-bottom crater indicates that the IPyC was not exposed. In contrast, the buffer and IPyC layers were burned out of the particle on the right, and the kernel was expanded as a result of conversion to U_3O_8; this confirms that the particle with the mottled appearing crater bottom had an exposed IPyC layer.

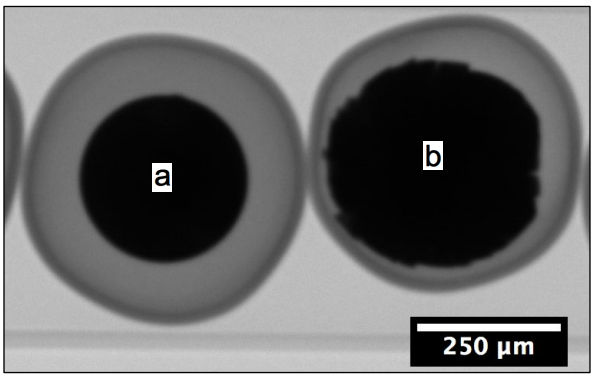

Figure 15. X-ray radiograph of the particles presented in Figure 12 after heating in air at 750°C for 60 hr: (a) particle with smooth crater bottom and (b) particle with mottled crater bottom.

After confirmation that the process of using a FIB to mill a large-diameter hole through the SiC provided reliable exposure of the IPyC, a test was performed to ensure that the process was controllable enough to prevent damage to the IPyC that might result in premature leaching. Ten particles with large-diameter, simulated postburn leach defects were fabricated, imaged by SEM and x-ray, and subjected to LBL analysis. The fabrication process utilized a 25 µm diameter raster pattern with a 30 kV, 30 nA Ga^+ ion beam. Simulated defects were introduced through the implementation of a stepwise process in which an initial 25 µm diameter crater was produced by a 73 min milling step followed by incremental milling for 2–4 min until the bottom of the crater showed the characteristic mottled surface that indicated the SiC had been penetrated and the IPyC was exposed.

Acceptance criteria were developed to ensure that the milling process was reproducibly providing the required microstructure and to document that microstructure. The crater of each particle was first imaged with SEM to verify that the bottom of the crater had the required mottled appearance, and then an x-ray radiograph was taken to verify that the crater did not penetrate more than 10 µm into the IPyC layer. An example of the acceptance analysis is shown in Figure 16. Because the crater bottom was sometimes difficult to identify in the x-ray radiographs, a small Pt dot was deposited at the bottom of each crater at the end of the milling process; this Pt deposit is also shown in Figure 16. The Pt was deposited using the FIB gas injection system, which can locally flood the target region with a Pt precursor gas. Platinum is deposited when the precursor gas interacts with the Ga^+ ion beam, and the deposition area can be controlled by rastering the beam. The Pt feature was deposited using a 30 kV, 0.5 nA Ga^+ beam and a 3.5 min, 3 µm diameter raster pattern. The higher atomic mass of the Pt relative to the TRISO layers provided additional x-ray imaging contrast to help confidently determine the ultimate depth of the crater. Additionally, the Pt was chemically stable and small enough to ensure that it would not interfere with the LBL process.

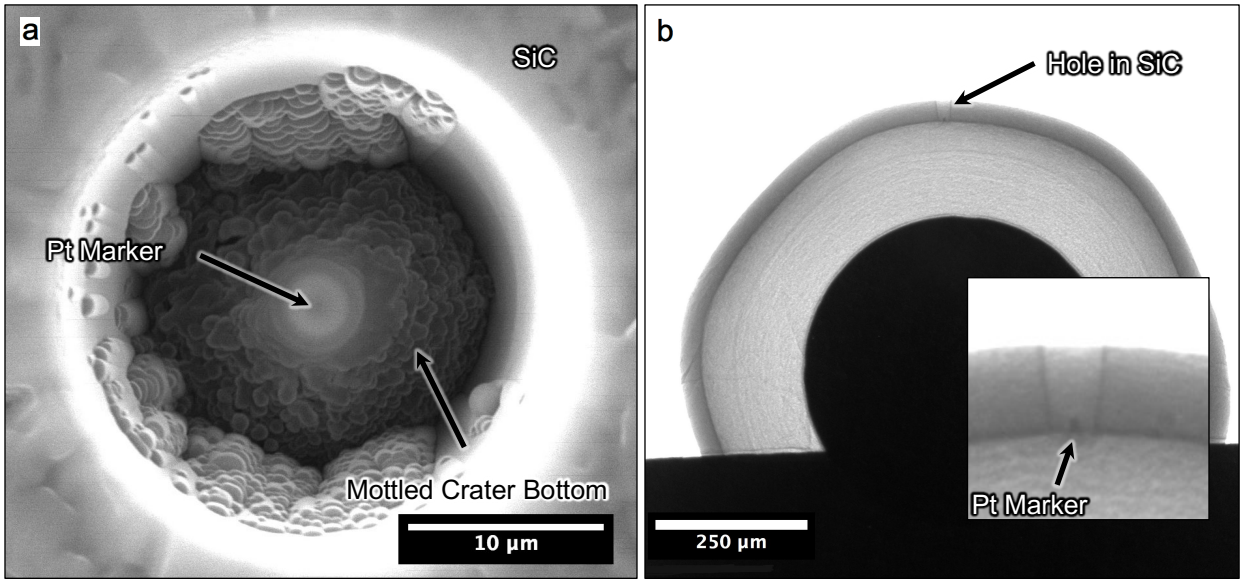

Figure 16. Two-part confirmation of acceptable microstructure for a simulated postburn leach defect consisting of (a) secondary electron SEM micrograph of the crater showing a mottled bottom with Pt marker, and (b) x-ray radiograph of the crater cross section indicating crater termination near the IPyC/SiC interface (inset shows close-up of the crater with platinum marker at the bottom).

The ten particles fabricated to test the LBL behavior of the simulated postburn leach defects met the required acceptance criteria and included the Pt marker. These particles were divided into two groups of five and were subjected to the standard ORNL LBL process (two 24 h leaches in boiling nitric acid before and after a 60 h burn at 750°C in air). Table 4 shows that 4–5% of the total uranium inventory was detected in the preburn leach solutions and the total amount of uranium leached was within the measurement uncertainty of the uranium inventory expected in each five-particle sample. Essentially all the exposed uranium detected during preburn leaching was found in the second 24 h leach, whereas the uranium measured during the postburn leach was essentially all in the first 24 h leach. This indicates that nitric acid was able to slowly permeate the IPyC layer and eventually extract a small fraction of uranium from the kernel during the preburn leach period, whereas the burn step resulted in complete exposure of the kernel material followed by effective dissolution of the uranium by the hot nitric acid. The small fraction of uranium leached through the IPyC layer prior to the burn will not adversely impact the primary goal of the round robin experiment, which is to count the number of particles with simulated LBL defects present in each round robin test sample (Table 1). Furthermore, the essentially complete postburn leaching of five kernels in each sample demonstrated that the simulated postburn leach defects will perform as needed.

Table 4. Results of LBL analysis on two test samples of five simulated postburn leach defects

Test sample	Uranium detected in preburn leach (kernel fraction)	Uranium detected in postburn leach (kernel fraction)	Total uranium detected by LBL (kernel fraction)
1	0.21 ± 0.02	4.58 ± 0.47	4.79 ± 0.47
2	0.26 ± 0.03	4.62 ± 0.47	4.88 ± 0.47

Reported kernel fractions are determined by dividing the mass of measured uranium in the leach solutions by the average mass of uranium in one kernel.

Figure 17 provides additional evidence of slow permeability of nitric acid through the IPyC layer in the particles with simulated postburn leach defects. In this x-ray tomograph, uranium leached from the kernel can be seen dispersed throughout the buffer and accumulated against the inside surface of the IPyC.

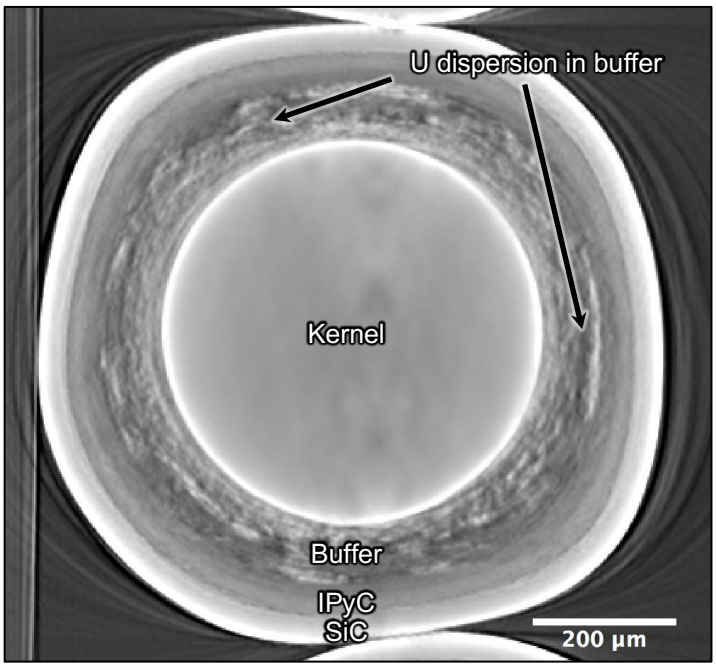

Figure 17. X-ray tomograph of a particle with a simulated postburn leach defect after preburn leaching: bright regions in the buffer layer indicate the presence of uranium that was extracted from the kernel as a result of nitric acid permeating the presumably intact IPyC layer.

Figure 18 shows an x-ray tomograph of a particle with a simulated postburn leach defect that was recovered after completion of postburn leaching. X-ray tomography provided additional confirmation of the successful postburn leach defect behavior. No buffer or IpyC layers were observed in the particles after postburn leaching. These carbon layers were oxidized and removed during the burn stage (as shown in Figure 15b), and the oxidized kernel was leached out of the SiC shell. There was also no evidence of residual dispersed uranium.

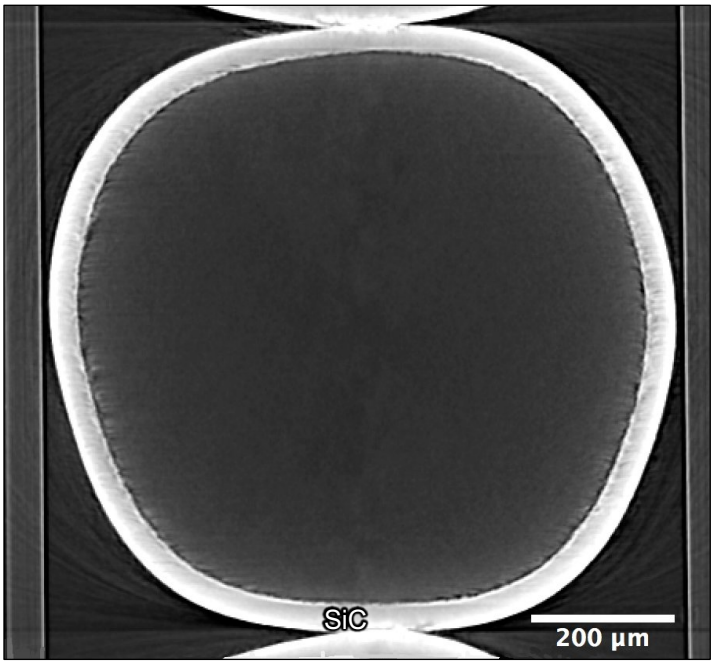

Figure 18. X-ray tomograph of a particle with a simulated postburn leach defect after postburn leaching: buffer and IPyC were oxidized and removed during the burn stage, and the kernel was completely leached during the postburn leach.

A total of 28 particles with simulated postburn leach defects was fabricated with the same 25 μm diameter raster pattern and stepwise milling procedure used to make the ten particles tested with LBL. These 28 particles are identified as FIB-01 through FIB-28. Twenty-one particles will be included in the LBL round robin experiment, and 7 are available as spares, as indicated in Table 5. Imaging with SEM and x-ray was performed on all 28 particles to determine if they met the acceptance criteria discussed above; Appendix F shows the results of this imaging, and Table 5 summarizes the status of the 28 particles. Appendix A identifies the sample assignment for each of these particles.

Table 5. Status of 28 particles from DUN500S-10A fabricated for inclusion in round robin experiment as simulated postburn leach defects using the FIB-milling method

Particle ID	Imaging status	Acceptable defect microstructure	Included in round robin
FIB-01	SEM/x-ray	Confirmed	Spare
FIB-02	SEM/x-ray	Confirmed	Yes
FIB-03	SEM/x-ray	Confirmed	Yes
FIB-04	SEM/x-ray	Confirmed	Spare
FIB-05	SEM/x-ray	Confirmed	Yes
FIB-06	SEM/x-ray	Confirmed	Yes
FIB-07	SEM/x-ray	Confirmed	Yes
FIB-08	SEM/x-ray	Confirmed	Yes
FIB-09	SEM/x-ray	Confirmed	Yes
FIB-10	SEM/x-ray	Confirmed	Yes
FIB-11	SEM/x-ray	Confirmed	Yes
FIB-12	SEM/x-ray	Confirmed	Spare
FIB-13	SEM/x-ray	Confirmed	Yes
FIB-14	SEM/x-ray	Confirmed	Yes
FIB-15	SEM/x-ray	Confirmed	Yes

Table 5. Status of 28 particles from DUN500S-10A fabricated for inclusion in round robin experiment as simulated postburn leach defects using FIB-milling method (continued)

Particle ID	Imaging status	Acceptable defect microstructure	Included in round robin
FIB-16	SEM/x-ray	Confirmed	Yes
FIB-17	SEM/x-ray	Confirmed	Yes
FIB-18	SEM/x-ray	Confirmed	Spare
FIB-19	SEM/x-ray	Confirmed	Yes
FIB-20	SEM/x-ray	Confirmed	Yes
FIB-21	SEM/x-ray	Confirmed	Yes
FIB-22	SEM/x-ray	Confirmed	Spare
FIB-23	SEM/x-ray	Confirmed	Yes
FIB-24	SEM/x-ray	Confirmed	Spare
FIB-25	SEM/x-ray	Confirmed	Yes
FIB-26	SEM/x-ray	Confirmed	Yes
FIB-27	SEM/x-ray	Confirmed	Yes
FIB-28	SEM/x-ray	Confirmed	Spare

6. SUMMARY

A cooperative round robin experiment to benchmark the LBL process has been undertaken by the GIF VHTR Fuel and Fuel Cycle Project Management Board. Primary participating countries in this LBL round robin are China, South Korea, and the United States, with corresponding organizations performing the LBL analysis being INET, KAERI, and ORNL, respectively. ORNL work scope has included the of simulated LBL defect particles and preparation of round robin test samples containing these particles and a coal impurity standard mixed with about 9,000 nonuranium-bearing surrogate coated particles.

Particles with simulated preburn and postburn leach defects were successfully fabricated from TRISO-coated DUO_2 particles. The vetting of the simulated defects included identification of the required defect behavior, development of fabrication methods to produce the defects, and validation of the simulated LBL defect particle performance. These particles will be shipped to INET and KAERI so they can proceed with round robin test sample analysis. Measurements have already been completed to determine the average uranium content per DUO_2 particle and average weight percent ^{235}U. Average uranium content is necessary for the LBL analysis to determine the number of DUO_2 kernels leached in each test sample. A data report form was developed by ORNL to assist in the collection of data and the analysis to determine the number of defective DUO_2 particles present in each sample based on the total amount of leached uranium in each leachate. This information will also be provided to each participant.

Preburn leach defects were simulated by designing a method to crack all the coating layers in a TRISO particle by transmitting the impact of a falling weight to one point on the surface of the particle through a small rod. This method successfully exposed the kernel without removing or excessively fracturing the TRISO coatings. Validation of all the simulated preburn leach defects to be included in the round robin experiment was accomplished by obtaining x-ray images of each particle to confirm that all coatings had through-layer cracks. One particle was subjected to destructive LBL analysis to verify that the simulated defect exhibited the proper preburn leach behavior, and this test showed full leaching of the kernel during the first 24 h leach.

Postburn leach defects were simulated by milling a hole through the SiC layer of each particle without excessively penetrating or damaging the overall integrity of the IPyC layer. To assist in the control of this process, the OPyC layer was first removed by burning it off in air at 750°C, and then a relatively large hole was milled with a FIB through the SiC using a 25 μm diameter raster pattern. This large hole allowed for sufficient control of the milling process, reduction in the interference from redeposited material, and direct imaging of the milled crater during fabrication. The size of the hole used to simulate the behavior of a postburn leach defect is not ideal from the standpoint of accurately replicating the smaller scale SiC defects that have been observed in TRISO particles or challenging the ultimate ability of air and liquid in penetrating very small defects. However, the experimental impact of simulated defects not performing as intended was an important consideration, and larger diameter holes were determined to be the best solution given the limitations of the available equipment and resources. Validation of the simulated postburn leach defects was accomplished by SEM and x-ray imaging of the FIB-produced crater in all particles to be used in the experiment. The combination of these two imaging techniques confirmed that each particle with a simulated burn-leach defect had a fully exposed IPyC layer without penetration beyond the outer 10 μm of IPyC. The LBL performance of the particles with simulated postburn leach defects was verified by subjecting ten particles to destructive LBL analysis: results indicate that the FIB-produced specimens behaved as required.

7. REFERENCES

Baldwin, C.A., J.D. Hunn, R.N. Morris, F.C. Montgomery, C.M. Silva, and P.A. Demkowicz. 2012. "First Elevated Temperature Performance Testing of Coated Particle Fuel Compacts from the AGR-1 Irradiation Experiment." Paper HTR2012-3-027 in *Proceedings of the 6th International Topical Meeting on High Temperature Reactor Technology—HTR 2012,* Tokyo, Japan, October 28–November 1, 2012. Also published in *Nuclear Engineering and Design* 271: 131–141.

Hunn, J.D. 2013. "Leach-Burn-Leach Analysis at ORNL for US VHTR Fuel Development and Qualification." Presented at the GIF-VHTR-Fuel and Fuel Cycle Project Management Board Meeting, Cadarache, France, December 12, 2013.

Hunn, J.D., R.N. Morris, C.A. Baldwin, F.C. Montgomery, C.M. Silva, and T.J. Gerczak. 2013. *AGR-1 Irradiated Compact 4-4-2 PIE Report: Evaluation of As-Irradiated Fuel Performance with Leach Burn Leach, IMGA, Materialography, and X-ray Tomography*. ORNL/TM-2013/236, Revision 0. Oak Ridge, Tennessee: Oak Ridge National Laboratory.

Lowden, R.A., and J.C. McLaughlin. 2004. *Fluidized Bed Coating of 500 um Depleted Uranium Oxide Kernels.* ORNL/CF-04/13, Revision 0. Oak Ridge, Tennessee: Oak Ridge National Laboratory.

Mackey, Elizabeth A., et al. 2011. *Certificate of Analysis Standard Reference Material 1632d Trace Elements in Coal*. Certificate issue date: October 14, 2014. Gaithersburg: National Institute of Standards and Technology.

Petti, D.A., J.T. Maki, J.D. Hunn, P.J. Pappano, C.M. Barnes, J.J. Saurwein, S.G. Nagley, J.M. Kendall, and R.R. Hobbins. 2010. "The DOE Advanced Gas Reactor Fuel Development and Qualification Program." *JOM* 62(9): 62–66.

APPENDIX A. SEEDING PLAN FOR SIMULATED LBL DEFECT PARTICLES

The following table identifies the specific particles with simulated LBL defects placed into each round robin test sample. Particles labeled "GIF" have simulated preburn leach defects, and particles labeled "FIB" have simulated postburn leach defects.

Table A.1. Specific DUN500S-10A particles with simulated LBL defects in each sample.

Ship round robin sample to:	Test sample ID	Particles to be added	Re-label for blind study (? = A–G)*
INET	INET-1	No defect particles added	INET-D
	INET-2	GIF-02	INET-E
	INET-3	GIF-03, GIF-06	INET-A
	INET-4	GIF-07, GIF-09, GIF-14, GIF-15	INET-F
	INET-5	FIB-02	INET-G
	INET-6	FIB-03, FIB-05	INET-C
	INET-7	FIB-06, FIB-07, FIB-08, FIB-09	INET-B
KAERI	KAERI-1	No defect particles added	KAERI-G
	KAERI-2	GIF-17	KAERI-B
	KAERI-3	GIF-19, GIF-27	KAERI-A
	KAERI-4	GIF-28, GIF-29. GIF-38, GIF-39	KAERI-D
	KAERI-5	FIB-10	KAERI-C
	KAERI-6	FIB-11, FIB-13	KAERI-F
	KAERI-7	FIB-14, FIB-15, FIB-16, FIB-17	KAERI-E
ORNL	ORNL-1	No defect particles added	ORNL-B
	ORNL-2	GIF-30	ORNL-C
	ORNL-3	GIF-41, GIF-42	ORNL-A
	ORNL-4	GIF-43, GIF-44, GIF-49, GIF-04	ORNL-F
	ORNL-5	FIB-19	ORNL-E
	ORNL-6	FIB-20, FIB-21	ORNL-D
	ORNL-7	FIB-23, FIB-25, FIB-26, FIB-27	ORNL-G

* When they were distributed to round-robin test participants for LBL, each sample set had been randomly re-labeled from 1–7 to A–G so that only the preparer knew the number and type of simulated defects in each sample. After LBL was completed, this table was revised to identify the assignments between the 1–7 labels and the A–G labels.

APPENDIX B. IMPURITIES IN SEEDED SAMPLES

After completion of LBL analysis by all participating institutions, this appendix was added to communicate the mass of each impurity contained in the standard reference material (SRM 1632d) that was mixed into each sample. Table B-1 through Table B-3 list the amount of dried SRM 1632d reference material that was added to each sample, as well as the mass of each impurity in each sample which was calculated by multiplying the mass fraction by the mass of added powder. Uncertainty in mass was propagated from the uncertainties in the mass fraction and measured powder mass.

Table B-1 through Table B-3 include information from the certificate of analysis for SRM 1632d (Mackey et al. 2011), which is maintained by NIST and can be downloaded from https://www-s.nist.gov/srmors/certificates/archives/1632d.pdf. The certificate of analysis provides detailed information on the standard reference material, including the mass fractions and uncertainties for each element listed in Table B-1 through Table B-3. Certified values are values reported to have the highest confidence for accuracy because all known or suspected biases have been considered. Reference values have uncertainties that may be based only on measurement precision, and some sources of uncertainty may not be included. Information values were provided by NIST because they may be of interest and use, but these were not reported with uncertainties as a result of insufficient information; therefore, uncertainties for these values are listed in the table as *not applicable (NA)*. Preparation of the simulated samples included acid washing of the ZrO-GIF particles used as a sample base to into which the particles with simulated defects and SRM 1632d powder were blended. As such, the impurities listed in the table should dominate the mass of impurities in each simulated sample, with the exception of uranium for the samples that include simulated defects. The uranium leached from those samples should be dominated by the uranium in the kernels of the particles with simulated defects. The average uranium content in the DUO_2 particles used to make the simulated defects (7.003E-4 g) was ~2,600× that of the uranium from the SRM 1632d powder included in each sample.

Table B-1. Impurity content in SRM 1632d added to each INET sample.

NIST SRM1632d Data			INET-A	INET-B	INET-C	INET-D	INET-E	INET-F	INET-G
Mass of dried SRM1632d powder added (g):			0.4945 ± 0.0005	0.5009 ± 0.0005	0.4849 ± 0.0005	0.5206 ± 0.0005	0.5076 ± 0.0005	0.4960 ± 0.0005	0.4911 ± 0.0005
Element	Quality	SRM1632 mass fraction	Mass in sample (g)	Mass in sample (g)	Mass in sample (g)	Mass in sample (g)	Mass in sample (g)	Mass in sample (g)	Mass in sample (g)
Al	reference	9.12E-03 ± 5E-05	4.51E-03 ± 2.5E-05	4.57E-03 ± 2.5E-05	4.42E-03 ± 2.5E-05	4.75E-03 ± 2.6E-05	4.63E-03 ± 2.6E-05	4.52E-03 ± 2.5E-05	4.48E-03 ± 2.5E-05
As	reference	6.1E-06 ± 2E-07	3.02E-06 ± 9.9E-08	3.06E-06 ± 1.0E-07	2.96E-06 ± 9.7E-08	3.18E-06 ± 1.0E-07	3.10E-06 ± 1.0E-07	3.03E-06 ± 9.9E-08	3.00E-06 ± 9.8E-08
B	reference	6.2E-05 ± 1E-06	3.07E-05 ± 5.0E-07	3.11E-05 ± 5.0E-07	3.01E-05 ± 4.9E-07	3.23E-05 ± 5.2E-07	3.15E-05 ± 5.1E-07	3.08E-05 ± 5.0E-07	3.04E-05 ± 4.9E-07
Ba	certified	4.042E-05 ± 8.9E-07	2.00E-05 ± 4.4E-07	2.02E-05 ± 4.5E-07	1.96E-05 ± 4.3E-07	2.10E-05 ± 4.6E-07	2.05E-05 ± 4.5E-07	2.00E-05 ± 4.4E-07	1.98E-05 ± 4.4E-07
C	reference	7.688E-01 ± 1.5E-03	3.80E-01 ± 8.3E-04	3.85E-01 ± 8.4E-04	3.73E-01 ± 8.2E-04	4.00E-01 ± 8.7E-04	3.90E-01 ± 8.5E-04	3.81E-01 ± 8.4E-04	3.78E-01 ± 8.3E-04
Ca	reference	1.44E-03 ± 3E-05	7.12E-04 ± 1.5E-05	7.21E-04 ± 1.5E-05	6.98E-04 ± 1.5E-05	7.50E-04 ± 1.6E-05	7.31E-04 ± 1.5E-05	7.14E-04 ± 1.5E-05	7.07E-04 ± 1.5E-05
Cd	reference	8E-08 ± 1E-08	3.96E-08 ± 4.9E-09	4.01E-08 ± 5.0E-09	3.88E-08 ± 4.8E-09	4.17E-08 ± 5.2E-09	4.06E-08 ± 5.1E-09	3.97E-08 ± 5.0E-09	3.93E-08 ± 4.9E-09
Ce	reference	1.17E-05 ± 4E-07	5.79E-06 ± 2.0E-07	5.86E-06 ± 2.0E-07	5.67E-06 ± 1.9E-07	6.09E-06 ± 2.1E-07	5.94E-06 ± 2.0E-07	5.80E-06 ± 2.0E-07	5.75E-06 ± 2.0E-07
Cl	certified	1.142E-03 ± 1.1E-05	5.65E-04 ± 5.5E-06	5.72E-04 ± 5.5E-06	5.54E-04 ± 5.4E-06	5.95E-04 ± 5.8E-06	5.80E-04 ± 5.6E-06	5.66E-04 ± 5.5E-06	5.61E-04 ± 5.4E-06
Co	certified	3.424E-06 ± 4.8E-08	1.69E-06 ± 2.4E-08	1.71E-06 ± 2.4E-08	1.66E-06 ± 2.3E-08	1.78E-06 ± 2.5E-08	1.74E-06 ± 2.4E-08	1.70E-06 ± 2.4E-08	1.68E-06 ± 2.4E-08
Cr	reference	1.37E-05 ± 1E-07	6.77E-06 ± 5.0E-08	6.86E-06 ± 5.1E-08	6.64E-06 ± 4.9E-08	7.13E-06 ± 5.3E-08	6.95E-06 ± 5.1E-08	6.79E-06 ± 5.0E-08	6.73E-06 ± 5.0E-08
Cs	reference	5.98E-07 ± 6E-09	2.96E-07 ± 3.0E-09	3.00E-07 ± 3.0E-09	2.90E-07 ± 2.9E-09	3.11E-07 ± 3.1E-09	3.04E-07 ± 3.1E-09	2.97E-07 ± 3.0E-09	2.94E-07 ± 3.0E-09
Cu	certified	5.83E-06 ± 3.1E-07	2.88E-06 ± 1.5E-07	2.92E-06 ± 1.6E-07	2.83E-06 ± 1.5E-07	3.04E-06 ± 1.6E-07	2.96E-06 ± 1.6E-07	2.89E-06 ± 1.5E-07	2.86E-06 ± 1.5E-07
Dy	information	9E-07 ± NA	4.45E-07 ± NA	4.51E-07 ± NA	4.36E-07 ± NA	4.69E-07 ± NA	4.57E-07 ± NA	4.46E-07 ± NA	4.42E-07 ± NA
Eu	reference	2.17E-07 ± 6E-09	1.07E-07 ± 3.0E-09	1.09E-07 ± 3.0E-09	1.05E-07 ± 2.9E-09	1.13E-07 ± 3.1E-09	1.10E-07 ± 3.0E-09	1.08E-07 ± 3.0E-09	1.07E-07 ± 2.9E-09
Fe	certified	7.49E-03 ± 1.6E-04	3.70E-03 ± 7.9E-05	3.75E-03 ± 8.0E-05	3.63E-03 ± 7.8E-05	3.90E-03 ± 8.3E-05	3.80E-03 ± 8.1E-05	3.71E-03 ± 7.9E-05	3.68E-03 ± 7.9E-05
H	certified	5.10E-02 ± 5E-04	2.52E-02 ± 2.5E-04	2.55E-02 ± 2.5E-04	2.47E-02 ± 2.4E-04	2.66E-02 ± 2.6E-04	2.59E-02 ± 2.6E-04	2.53E-02 ± 2.5E-04	2.50E-02 ± 2.5E-04
Hf	information	5E-07 ± NA	2.47E-07 ± NA	2.50E-07 ± NA	2.42E-07 ± NA	2.60E-07 ± NA	2.54E-07 ± NA	2.48E-07 ± NA	2.46E-07 ± NA
Hg	certified	9.28E-08 ± 3.3E-09	4.59E-08 ± 1.6E-09	4.65E-08 ± 1.7E-09	4.50E-08 ± 1.6E-09	4.83E-08 ± 1.7E-09	4.71E-08 ± 1.7E-09	4.60E-08 ± 1.6E-09	4.56E-08 ± 1.6E-09
K	certified	1.094E-03 ± 2.6E-05	5.41E-04 ± 1.3E-05	5.48E-04 ± 1.3E-05	5.30E-04 ± 1.3E-05	5.70E-04 ± 1.4E-05	5.55E-04 ± 1.3E-05	5.43E-04 ± 1.3E-05	5.37E-04 ± 1.3E-05
La	information	6E-06 ± NA	2.97E-06 ± NA	3.01E-06 ± NA	2.91E-06 ± NA	3.12E-06 ± NA	3.05E-06 ± NA	2.98E-06 ± NA	2.95E-06 ± NA
Mg	reference	3.90E-04 ± 6E-06	1.93E-04 ± 3.0E-06	1.95E-04 ± 3.0E-06	1.89E-04 ± 2.9E-06	2.03E-04 ± 3.1E-06	1.98E-04 ± 3.1E-06	1.93E-04 ± 3.0E-06	1.92E-04 ± 3.0E-06
Mn	reference	1.31E-05 ± 4E-07	6.48E-06 ± 2.0E-07	6.56E-06 ± 2.0E-07	6.35E-06 ± 1.9E-07	6.82E-06 ± 2.1E-07	6.65E-06 ± 2.0E-07	6.50E-06 ± 2.0E-07	6.43E-06 ± 2.0E-07
N	reference	1.59E-02 ± 1E-04	7.86E-03 ± 5.0E-05	7.96E-03 ± 5.1E-05	7.71E-03 ± 4.9E-05	8.28E-03 ± 5.3E-05	8.07E-03 ± 5.1E-05	7.89E-03 ± 5.0E-05	7.81E-03 ± 5.0E-05
Na	certified	2.969E-04 ± 4.2E-06	1.47E-04 ± 2.1E-06	1.49E-04 ± 2.1E-06	1.44E-04 ± 2.0E-06	1.55E-04 ± 2.2E-06	1.51E-04 ± 2.1E-06	1.47E-04 ± 2.1E-06	1.46E-04 ± 2.1E-06
Ni	information	1.0E-05 ± NA	4.95E-06 ± NA	5.01E-06 ± NA	4.85E-06 ± NA	5.21E-06 ± NA	5.08E-06 ± NA	4.96E-06 ± NA	4.91E-06 ± NA
Pb	certified	3.845E-06 ± 4.2E-08	1.90E-06 ± 2.1E-08	1.93E-06 ± 2.1E-08	1.86E-06 ± 2.0E-08	2.00E-06 ± 2.2E-08	1.95E-06 ± 2.1E-08	1.91E-06 ± 2.1E-08	1.89E-06 ± 2.1E-08
Rb	certified	7.36E-06 ± 2.0E-07	3.64E-06 ± 9.9E-08	3.69E-06 ± 1.0E-07	3.57E-06 ± 9.7E-08	3.83E-06 ± 1.0E-07	3.74E-06 ± 1.0E-07	3.65E-06 ± 9.9E-08	3.61E-06 ± 9.8E-08
S	certified	1.462E-02 ± 7.4E-04	7.23E-03 ± 3.7E-04	7.32E-03 ± 3.7E-04	7.09E-03 ± 3.6E-04	7.61E-03 ± 3.9E-04	7.42E-03 ± 3.8E-04	7.25E-03 ± 3.7E-04	7.18E-03 ± 3.6E-04
Sb	certified	4.45E-07 ± 1.5E-08	2.20E-07 ± 7.4E-09	2.23E-07 ± 7.5E-09	2.16E-07 ± 7.3E-09	2.32E-07 ± 7.8E-09	2.26E-07 ± 7.6E-09	2.21E-07 ± 7.4E-09	2.19E-07 ± 7.4E-09
Sc	reference	2.89E-06 ± 3E-08	1.43E-06 ± 1.5E-08	1.45E-06 ± 1.5E-08	1.40E-06 ± 1.5E-08	1.50E-06 ± 1.6E-08	1.47E-06 ± 1.5E-08	1.43E-06 ± 1.5E-08	1.42E-06 ± 1.5E-08
Se	reference	1.29E-06 ± 3E-08	6.38E-07 ± 1.5E-08	6.46E-07 ± 1.5E-08	6.26E-07 ± 1.5E-08	6.72E-07 ± 1.6E-08	6.55E-07 ± 1.5E-08	6.40E-07 ± 1.5E-08	6.33E-07 ± 1.5E-08
Si	reference	1.65E-02 ± 3E-04	8.16E-03 ± 1.5E-04	8.26E-03 ± 1.5E-04	8.00E-03 ± 1.5E-04	8.59E-03 ± 1.6E-04	8.38E-03 ± 1.5E-04	8.18E-03 ± 1.5E-04	8.10E-03 ± 1.5E-04
Sm	information	1E-06 ± NA	4.95E-07 ± NA	5.01E-07 ± NA	4.85E-07 ± NA	5.21E-07 ± NA	5.08E-07 ± NA	4.96E-07 ± NA	4.91E-07 ± NA
Sr	certified	6.35E-05 ± 1.2E-06	3.14E-05 ± 5.9E-07	3.18E-05 ± 6.0E-07	3.08E-05 ± 5.8E-07	3.31E-05 ± 6.3E-07	3.22E-05 ± 6.1E-07	3.15E-05 ± 6.0E-07	3.12E-05 ± 5.9E-07
Th	certified	1.428E-06 ± 3.5E-08	7.06E-07 ± 1.7E-08	7.15E-07 ± 1.8E-08	6.92E-07 ± 1.7E-08	7.43E-07 ± 1.8E-08	7.25E-07 ± 1.8E-08	7.08E-07 ± 1.7E-08	7.01E-07 ± 1.7E-08
Ti	certified	4.77E-04 ± 1.0E-05	2.36E-04 ± 5.0E-06	2.39E-04 ± 5.0E-06	2.31E-04 ± 4.9E-06	2.48E-04 ± 5.2E-06	2.42E-04 ± 5.1E-06	2.37E-04 ± 5.0E-06	2.34E-04 ± 4.9E-06
U	certified	5.17E-07 ± 1.2E-08	2.56E-07 ± 5.9E-09	2.59E-07 ± 6.0E-09	2.51E-07 ± 5.8E-09	2.69E-07 ± 6.3E-09	2.62E-07 ± 6.1E-09	2.56E-07 ± 6.0E-09	2.54E-07 ± 5.9E-09
V	certified	2.374E-05 ± 1.0E-07	1.17E-05 ± 5.1E-08	1.19E-05 ± 5.1E-08	1.15E-05 ± 5.0E-08	1.24E-05 ± 5.3E-08	1.21E-05 ± 5.2E-08	1.18E-05 ± 5.1E-08	1.17E-05 ± 5.0E-08
Zn	reference	1.29E-05 ± 1.2E-06	6.38E-06 ± 5.9E-07	6.46E-06 ± 6.0E-07	6.26E-06 ± 5.8E-07	6.72E-06 ± 6.2E-07	6.55E-06 ± 6.1E-07	6.40E-06 ± 6.0E-07	6.33E-06 ± 5.9E-07

Note: Listed values for mass fraction ± uncertainty were obtained from NIST SRM 1632d Certificate of Analysis (https://www-s.nist.gov/srmors/certificates/archives/1632d.pdf).

Note: Listed values for mass in sample ± uncertainty were calculated from mass fraction data and measured mass of dry powder added.

Note: Yellow highlight indicates elements of interest for QC of TRISO fuel and blue highlight indicates elements of interest for PIE of TRISO fuel.

Table B-2. Impurity content in SRM 1632d added to each KAERI sample.

NIST SRM1632d Data			KAERI-A	KAERI-B	KAERI-C	KAERI-D	KAERI-E	KAERI-F	KAERI-G
Mass of dried SRM1632d powder added (g):			0.4887 ± 0.0005	0.4860 ± 0.0005	0.5045 ± 0.0005	0.4895 ± 0.0005	0.5006 ± 0.0005	0.4922 ± 0.0005	0.4905 ± 0.0005
Element	Quality	SRM1632 mass fraction	Mass in sample (g)	Mass in sample (g)	Mass in sample (g)	Mass in sample (g)	Mass in sample (g)	Mass in sample (g)	Mass in sample (g)
Al	reference	9.12E-03 ± 5E-05	4.46E-03 ± 2.5E-05	4.43E-03 ± 2.5E-05	4.60E-03 ± 2.6E-05	4.46E-03 ± 2.5E-05	4.57E-03 ± 2.5E-05	4.49E-03 ± 2.5E-05	4.47E-03 ± 2.5E-05
As	reference	6.1E-06 ± 2E-07	2.98E-06 ± 9.8E-08	2.96E-06 ± 9.7E-08	3.08E-06 ± 1.0E-07	2.99E-06 ± 9.8E-08	3.05E-06 ± 1.0E-07	3.00E-06 ± 9.8E-08	2.99E-06 ± 9.8E-08
B	reference	6.2E-05 ± 1E-06	3.03E-05 ± 4.9E-07	3.01E-05 ± 4.9E-07	3.13E-05 ± 5.1E-07	3.03E-05 ± 4.9E-07	3.10E-05 ± 5.0E-07	3.05E-05 ± 4.9E-07	3.04E-05 ± 4.9E-07
Ba	certified	4.042E-05 ± 8.9E-07	1.98E-05 ± 4.4E-07	1.96E-05 ± 4.3E-07	2.04E-05 ± 4.5E-07	1.98E-05 ± 4.4E-07	2.02E-05 ± 4.5E-07	1.99E-05 ± 4.4E-07	1.98E-05 ± 4.4E-07
C	reference	7.688E-01 ± 1.5E-03	3.76E-01 ± 8.2E-04	3.74E-01 ± 8.2E-04	3.88E-01 ± 8.5E-04	3.76E-01 ± 8.3E-04	3.85E-01 ± 8.4E-04	3.78E-01 ± 8.3E-04	3.77E-01 ± 8.3E-04
Ca	reference	1.44E-03 ± 3E-05	7.04E-04 ± 1.5E-05	7.00E-04 ± 1.5E-05	7.26E-04 ± 1.5E-05	7.05E-04 ± 1.5E-05	7.21E-04 ± 1.5E-05	7.09E-04 ± 1.5E-05	7.06E-04 ± 1.5E-05
Cd	reference	8E-08 ± 1E-08	3.91E-08 ± 4.9E-09	3.89E-08 ± 4.9E-09	4.04E-08 ± 5.0E-09	3.92E-08 ± 4.9E-09	4.00E-08 ± 5.0E-09	3.94E-08 ± 4.9E-09	3.92E-08 ± 4.9E-09
Ce	reference	1.17E-05 ± 4E-07	5.72E-06 ± 2.0E-07	5.69E-06 ± 1.9E-07	5.90E-06 ± 2.0E-07	5.73E-06 ± 2.0E-07	5.86E-06 ± 2.0E-07	5.76E-06 ± 2.0E-07	5.74E-06 ± 2.0E-07
Cl	certified	1.142E-03 ± 1.1E-05	5.58E-04 ± 5.4E-06	5.55E-04 ± 5.4E-06	5.76E-04 ± 5.6E-06	5.59E-04 ± 5.4E-06	5.72E-04 ± 5.5E-06	5.62E-04 ± 5.4E-06	5.60E-04 ± 5.4E-06
Co	certified	3.424E-06 ± 4.8E-08	1.67E-06 ± 2.4E-08	1.66E-06 ± 2.3E-08	1.73E-06 ± 2.4E-08	1.68E-06 ± 2.4E-08	1.71E-06 ± 2.4E-08	1.69E-06 ± 2.4E-08	1.68E-06 ± 2.4E-08
Cr	reference	1.37E-05 ± 1E-07	6.70E-06 ± 4.9E-08	6.66E-06 ± 4.9E-08	6.91E-06 ± 5.1E-08	6.71E-06 ± 4.9E-08	6.86E-06 ± 5.1E-08	6.74E-06 ± 5.0E-08	6.72E-06 ± 5.0E-08
Cs	reference	5.98E-07 ± 6E-09	2.92E-07 ± 2.9E-09	2.91E-07 ± 2.9E-09	3.02E-07 ± 3.0E-09	2.93E-07 ± 3.0E-09	2.99E-07 ± 3.0E-09	2.94E-07 ± 3.0E-09	2.93E-07 ± 3.0E-09
Cu	certified	5.83E-06 ± 3.1E-07	2.85E-06 ± 1.5E-07	2.83E-06 ± 1.5E-07	2.94E-06 ± 1.6E-07	2.85E-06 ± 1.5E-07	2.92E-06 ± 1.6E-07	2.87E-06 ± 1.5E-07	2.86E-06 ± 1.5E-07
Dy	information	9E-07 ± NA	4.40E-07 ± NA	4.37E-07 ± NA	4.54E-07 ± NA	4.41E-07 ± NA	4.51E-07 ± NA	4.43E-07 ± NA	4.41E-07 ± NA
Eu	reference	2.17E-07 ± 6E-09	1.06E-07 ± 2.9E-09	1.05E-07 ± 2.9E-09	1.09E-07 ± 3.0E-09	1.06E-07 ± 2.9E-09	1.09E-07 ± 3.0E-09	1.07E-07 ± 3.0E-09	1.06E-07 ± 2.9E-09
Fe	certified	7.49E-03 ± 1.6E-04	3.66E-03 ± 7.8E-05	3.64E-03 ± 7.8E-05	3.78E-03 ± 8.1E-05	3.67E-03 ± 7.8E-05	3.75E-03 ± 8.0E-05	3.69E-03 ± 7.9E-05	3.67E-03 ± 7.9E-05
H	certified	5.10E-02 ± 5E-04	2.49E-02 ± 2.5E-04	2.48E-02 ± 2.4E-04	2.57E-02 ± 2.5E-04	2.50E-02 ± 2.5E-04	2.55E-02 ± 2.5E-04	2.51E-02 ± 2.5E-04	2.50E-02 ± 2.5E-04
Hf	information	5E-07 ± NA	2.44E-07 ± NA	2.43E-07 ± NA	2.52E-07 ± NA	2.45E-07 ± NA	2.50E-07 ± NA	2.46E-07 ± NA	2.45E-07 ± NA
Hg	certified	9.28E-08 ± 3.3E-09	4.54E-08 ± 1.6E-09	4.51E-08 ± 1.6E-09	4.68E-08 ± 1.7E-09	4.54E-08 ± 1.6E-09	4.65E-08 ± 1.7E-09	4.57E-08 ± 1.6E-09	4.55E-08 ± 1.6E-09
K	certified	1.094E-03 ± 2.6E-05	5.35E-04 ± 1.3E-05	5.32E-04 ± 1.3E-05	5.52E-04 ± 1.3E-05	5.36E-04 ± 1.3E-05	5.48E-04 ± 1.3E-05	5.38E-04 ± 1.3E-05	5.37E-04 ± 1.3E-05
La	information	6E-06 ± NA	2.93E-06 ± NA	2.92E-06 ± NA	3.03E-06 ± NA	2.94E-06 ± NA	3.00E-06 ± NA	2.95E-06 ± NA	2.94E-06 ± NA
Mg	reference	3.90E-04 ± 6E-06	1.91E-04 ± 2.9E-06	1.90E-04 ± 2.9E-06	1.97E-04 ± 3.0E-06	1.91E-04 ± 2.9E-06	1.95E-04 ± 3.0E-06	1.92E-04 ± 3.0E-06	1.91E-04 ± 2.9E-06
Mn	reference	1.31E-05 ± 4E-07	6.40E-06 ± 2.0E-07	6.37E-06 ± 1.9E-07	6.61E-06 ± 2.0E-07	6.41E-06 ± 2.0E-07	6.56E-06 ± 2.0E-07	6.45E-06 ± 2.0E-07	6.43E-06 ± 2.0E-07
N	reference	1.59E-02 ± 1E-04	7.77E-03 ± 4.9E-05	7.73E-03 ± 4.9E-05	8.02E-03 ± 5.1E-05	7.78E-03 ± 5.0E-05	7.96E-03 ± 5.1E-05	7.83E-03 ± 5.0E-05	7.80E-03 ± 5.0E-05
Na	certified	2.969E-04 ± 4.2E-06	1.45E-04 ± 2.1E-06	1.44E-04 ± 2.0E-06	1.50E-04 ± 2.1E-06	1.45E-04 ± 2.1E-06	1.49E-04 ± 2.1E-06	1.46E-04 ± 2.1E-06	1.46E-04 ± 2.1E-06
Ni	information	1.0E-05 ± NA	4.89E-06 ± NA	4.86E-06 ± NA	5.04E-06 ± NA	4.90E-06 ± NA	5.01E-06 ± NA	4.92E-06 ± NA	4.90E-06 ± NA
Pb	certified	3.845E-06 ± 4.2E-08	1.88E-06 ± 2.1E-08	1.87E-06 ± 2.0E-08	1.94E-06 ± 2.1E-08	1.88E-06 ± 2.1E-08	1.92E-06 ± 2.1E-08	1.89E-06 ± 2.1E-08	1.89E-06 ± 2.1E-08
Rb	certified	7.36E-06 ± 2.0E-07	3.60E-06 ± 9.8E-08	3.58E-06 ± 9.7E-08	3.71E-06 ± 1.0E-07	3.60E-06 ± 9.8E-08	3.68E-06 ± 1.0E-07	3.62E-06 ± 9.8E-08	3.61E-06 ± 9.8E-08
S	certified	1.462E-02 ± 7.4E-04	7.15E-03 ± 3.6E-04	7.11E-03 ± 3.6E-04	7.38E-03 ± 3.7E-04	7.16E-03 ± 3.6E-04	7.32E-03 ± 3.7E-04	7.20E-03 ± 3.6E-04	7.17E-03 ± 3.6E-04
Sb	certified	4.45E-07 ± 1.5E-08	2.17E-07 ± 7.3E-09	2.16E-07 ± 7.3E-09	2.24E-07 ± 7.6E-09	2.18E-07 ± 7.3E-09	2.23E-07 ± 7.5E-09	2.19E-07 ± 7.4E-09	2.18E-07 ± 7.4E-09
Sc	reference	2.89E-06 ± 3E-08	1.41E-06 ± 1.5E-08	1.40E-06 ± 1.5E-08	1.46E-06 ± 1.5E-08	1.41E-06 ± 1.5E-08	1.45E-06 ± 1.5E-08	1.42E-06 ± 1.5E-08	1.42E-06 ± 1.5E-08
Se	reference	1.29E-06 ± 3E-08	6.30E-07 ± 1.5E-08	6.27E-07 ± 1.5E-08	6.51E-07 ± 1.5E-08	6.31E-07 ± 1.5E-08	6.46E-07 ± 1.5E-08	6.35E-07 ± 1.5E-08	6.33E-07 ± 1.5E-08
Si	reference	1.65E-02 ± 3E-04	8.06E-03 ± 1.5E-04	8.02E-03 ± 1.5E-04	8.32E-03 ± 1.5E-04	8.08E-03 ± 1.5E-04	8.26E-03 ± 1.5E-04	8.12E-03 ± 1.5E-04	8.09E-03 ± 1.5E-04
Sm	information	1E-06 ± NA	4.89E-07 ± NA	4.86E-07 ± NA	5.04E-07 ± NA	4.90E-07 ± NA	5.01E-07 ± NA	4.92E-07 ± NA	4.90E-07 ± NA
Sr	certified	6.35E-05 ± 1.2E-06	3.10E-05 ± 5.9E-07	3.09E-05 ± 5.8E-07	3.20E-05 ± 6.1E-07	3.11E-05 ± 5.9E-07	3.18E-05 ± 6.0E-07	3.13E-05 ± 5.9E-07	3.11E-05 ± 5.9E-07
Th	certified	1.428E-06 ± 3.5E-08	6.98E-07 ± 1.7E-08	6.94E-07 ± 1.7E-08	7.20E-07 ± 1.8E-08	6.99E-07 ± 1.7E-08	7.15E-07 ± 1.8E-08	7.03E-07 ± 1.7E-08	7.00E-07 ± 1.7E-08
Ti	certified	4.77E-04 ± 1.0E-05	2.33E-04 ± 4.9E-06	2.32E-04 ± 4.9E-06	2.41E-04 ± 5.1E-06	2.33E-04 ± 4.9E-06	2.39E-04 ± 5.0E-06	2.35E-04 ± 4.9E-06	2.34E-04 ± 4.9E-06
U	certified	5.17E-07 ± 1.2E-08	2.53E-07 ± 5.9E-09	2.51E-07 ± 5.8E-09	2.61E-07 ± 6.1E-09	2.53E-07 ± 5.9E-09	2.59E-07 ± 6.0E-09	2.54E-07 ± 5.9E-09	2.54E-07 ± 5.9E-09
V	certified	2.374E-05 ± 1.0E-07	1.16E-05 ± 5.0E-08	1.15E-05 ± 5.0E-08	1.20E-05 ± 5.2E-08	1.16E-05 ± 5.0E-08	1.19E-05 ± 5.1E-08	1.17E-05 ± 5.1E-08	1.16E-05 ± 5.0E-08
Zn	reference	1.29E-05 ± 1.2E-06	6.30E-06 ± 5.9E-07	6.27E-06 ± 5.8E-07	6.51E-06 ± 6.1E-07	6.31E-06 ± 5.9E-07	6.46E-06 ± 6.0E-07	6.35E-06 ± 5.9E-07	6.33E-06 ± 5.9E-07

Note: Listed values for mass fraction ± uncertainty were obtained from NIST SRM 1632d Certificate of Analysis (https://www-s.nist.gov/srmors/certificates/archives/1632d.pdf).

Note: Listed values for mass in sample ± uncertainty were calculated from mass fraction data and measured mass of dry powder added.

Note: Yellow highlight indicates elements of interest for QC of TRISO fuel and blue highlight indicates elements of interest for PIE of TRISO fuel.

Table B-3. Impurity content in SRM 1632d added to each ORNL sample.

NIST SRM1632d Data			ORNL-A	ORNL-B	ORNL-C	ORNL-D	ORNL-E	ORNL-F	ORNL-G
Mass of dried SRM1632d powder added (g):			0.5529 ± 0.0005	0.4850 ± 0.0005	0.5264 ± 0.0005	0.4922 ± 0.0005	0.4969 ± 0.0005	0.4904 ± 0.0005	0.4672 ± 0.0005
Element	Quality	SRM1632 mass fraction	Mass in sample (g)	Mass in sample (g)	Mass in sample (g)	Mass in sample (g)	Mass in sample (g)	Mass in sample (g)	Mass in sample (g)
Al	reference	9.12E-03 ± 5E-05	5.04E-03 ± 2.8E-05	4.42E-03 ± 2.5E-05	4.80E-03 ± 2.7E-05	4.49E-03 ± 2.5E-05	4.53E-03 ± 2.5E-05	4.47E-03 ± 2.5E-05	4.26E-03 ± 2.4E-05
As	reference	6.1E-06 ± 2E-07	3.37E-06 ± 1.1E-07	2.96E-06 ± 9.7E-08	3.21E-06 ± 1.1E-07	3.00E-06 ± 9.8E-08	3.03E-06 ± 9.9E-08	2.99E-06 ± 9.8E-08	2.85E-06 ± 9.3E-08
B	reference	6.2E-05 ± 1E-06	3.43E-05 ± 5.5E-07	3.01E-05 ± 4.9E-07	3.26E-05 ± 5.3E-07	3.05E-05 ± 4.9E-07	3.08E-05 ± 5.0E-07	3.04E-05 ± 4.9E-07	2.90E-05 ± 4.7E-07
Ba	certified	4.042E-05 ± 8.9E-07	2.23E-05 ± 4.9E-07	1.96E-05 ± 4.3E-07	2.13E-05 ± 4.7E-07	1.99E-05 ± 4.4E-07	2.01E-05 ± 4.4E-07	1.98E-05 ± 4.4E-07	1.89E-05 ± 4.2E-07
C	reference	7.688E-01 ± 1.5E-03	4.25E-01 ± 9.3E-04	3.73E-01 ± 8.2E-04	4.05E-01 ± 8.8E-04	3.78E-01 ± 8.3E-04	3.82E-01 ± 8.4E-04	3.77E-01 ± 8.3E-04	3.59E-01 ± 7.9E-04
Ca	reference	1.44E-03 ± 3E-05	7.96E-04 ± 1.7E-05	6.98E-04 ± 1.5E-05	7.58E-04 ± 1.6E-05	7.09E-04 ± 1.5E-05	7.15E-04 ± 1.5E-05	7.06E-04 ± 1.5E-05	6.73E-04 ± 1.4E-05
Cd	reference	8E-08 ± 1E-08	4.42E-08 ± 5.5E-09	3.88E-08 ± 4.9E-09	4.21E-08 ± 5.3E-09	3.94E-08 ± 4.9E-09	3.97E-08 ± 5.0E-09	3.92E-08 ± 4.9E-09	3.74E-08 ± 4.7E-09
Ce	reference	1.17E-05 ± 4E-07	6.47E-06 ± 2.2E-07	5.67E-06 ± 1.9E-07	6.16E-06 ± 2.1E-07	5.76E-06 ± 2.0E-07	5.81E-06 ± 2.0E-07	5.74E-06 ± 2.0E-07	5.47E-06 ± 1.9E-07
Cl	certified	1.142E-03 ± 1.1E-05	6.31E-04 ± 6.1E-06	5.54E-04 ± 5.4E-06	6.01E-04 ± 5.8E-06	5.62E-04 ± 5.4E-06	5.67E-04 ± 5.5E-06	5.60E-04 ± 5.4E-06	5.34E-04 ± 5.2E-06
Co	certified	3.424E-06 ± 4.8E-08	1.89E-06 ± 2.7E-08	1.66E-06 ± 2.3E-08	1.80E-06 ± 2.5E-08	1.69E-06 ± 2.4E-08	1.70E-06 ± 2.4E-08	1.68E-06 ± 2.4E-08	1.60E-06 ± 2.2E-08
Cr	reference	1.37E-05 ± 1E-07	7.57E-06 ± 5.6E-08	6.64E-06 ± 4.9E-08	7.21E-06 ± 5.3E-08	6.74E-06 ± 5.0E-08	6.81E-06 ± 5.0E-08	6.72E-06 ± 4.9E-08	6.40E-06 ± 4.7E-08
Cs	reference	5.98E-07 ± 6E-09	3.31E-07 ± 3.3E-09	2.90E-07 ± 2.9E-09	3.15E-07 ± 3.2E-09	2.94E-07 ± 3.0E-09	2.97E-07 ± 3.0E-09	2.93E-07 ± 3.0E-09	2.79E-07 ± 2.8E-09
Cu	certified	5.83E-06 ± 3.1E-07	3.22E-06 ± 1.7E-07	2.83E-06 ± 1.5E-07	3.07E-06 ± 1.6E-07	2.87E-06 ± 1.5E-07	2.90E-06 ± 1.5E-07	2.86E-06 ± 1.5E-07	2.72E-06 ± 1.4E-07
Dy	information	9E-07 ± NA	4.98E-07 ± NA	4.37E-07 ± NA	4.74E-07 ± NA	4.43E-07 ± NA	4.47E-07 ± NA	4.41E-07 ± NA	4.20E-07 ± NA
Eu	reference	2.17E-07 ± 6E-09	1.20E-07 ± 3.3E-09	1.05E-07 ± 2.9E-09	1.14E-07 ± 3.2E-09	1.07E-07 ± 3.0E-09	1.08E-07 ± 3.0E-09	1.06E-07 ± 2.9E-09	1.01E-07 ± 2.8E-09
Fe	certified	7.49E-03 ± 1.6E-04	4.14E-03 ± 8.9E-05	3.63E-03 ± 7.8E-05	3.94E-03 ± 8.4E-05	3.69E-03 ± 7.9E-05	3.72E-03 ± 8.0E-05	3.67E-03 ± 7.9E-05	3.50E-03 ± 7.5E-05
H	certified	5.10E-02 ± 5E-04	2.82E-02 ± 2.8E-04	2.47E-02 ± 2.4E-04	2.68E-02 ± 2.6E-04	2.51E-02 ± 2.5E-04	2.53E-02 ± 2.5E-04	2.50E-02 ± 2.5E-04	2.38E-02 ± 2.3E-04
Hf	information	5E-07 ± NA	2.76E-07 ± NA	2.43E-07 ± NA	2.63E-07 ± NA	2.46E-07 ± NA	2.48E-07 ± NA	2.45E-07 ± NA	2.34E-07 ± NA
Hg	certified	9.28E-08 ± 3.3E-09	5.13E-08 ± 1.8E-09	4.50E-08 ± 1.6E-09	4.89E-08 ± 1.7E-09	4.57E-08 ± 1.6E-09	4.61E-08 ± 1.6E-09	4.55E-08 ± 1.6E-09	4.34E-08 ± 1.5E-09
K	certified	1.094E-03 ± 2.6E-05	6.05E-04 ± 1.4E-05	5.31E-04 ± 1.3E-05	5.76E-04 ± 1.4E-05	5.39E-04 ± 1.3E-05	5.44E-04 ± 1.3E-05	5.36E-04 ± 1.3E-05	5.11E-04 ± 1.2E-05
La	information	6E-06 ± NA	3.32E-06 ± NA	2.91E-06 ± NA	3.16E-06 ± NA	2.95E-06 ± NA	2.98E-06 ± NA	2.94E-06 ± NA	2.80E-06 ± NA
Mg	reference	3.90E-04 ± 6E-06	2.16E-04 ± 3.3E-06	1.89E-04 ± 2.9E-06	2.05E-04 ± 3.2E-06	1.92E-04 ± 3.0E-06	1.94E-04 ± 3.0E-06	1.91E-04 ± 2.9E-06	1.82E-04 ± 2.8E-06
Mn	reference	1.31E-05 ± 4E-07	7.24E-06 ± 2.2E-07	6.35E-06 ± 1.9E-07	6.90E-06 ± 2.1E-07	6.45E-06 ± 2.0E-07	6.51E-06 ± 2.0E-07	6.42E-06 ± 2.0E-07	6.12E-06 ± 1.9E-07
N	reference	1.59E-02 ± 1E-04	8.79E-03 ± 5.6E-05	7.71E-03 ± 4.9E-05	8.37E-03 ± 5.3E-05	7.83E-03 ± 5.0E-05	7.90E-03 ± 5.0E-05	7.80E-03 ± 5.0E-05	7.43E-03 ± 4.7E-05
Na	certified	2.969E-04 ± 4.2E-06	1.64E-04 ± 2.3E-06	1.44E-04 ± 2.0E-06	1.56E-04 ± 2.2E-06	1.46E-04 ± 2.1E-06	1.48E-04 ± 2.1E-06	1.46E-04 ± 2.1E-06	1.39E-04 ± 2.0E-06
Ni	information	1.0E-05 ± NA	5.53E-06 ± NA	4.85E-06 ± NA	5.26E-06 ± NA	4.92E-06 ± NA	4.97E-06 ± NA	4.90E-06 ± NA	4.67E-06 ± NA
Pb	certified	3.845E-06 ± 4.2E-08	2.13E-06 ± 2.3E-08	1.86E-06 ± 2.0E-08	2.02E-06 ± 2.2E-08	1.89E-06 ± 2.1E-08	1.91E-06 ± 2.1E-08	1.89E-06 ± 2.1E-08	1.80E-06 ± 2.0E-08
Rb	certified	7.36E-06 ± 2.0E-07	4.07E-06 ± 1.1E-07	3.57E-06 ± 9.7E-08	3.87E-06 ± 1.1E-07	3.62E-06 ± 9.9E-08	3.66E-06 ± 9.9E-08	3.61E-06 ± 9.8E-08	3.44E-06 ± 9.4E-08
S	certified	1.462E-02 ± 7.4E-04	8.08E-03 ± 4.1E-04	7.09E-03 ± 3.6E-04	7.70E-03 ± 3.9E-04	7.20E-03 ± 3.6E-04	7.26E-03 ± 3.7E-04	7.17E-03 ± 3.6E-04	6.83E-03 ± 3.5E-04
Sb	certified	4.45E-07 ± 1.5E-08	2.46E-07 ± 8.3E-09	2.16E-07 ± 7.3E-09	2.34E-07 ± 7.9E-09	2.19E-07 ± 7.4E-09	2.21E-07 ± 7.5E-09	2.18E-07 ± 7.4E-09	2.08E-07 ± 7.0E-09
Sc	reference	2.89E-06 ± 3E-08	1.60E-06 ± 1.7E-08	1.40E-06 ± 1.5E-08	1.52E-06 ± 1.6E-08	1.42E-06 ± 1.5E-08	1.44E-06 ± 1.5E-08	1.42E-06 ± 1.5E-08	1.35E-06 ± 1.4E-08
Se	reference	1.29E-06 ± 3E-08	7.13E-07 ± 1.7E-08	6.26E-07 ± 1.5E-08	6.79E-07 ± 1.6E-08	6.35E-07 ± 1.5E-08	6.41E-07 ± 1.5E-08	6.33E-07 ± 1.5E-08	6.03E-07 ± 1.4E-08
Si	reference	1.65E-02 ± 3E-04	9.12E-03 ± 1.7E-04	8.00E-03 ± 1.5E-04	8.69E-03 ± 1.6E-04	8.12E-03 ± 1.5E-04	8.20E-03 ± 1.5E-04	8.09E-03 ± 1.5E-04	7.71E-03 ± 1.4E-04
Sm	information	1E-06 ± NA	5.53E-07 ± NA	4.85E-07 ± NA	5.26E-07 ± NA	4.92E-07 ± NA	4.97E-07 ± NA	4.90E-07 ± NA	4.67E-07 ± NA
Sr	certified	6.35E-05 ± 1.2E-06	3.51E-05 ± 6.6E-07	3.08E-05 ± 5.8E-07	3.34E-05 ± 6.3E-07	3.13E-05 ± 5.9E-07	3.16E-05 ± 6.0E-07	3.11E-05 ± 5.9E-07	2.97E-05 ± 5.6E-07
Th	certified	1.428E-06 ± 3.5E-08	7.89E-07 ± 1.9E-08	6.93E-07 ± 1.7E-08	7.52E-07 ± 1.8E-08	7.03E-07 ± 1.7E-08	7.10E-07 ± 1.7E-08	7.00E-07 ± 1.7E-08	6.67E-07 ± 1.6E-08
Ti	certified	4.77E-04 ± 1.0E-05	2.64E-04 ± 5.5E-06	2.31E-04 ± 4.9E-06	2.51E-04 ± 5.3E-06	2.35E-04 ± 4.9E-06	2.37E-04 ± 5.0E-06	2.34E-04 ± 4.9E-06	2.23E-04 ± 4.7E-06
U	certified	5.17E-07 ± 1.2E-08	2.86E-07 ± 6.6E-09	2.51E-07 ± 5.8E-09	2.72E-07 ± 6.3E-09	2.54E-07 ± 5.9E-09	2.57E-07 ± 6.0E-09	2.54E-07 ± 5.9E-09	2.42E-07 ± 5.6E-09
V	certified	2.374E-05 ± 1.0E-07	1.31E-05 ± 5.7E-08	1.15E-05 ± 5.0E-08	1.25E-05 ± 5.4E-08	1.17E-05 ± 5.1E-08	1.18E-05 ± 5.1E-08	1.16E-05 ± 5.0E-08	1.11E-05 ± 4.8E-08
Zn	reference	1.29E-05 ± 1.2E-06	7.13E-06 ± 6.6E-07	6.26E-06 ± 5.8E-07	6.79E-06 ± 6.3E-07	6.35E-06 ± 5.9E-07	6.41E-06 ± 6.0E-07	6.33E-06 ± 5.9E-07	6.03E-06 ± 5.6E-07

Note: Listed values for mass fraction ± uncertainty were obtained from NIST SRM 1632d Certificate of Analysis (https://www-s.nist.gov/srmors/certificates/archives/1632d.pdf).

Note: Listed values for mass in sample ± uncertainty were calculated from mass fraction data and measured mass of dry powder added.

Note: Yellow highlight indicates elements of interest for QC of TRISO fuel and blue highlight indicates elements of interest for PIE of TRISO fuel.

APPENDIX C. EXAMPLE OF EXCEL DATA REPORT FORM FOR ROUND ROBIN EXPERIMENT

The following table is an example of a completed data report form in the Excel workbook designed to compile data from the round robin experiment. Data is input into the green cells. Blue cell are results of Excel calculations using data in the green cells. This spreadsheet includes impurities typically specified for HTGR fuel. Other impurities present in the NIST SRM 1632d impurity standard may be measured as an option.

Data from Preliminary Measurements		Units	Notes
Average total U in DUN500S-10A particle	7.003E-04 +/- 1.7E-06	grams U/particle	Value provided by ORNL
Fraction U-235 in DUN500S-10A particle	0.00217 +/- 0.00003	grams U-235/grams U	Value provided by ORNL

	Leach-Burn-Leach Analysis of Round Robin Samples with Simulated LBL Defects and Impurities								
	EXAMPLE-A	EXAMPLE-B	EXAMPLE-C	EXAMPLE-D	EXAMPLE-E	EXAMPLE-F	EXAMPLE-G	Units	Notes
Pre-burn Leach Data									
Total U leached (g)	7.003E-04 +/- 6.0E-05	2.040E-03 +/- 6.5E-05	2.840E-06 +/- 1.0E-06	2.940E-06 +/- 1.0E-06	6.230E-04 +/- 7.5E-05	2.800E-03 +/- 8.5E-05	2.940E-06 +/- 1.2E-06	grams	Measured by participating organization
Effective number of exposed DU kernels	1.00 +/- 0.09	2.91 +/- 0.09	0.00 +/- 0.00	0.00 +/- 0.00	0.89 +/- 0.11	4.00 +/- 0.12	0.00 +/- 0.00	kernels	Calculated by spreadsheet
Aluminum (Al) leached (g)	1.89E-06 +/- 1.9E-07	1.51E-07 +/- 2.1E-07	1.51E-07 +/- 1.5E-08	1.51E-07 +/- 1.5E-08	1.51E-07 +/- 1.5E-08	1.51E-07 +/- 1.5E-08	1.51E-07 +/- 1.5E-08	grams	Measured by participating organization
Calcium (Ca) leached (g)	1.41E-06 +/- 1.4E-07	1.69E-06 +/- 2.8E-07	1.69E-06 +/- 1.7E-07	1.69E-06 +/- 1.7E-07	1.69E-06 +/- 1.7E-07	1.69E-06 +/- 1.7E-07	1.69E-06 +/- 1.7E-07	grams	Measured by participating organization
Titanium (Ti) leached (g)	2.00E-07 +/- 2.0E-08	1.20E-07 +/- 3.6E-08	1.20E-07 +/- 1.2E-08	1.20E-07 +/- 1.2E-08	1.20E-07 +/- 1.2E-08	1.20E-07 +/- 1.2E-08	1.20E-07 +/- 1.2E-08	grams	Measured by participating organization
Vanadium (V leached (g)	1.52E-04 +/- 3.1E-06	2.12E-05 +/- 5.8E-08	4.56E-08 +/- 2.3E-09	7.46E-06 +/- 5.2E-09	4.20E-05 +/- 4.2E-08	7.58E-04 +/- 5.6E-07	4.86E-05 +/- 7.8E-07	grams	Measured by participating organization
Chromium (Cr) leached (g)	5.60E-07 +/- 5.6E-08	1.12E-06 +/- 5.0E-08	1.12E-06 +/- 1.1E-07	1.12E-06 +/- 1.1E-07	1.12E-06 +/- 1.1E-07	1.12E-06 +/- 1.1E-07	1.12E-06 +/- 1.1E-07	grams	Measured by participating organization
Manganese (Mn) leached (g)	1.00E-06 +/- 1.0E-07	1.30E-06 +/- 7.0E-08	1.30E-06 +/- 1.3E-07	1.30E-06 +/- 1.3E-07	1.30E-06 +/- 1.3E-07	1.30E-06 +/- 1.3E-07	1.30E-06 +/- 1.3E-07	grams	Measured by participating organization
Iron (Fe) leached (g)	1.40E-05 +/- 1.4E-06	1.96E-05 +/- 2.0E-06	1.96E-05 +/- 2.0E-06	1.96E-05 +/- 2.0E-06	1.96E-05 +/- 2.0E-06	1.96E-05 +/- 2.0E-06	1.96E-05 +/- 2.0E-06	grams	Measured by participating organization
Cobalt (Co) leached (g)	4.96E-06 +/- 5.0E-07	3.97E-06 +/- 5.0E-07	3.97E-06 +/- 4.0E-07	3.97E-06 +/- 4.0E-07	3.97E-06 +/- 4.0E-07	3.97E-06 +/- 4.0E-07	3.97E-06 +/- 4.0E-07	grams	Measured by participating organization
Nickel (Ni) leached (g)	2.25E-05 +/- 2.3E-06	2.70E-05 +/- 2.5E-06	2.70E-05 +/- 2.7E-06	2.70E-05 +/- 2.7E-06	2.70E-05 +/- 2.7E-06	2.70E-05 +/- 2.7E-06	2.70E-05 +/- 2.7E-06	grams	Measured by participating organization
Post-burn Leach Data									
Total U leached (g)	2.840E-06 +/- 3.0E-07	2.940E-06 +/- 1.0E-07	1.400E-03 +/- 4.9E-05	3.940E-06 +/- 2.1E-07	2.900E-03 +/- 3.5E-04	9.840E-06 +/- 3.0E-07	2.650E-03 +/- 6.5E-05	grams	Measured by participating organization
Effective number of exposed DU kernels	0.00 +/- 0.00	0.00 +/- 0.00	2.00 +/- 0.07	0.01 +/- 0.00	4.14 +/- 0.50	0.01 +/- 0.00	3.78 +/- 0.09	kernels	Calculated by spreadsheet
Aluminum (Al) leached (g)	1.89E-06 +/- 1.9E-07	1.51E-07 +/- 2.1E-07	1.51E-07 +/- 1.5E-08	1.51E-07 +/- 1.5E-08	1.51E-07 +/- 1.5E-08	1.51E-07 +/- 1.5E-08	1.51E-07 +/- 1.5E-08	grams	Measured by participating organization
Calcium (Ca) leached (g)	1.41E-06 +/- 1.4E-07	1.69E-06 +/- 2.8E-07	1.69E-06 +/- 1.7E-07	1.69E-06 +/- 1.7E-07	1.69E-06 +/- 1.7E-07	1.69E-06 +/- 1.7E-07	1.69E-06 +/- 1.7E-07	grams	Measured by participating organization
Titanium (Ti) leached (g)	2.00E-07 +/- 2.0E-08	1.20E-07 +/- 3.6E-08	1.20E-07 +/- 1.2E-08	1.20E-07 +/- 1.2E-08	1.20E-07 +/- 1.2E-08	1.20E-07 +/- 1.2E-08	1.20E-07 +/- 1.2E-08	grams	Measured by participating organization
Vanadium (V leached (g)	1.65E-05 +/- 1.2E-07	8.56E-07 +/- 2.6E-09	5.80E-07 +/- 6.5E-09	5.98E-08 +/- 2.5E-10	2.58E-07 +/- 1.3E-09	2.65E-06 +/- 4.5E-08	2.50E-08 +/- 2.1E-10	grams	Measured by participating organization
Chromium (Cr) leached (g)	5.60E-07 +/- 5.6E-08	1.12E-06 +/- 5.0E-08	1.12E-06 +/- 1.1E-07	1.12E-06 +/- 1.1E-07	1.12E-06 +/- 1.1E-07	1.12E-06 +/- 1.1E-07	1.12E-06 +/- 1.1E-07	grams	Measured by participating organization
Manganese (Mn) leached (g)	1.00E-06 +/- 1.0E-07	1.30E-06 +/- 7.0E-08	1.30E-06 +/- 1.3E-07	1.30E-06 +/- 1.3E-07	1.30E-06 +/- 1.3E-07	1.30E-06 +/- 1.3E-07	1.30E-06 +/- 1.3E-07	grams	Measured by participating organization
Iron (Fe) leached (g)	1.40E-05 +/- 1.4E-06	1.96E-05 +/- 2.0E-06	1.96E-05 +/- 2.0E-06	1.96E-05 +/- 2.0E-06	1.96E-05 +/- 2.0E-06	1.96E-05 +/- 2.0E-06	1.96E-05 +/- 2.0E-06	grams	Measured by participating organization
Cobalt (Co) leached (g)	4.96E-06 +/- 5.0E-07	3.97E-06 +/- 5.0E-07	3.97E-06 +/- 4.0E-07	3.97E-06 +/- 4.0E-07	3.97E-06 +/- 4.0E-07	3.97E-06 +/- 4.0E-07	3.97E-06 +/- 4.0E-07	grams	Measured by participating organization
Nickel (Ni) leached (g)	2.25E-05 +/- 2.3E-06	2.70E-05 +/- 2.5E-06	2.70E-05 +/- 2.7E-06	2.70E-05 +/- 2.7E-06	2.70E-05 +/- 2.7E-06	2.70E-05 +/- 2.7E-06	2.70E-05 +/- 2.7E-06	grams	Measured by participating organization
Combined Impurity Data									
Total U leached (g)	7.03E-04 +/- 6.00E-05	2.04E-03 +/- 6.52E-05	1.40E-03 +/- 4.87E-05	6.88E-06 +/- 1.02E-06	3.52E-03 +/- 3.60E-04	2.81E-03 +/- 8.52E-05	2.65E-03 +/- 6.52E-05	grams	Calculated by spreadsheet
Aluminum (Al) leached (g)	3.78E-06 +/- 2.67E-07	3.02E-07 +/- 2.94E-07	3.02E-07 +/- 2.14E-08	3.02E-07 +/- 2.14E-08	3.02E-07 +/- 2.14E-08	3.02E-07 +/- 2.14E-08	3.02E-07 +/- 2.14E-08	grams	Calculated by spreadsheet
Calcium (Ca) leached (g)	2.82E-06 +/- 1.99E-07	3.38E-06 +/- 3.99E-07	3.38E-06 +/- 2.39E-07	3.38E-06 +/- 2.39E-07	3.38E-06 +/- 2.39E-07	3.38E-06 +/- 2.39E-07	3.38E-06 +/- 2.39E-07	grams	Calculated by spreadsheet
Titanium (Ti) leached (g)	4.00E-07 +/- 2.83E-08	2.40E-07 +/- 5.09E-08	2.40E-07 +/- 1.70E-08	2.40E-07 +/- 1.70E-08	2.40E-07 +/- 1.70E-08	2.40E-07 +/- 1.70E-08	2.40E-07 +/- 1.70E-08	grams	Calculated by spreadsheet
Vanadium (V leached (g)	1.69E-04 +/- 3.10E-06	2.21E-05 +/- 5.81E-08	6.26E-07 +/- 6.89E-09	7.52E-06 +/- 5.21E-09	4.23E-05 +/- 4.20E-08	7.61E-04 +/- 5.62E-07	4.86E-05 +/- 7.80E-07	grams	Calculated by spreadsheet
Chromium (Cr) leached (g)	1.12E-06 +/- 7.92E-08	2.24E-06 +/- 7.13E-08	2.24E-06 +/- 1.58E-07	2.24E-06 +/- 1.58E-07	2.24E-06 +/- 1.58E-07	2.24E-06 +/- 1.58E-07	2.24E-06 +/- 1.58E-07	grams	Calculated by spreadsheet
Manganese (Mn) leached (g)	2.00E-06 +/- 1.41E-07	2.60E-06 +/- 9.90E-08	2.60E-06 +/- 1.84E-07	2.60E-06 +/- 1.84E-07	2.60E-06 +/- 1.84E-07	2.60E-06 +/- 1.84E-07	2.60E-06 +/- 1.84E-07	grams	Calculated by spreadsheet
Iron (Fe) leached (g)	2.80E-05 +/- 1.98E-06	3.92E-05 +/- 2.77E-06	3.92E-05 +/- 2.77E-06	3.92E-05 +/- 2.77E-06	3.92E-05 +/- 2.77E-06	3.92E-05 +/- 2.77E-06	3.92E-05 +/- 2.77E-06	grams	Calculated by spreadsheet
Cobalt (Co) leached (g)	9.92E-06 +/- 7.01E-07	7.94E-06 +/- 7.01E-07	7.94E-06 +/- 5.61E-07	7.94E-06 +/- 5.61E-07	7.94E-06 +/- 5.61E-07	7.94E-06 +/- 5.61E-07	7.94E-06 +/- 5.61E-07	grams	Calculated by spreadsheet
Nickel (Ni) leached (g)	4.50E-05 +/- 3.18E-06	5.40E-05 +/- 3.50E-06	5.40E-05 +/- 3.82E-06	5.40E-05 +/- 3.82E-06	5.40E-05 +/- 3.82E-06	5.40E-05 +/- 3.82E-06	5.40E-05 +/- 3.82E-06	grams	Calculated by spreadsheet

APPENDIX D. OPTICAL IMAGES OF SIMULATED PREBURN LEACH DEFECTS IN DUN500S-10A PARTICLES BEFORE REMOVAL FROM THE CRYSTALBOND EPOXY

Each particle is shown as it appeared after impact with the ram (see Figure 1). Cracks in the Crystalbond epoxy provided visible feedback regarding the extent of the fracturing in the TRISO coating caused by the impact of the ram on the exposed top of the particle and were used for initial selection of particles (Table 3) prior to x-ray confirmation of the required crack microstructure (Appendix E).

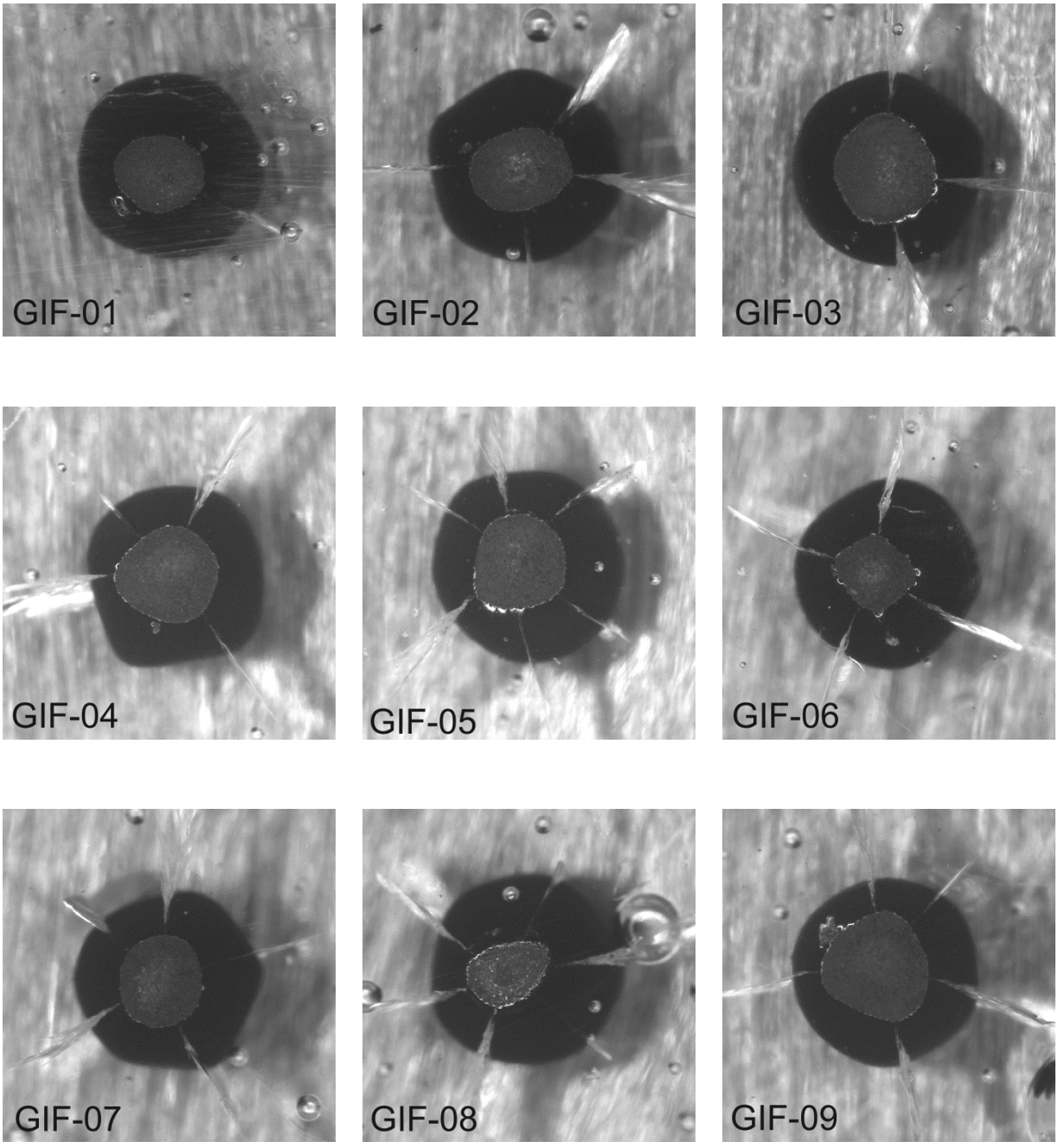

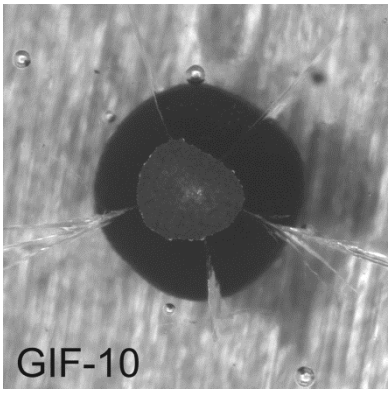
GIF-10

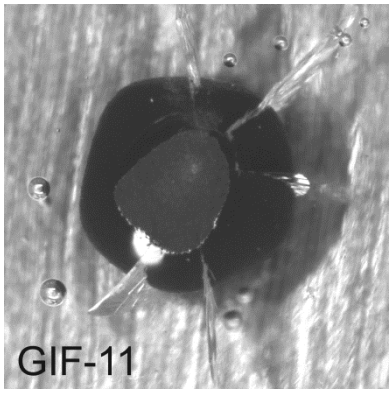
GIF-11

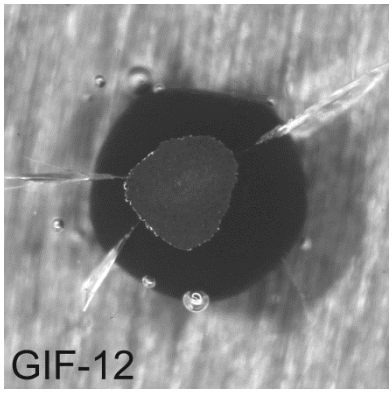
GIF-12

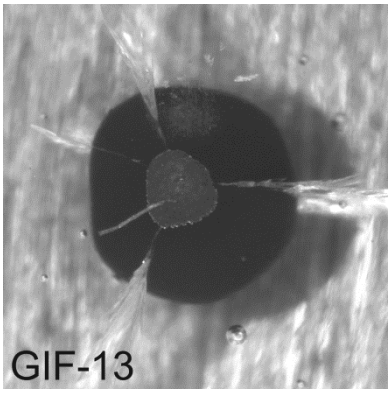
GIF-13

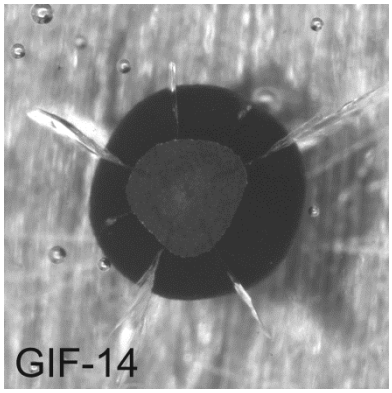
GIF-14

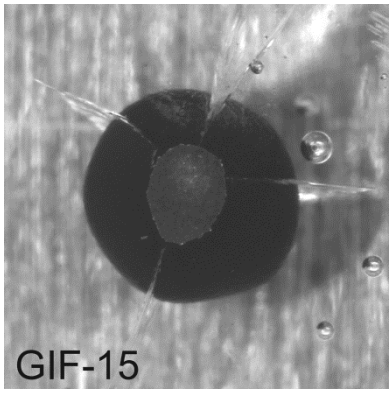
GIF-15

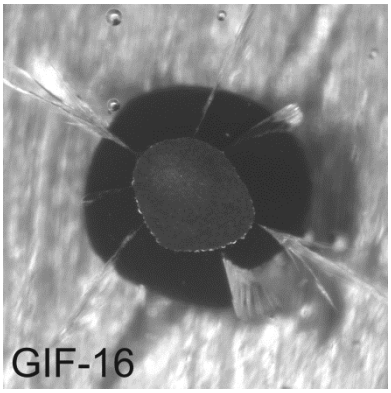
GIF-16

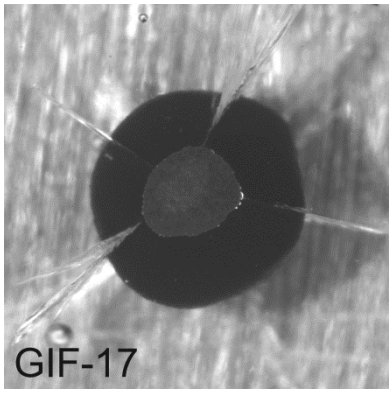
GIF-17

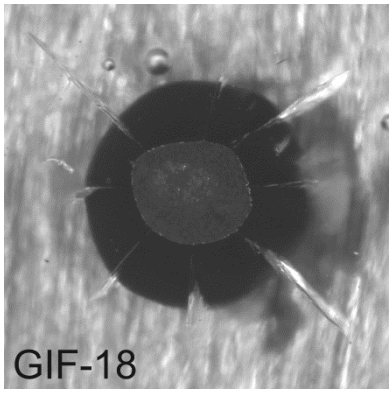
GIF-18

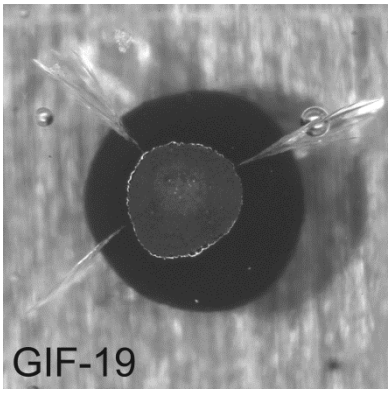
GIF-19

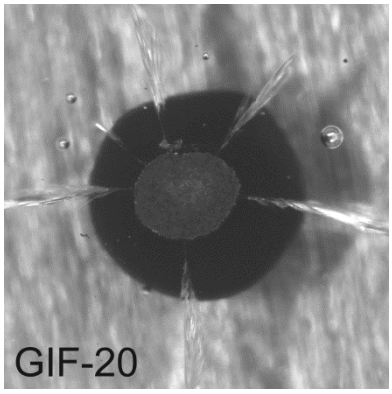
GIF-20

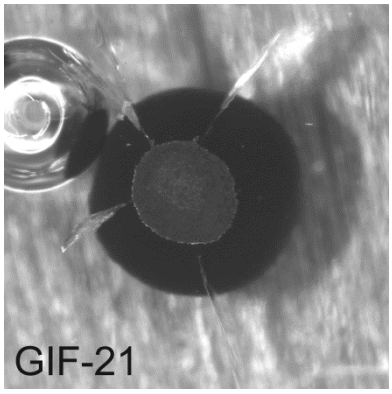
GIF-21

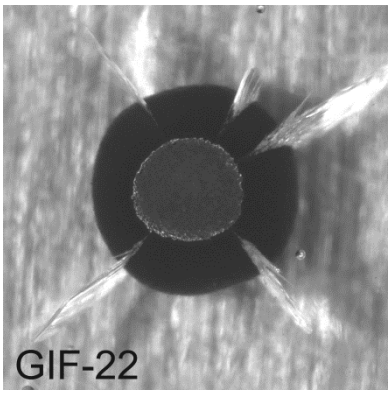
GIF-22

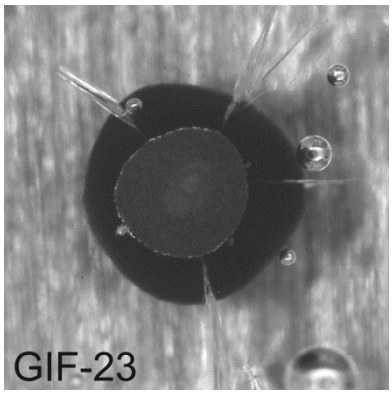
GIF-23

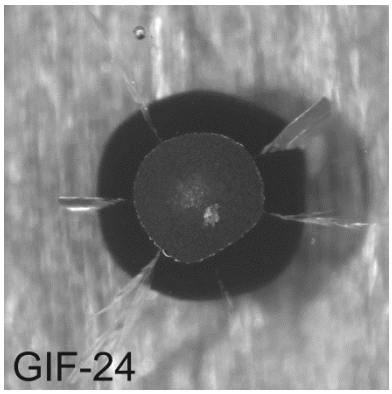
GIF-24

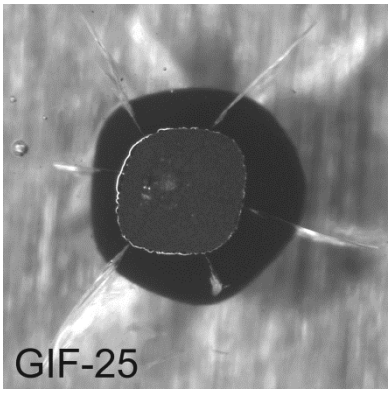
GIF-25

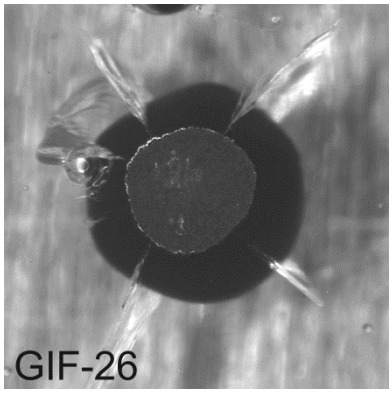
GIF-26

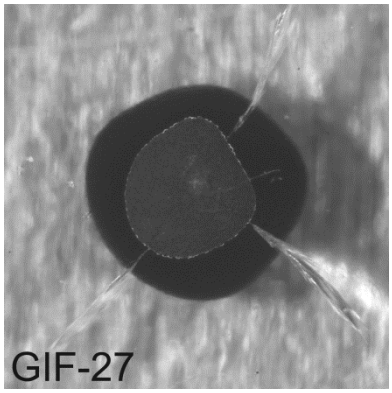
GIF-27

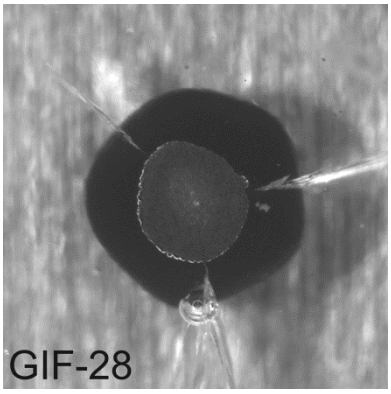
GIF-28

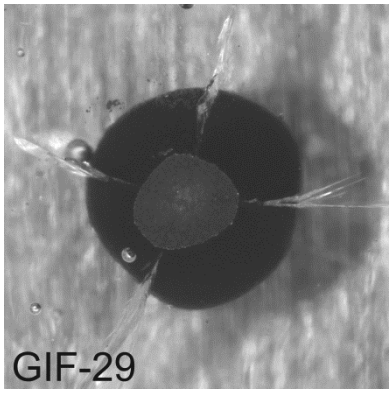
GIF-29

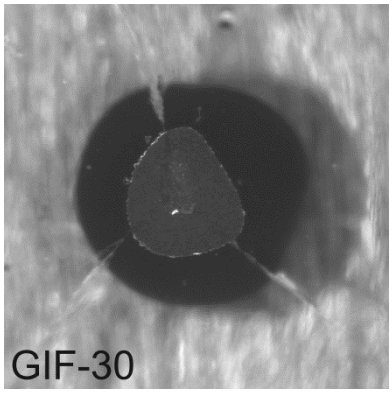
GIF-30

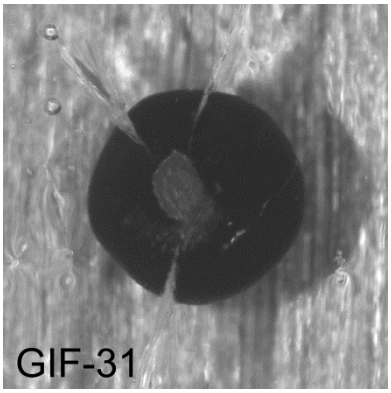
GIF-31

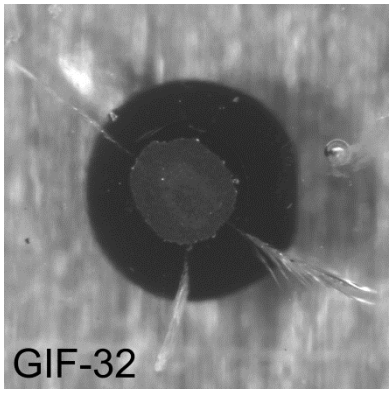
GIF-32

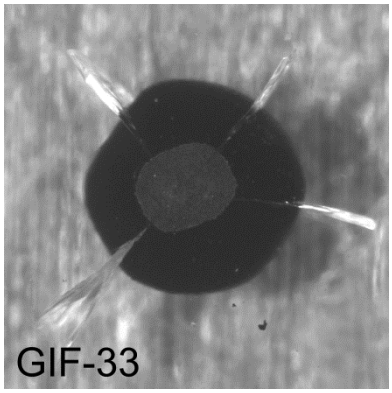
GIF-33

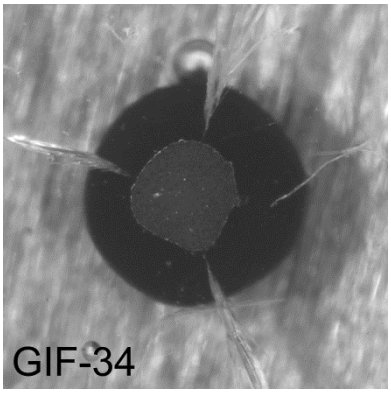
GIF-34

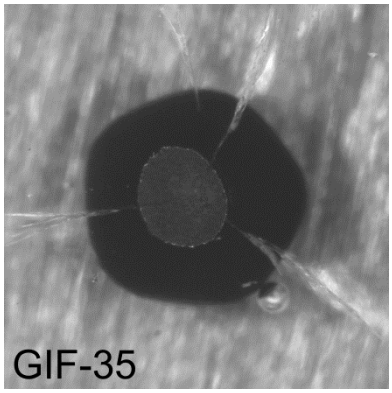
GIF-35

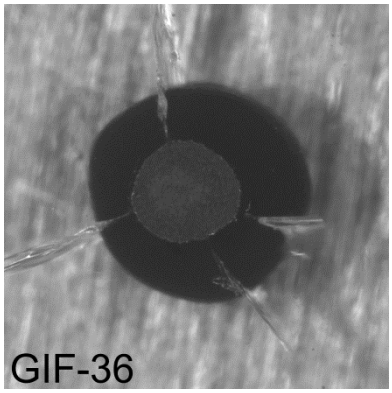
GIF-36

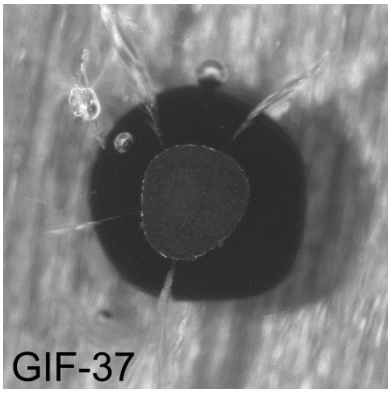
GIF-37

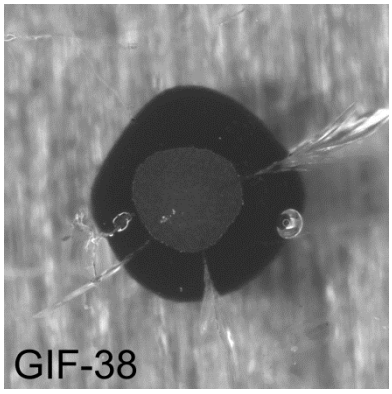
GIF-38

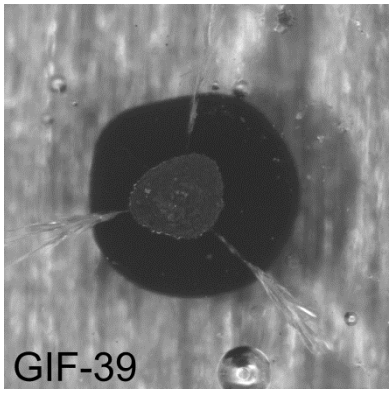
GIF-39

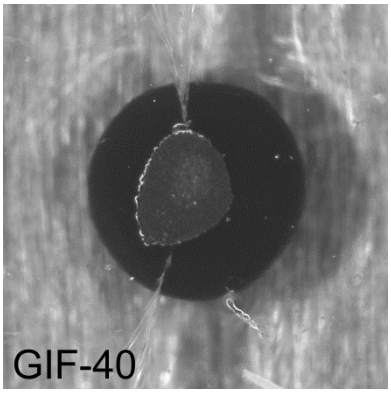
GIF-40

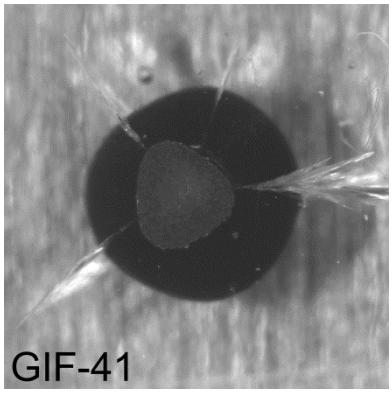
GIF-41

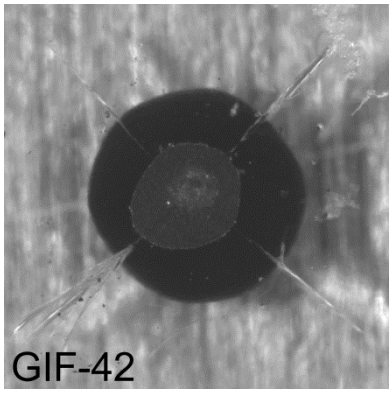
GIF-42

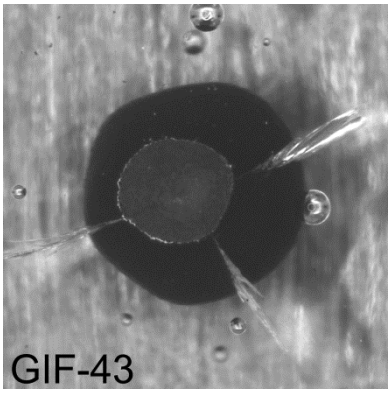
GIF-43


GIF-44

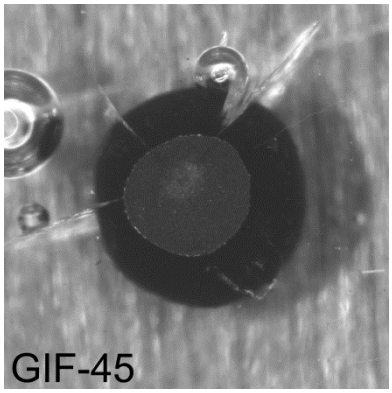
GIF-45

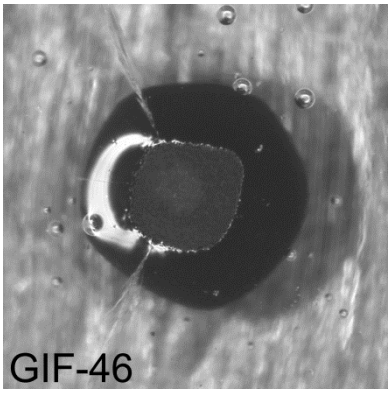
GIF-46

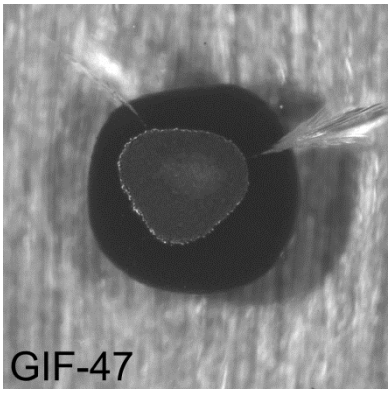
GIF-47

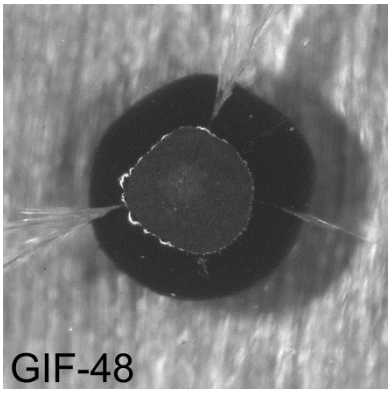
GIF-48

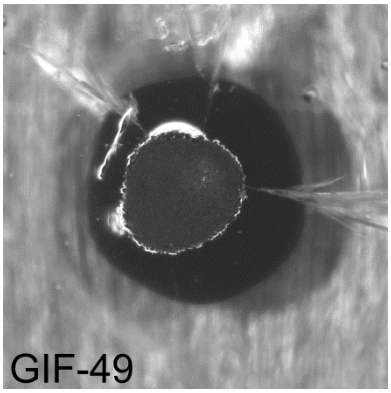
GIF-49

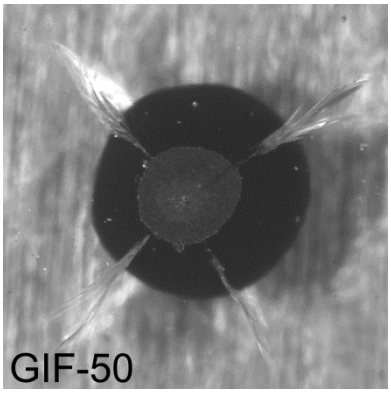
GIF-50

APPENDIX E. X-RAY TOMOGRAPHS OF SIMULATED PREBURN LEACH DEFECTS IN DUN500S-10A PARTICLES AFTER REMOVAL FROM THE CRYSTALBOND EPOXY

X-ray tomography was performed on all particles selected for use in the round robin experiment after removal of each particle from the Crystalbond (as shown in Appendix A) by dissolving the epoxy in acetone. The locations of the TRISO layer fractures visible in each tomograph are indicated by arrows.

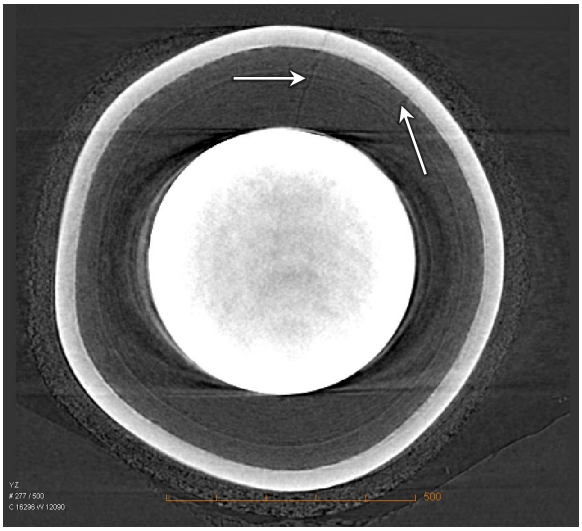

GIF-02

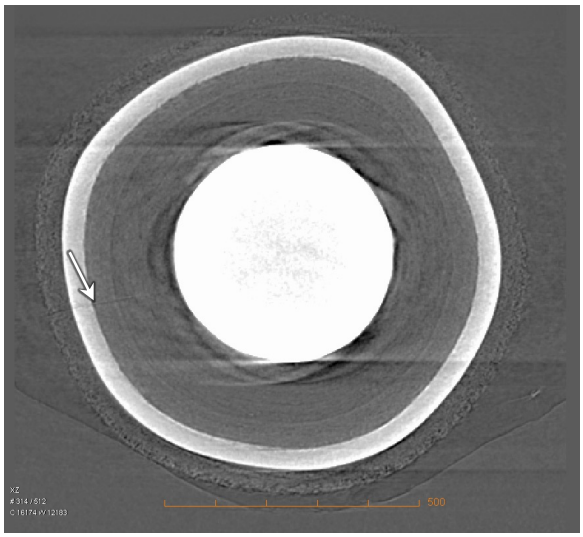

GIF-03

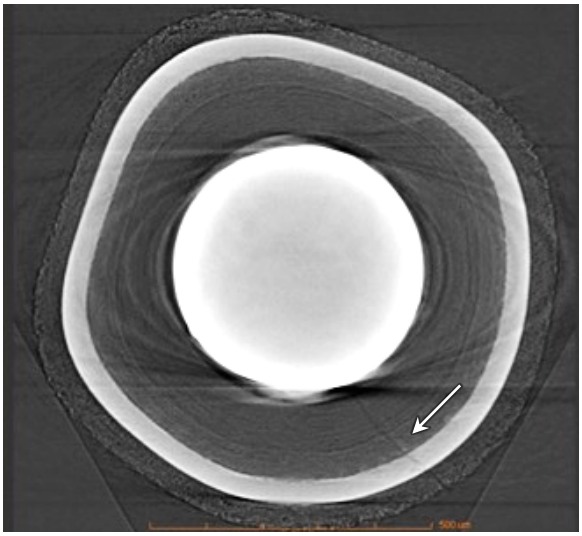

GIF-04

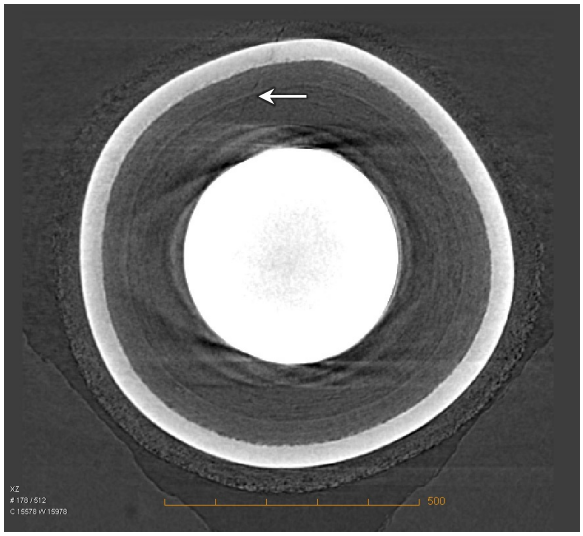

GIF-06

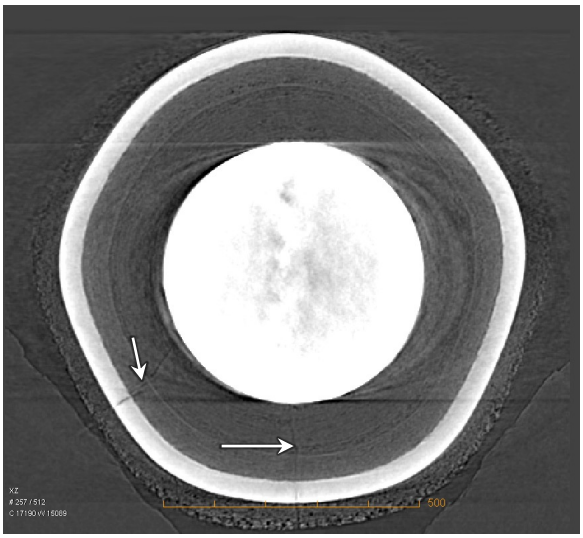

GIF-07

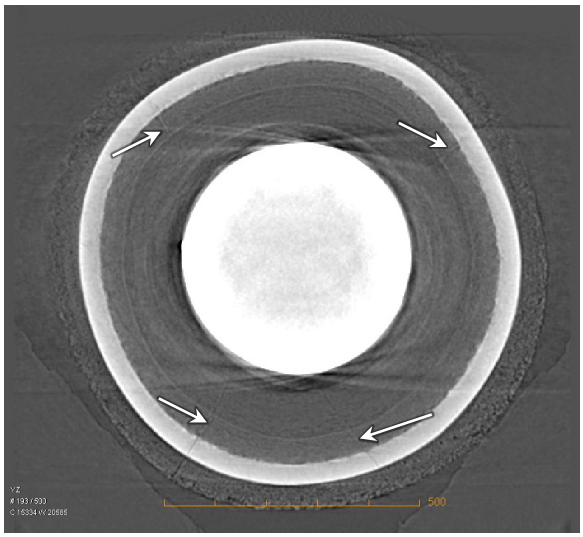

GIF-09

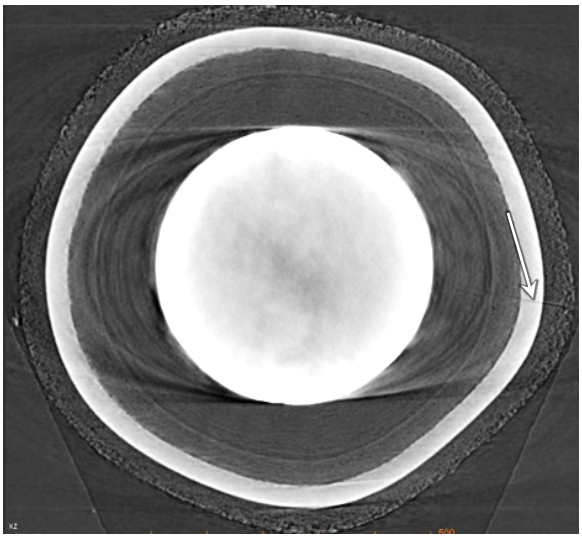

GIF-12

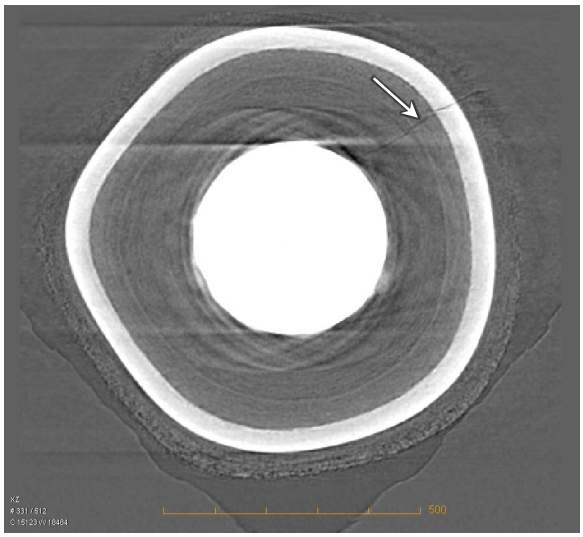

GIF-14

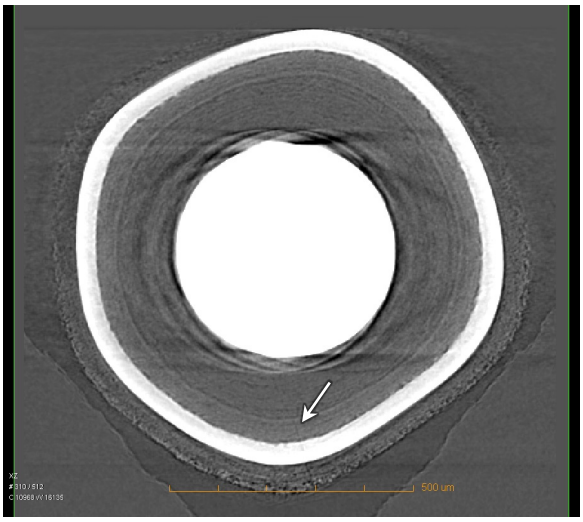

GIF-15

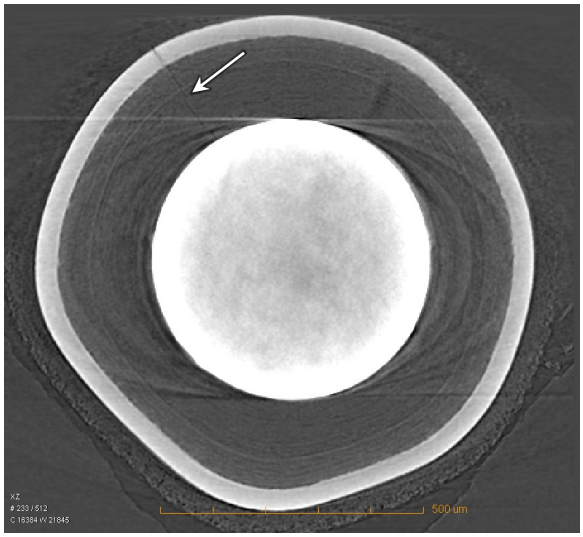

GIF-17

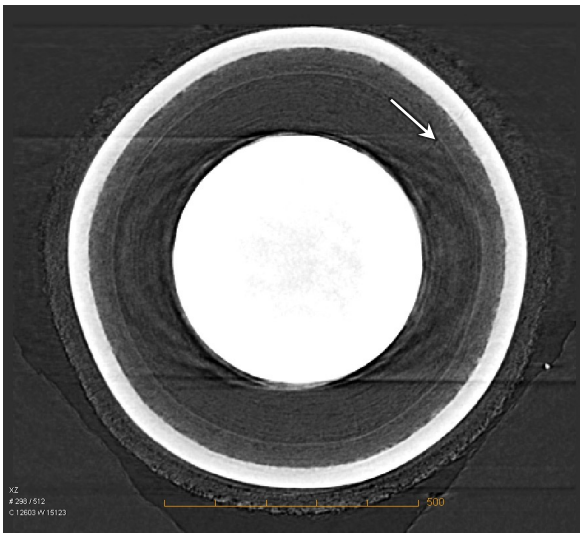

GIF-19

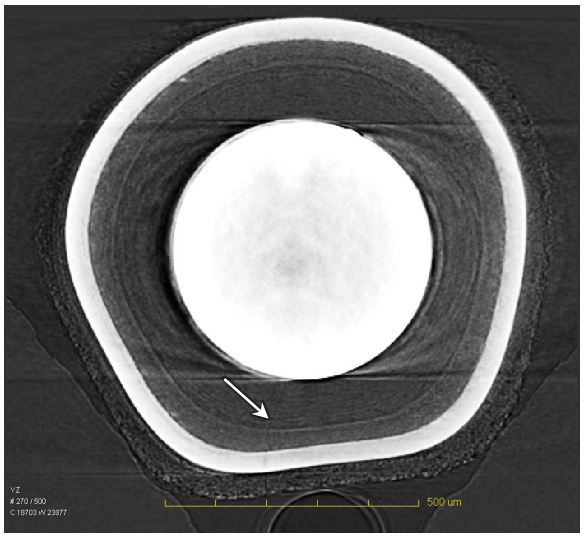

GIF-27

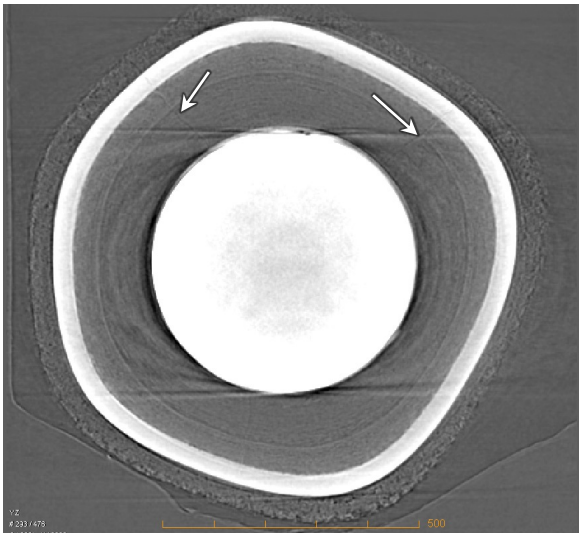

GIF-28

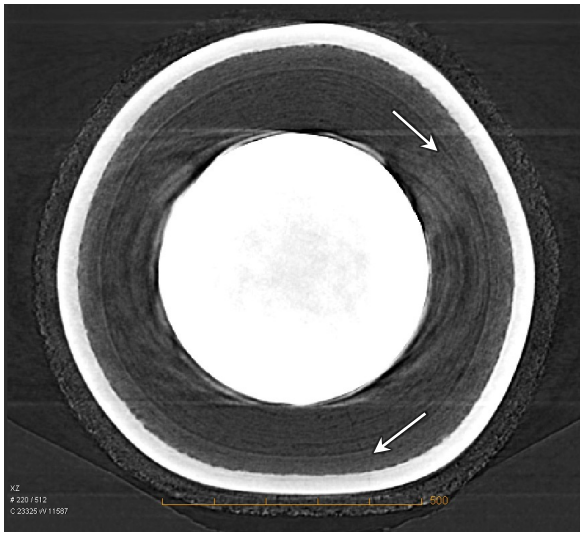

GIF-29

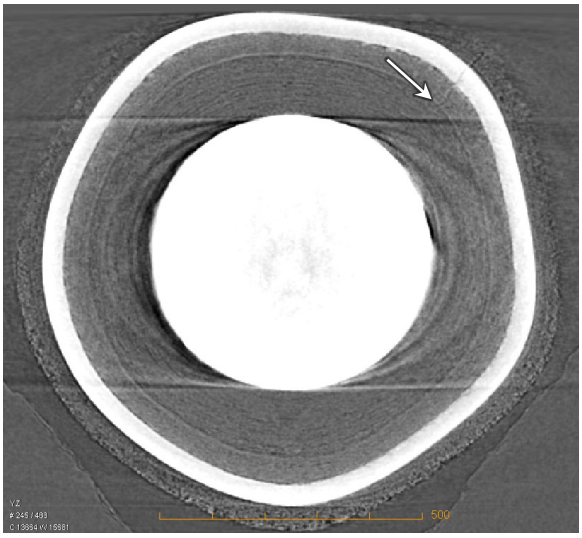

GIF-30

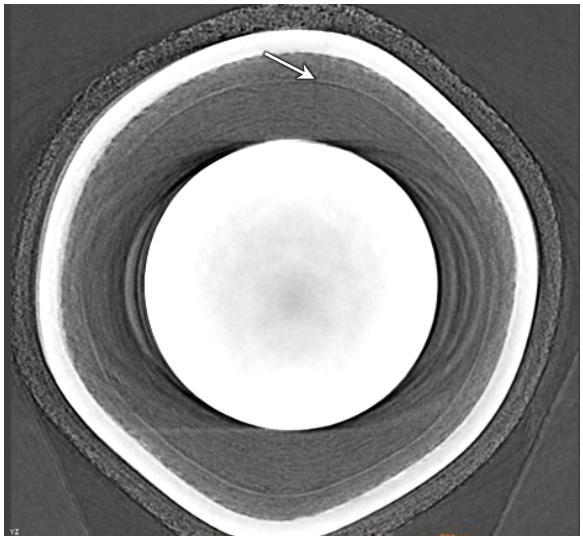

GIF-33

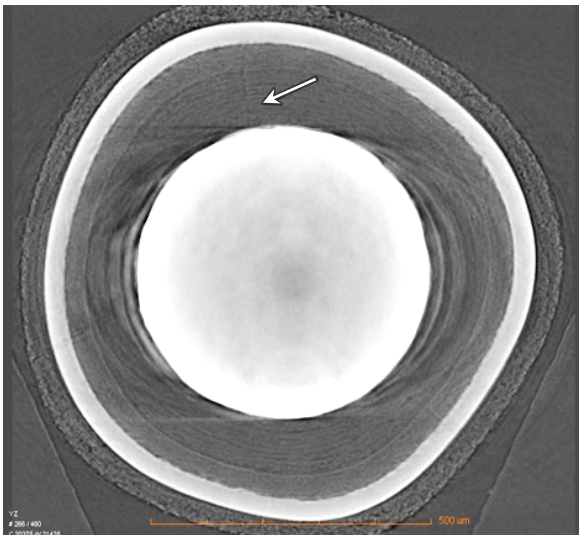

GIF-34

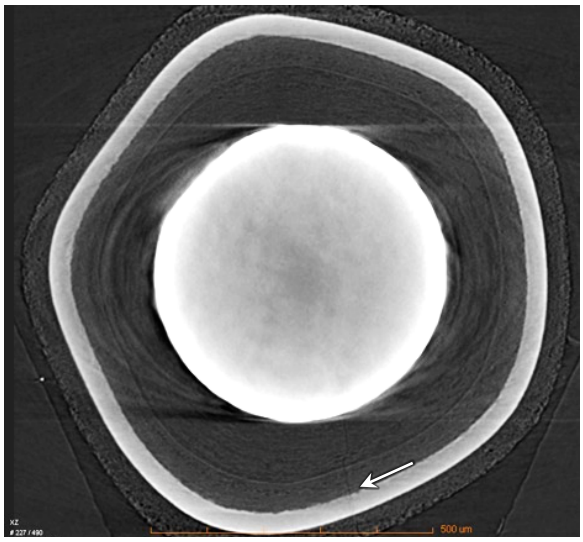

GIF-35

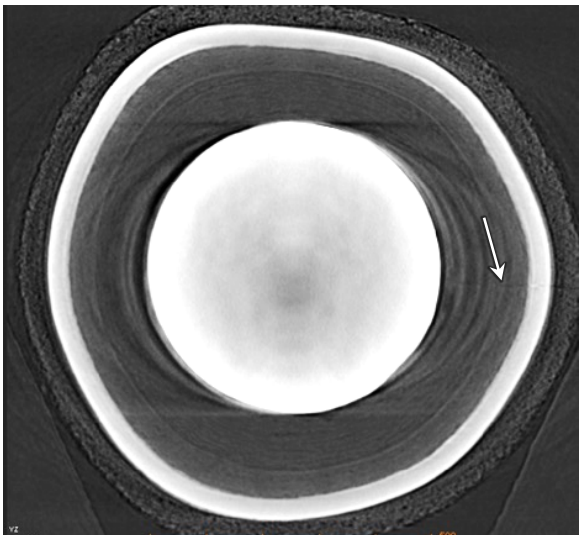

GIF-36

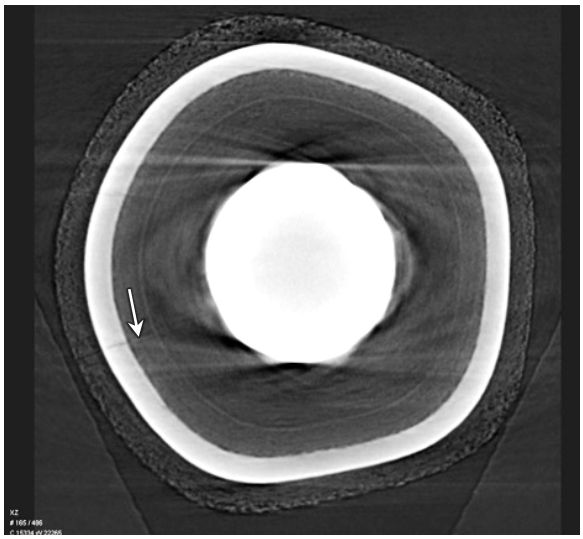

GIF-37

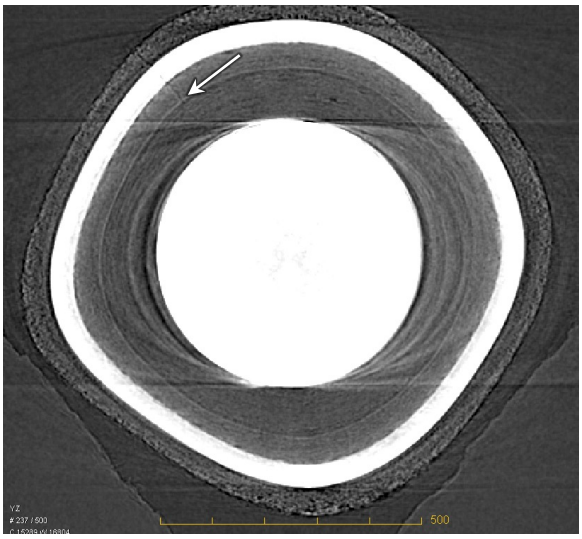

GIF-38

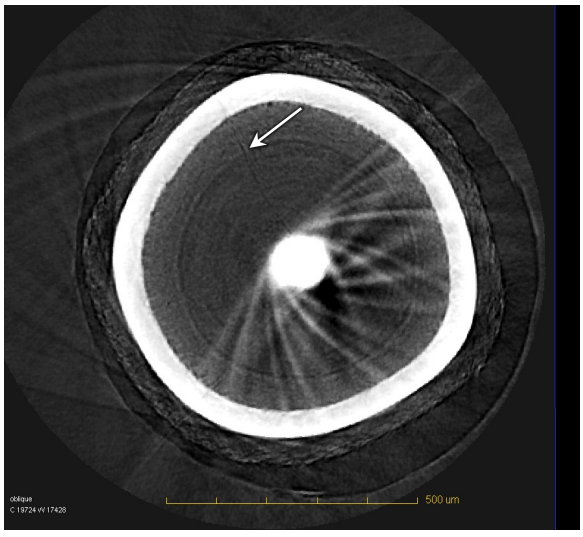

GIF-39 (oblique tomograph)

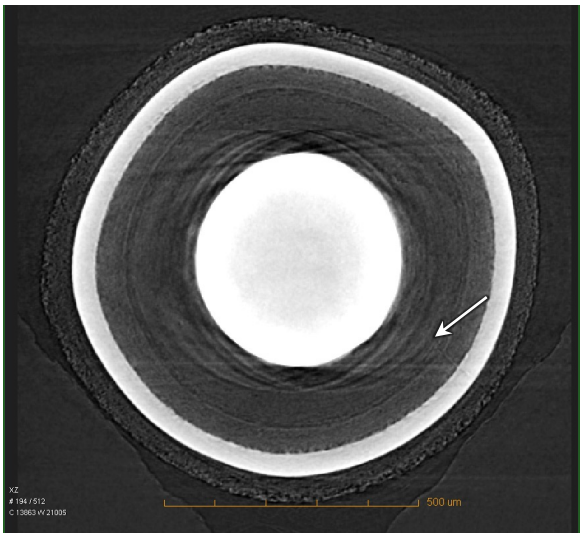

GIF-41

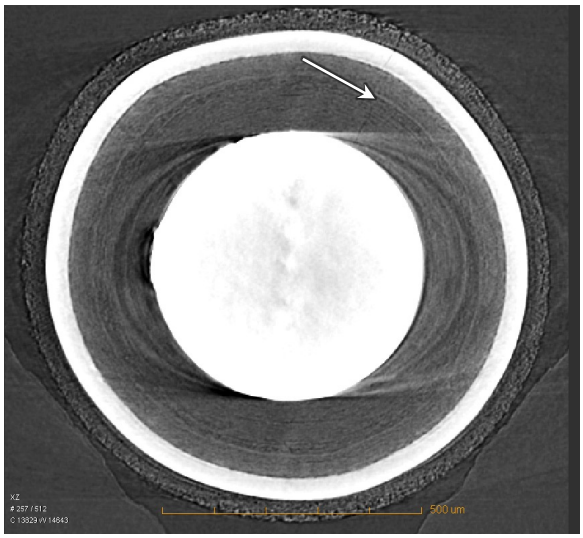

GIF-42

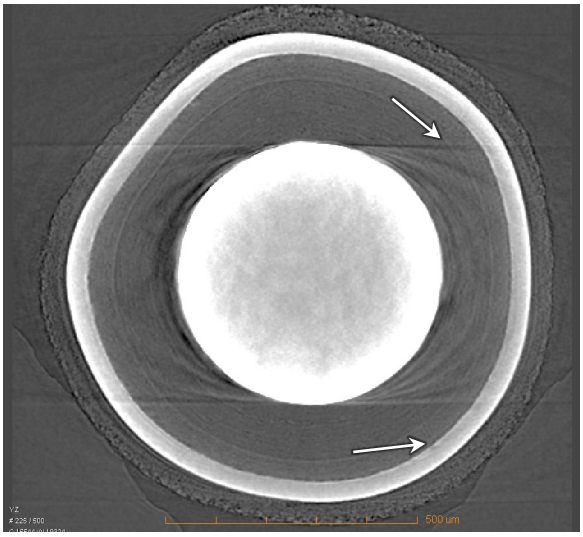

GIF-43

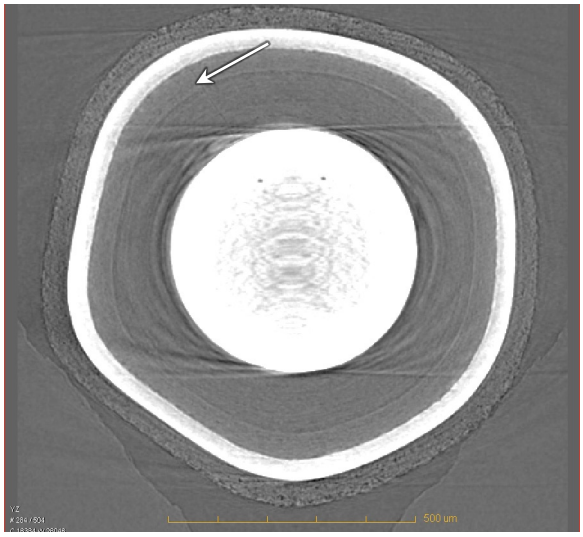

GIF-44

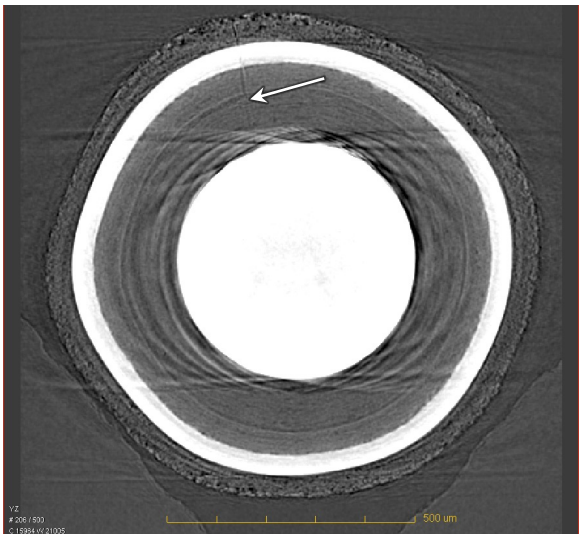

GIF-49

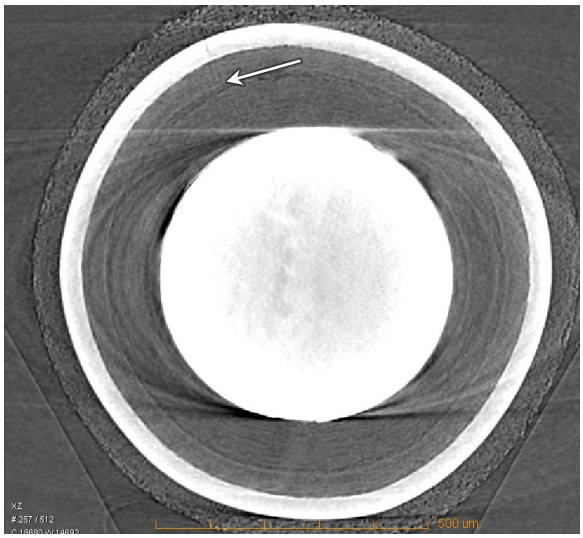

GIF-50

APPENDIX F. SEM IMAGES AND X-RAY RADIOGRAPHS OF SIMULATED POSTBURN LEACH DEFECTS IN DUN500S-10A PARTICLES

Secondary electron images (left) show the side and bottom of the hole through the SiC layer after completion of the milling process in the FIB to expose the IPyC layer. X-ray radiographs (right) show a vertical cross section through the crater at an optimized angle. A spot of platinum deposited at the bottom of each crater can be seen as a lighter contrast circle in the SEM images and as a dark spot in the radiographs. The mottled appearance of the IPyC material at the bottom of each crater (evident in the SEM images) and the vertical location of the platinum spot (evident in the radiographs) provide evidence of the successful exposure of the IPyC layer in each particle without penetrating more than 10 µm into the layer.

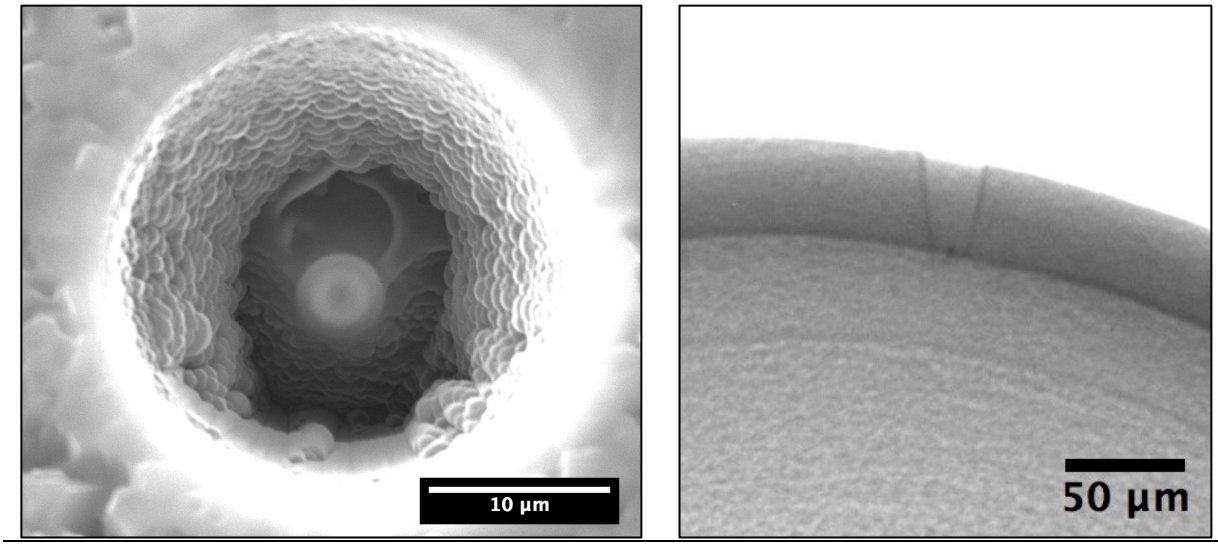

FIB-01

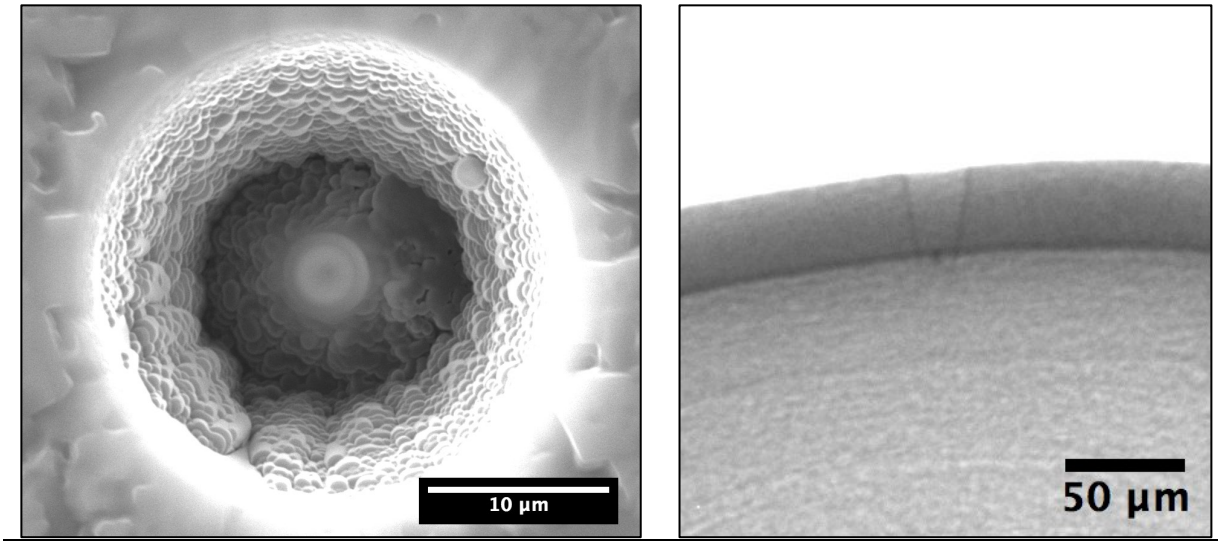

FIB-02

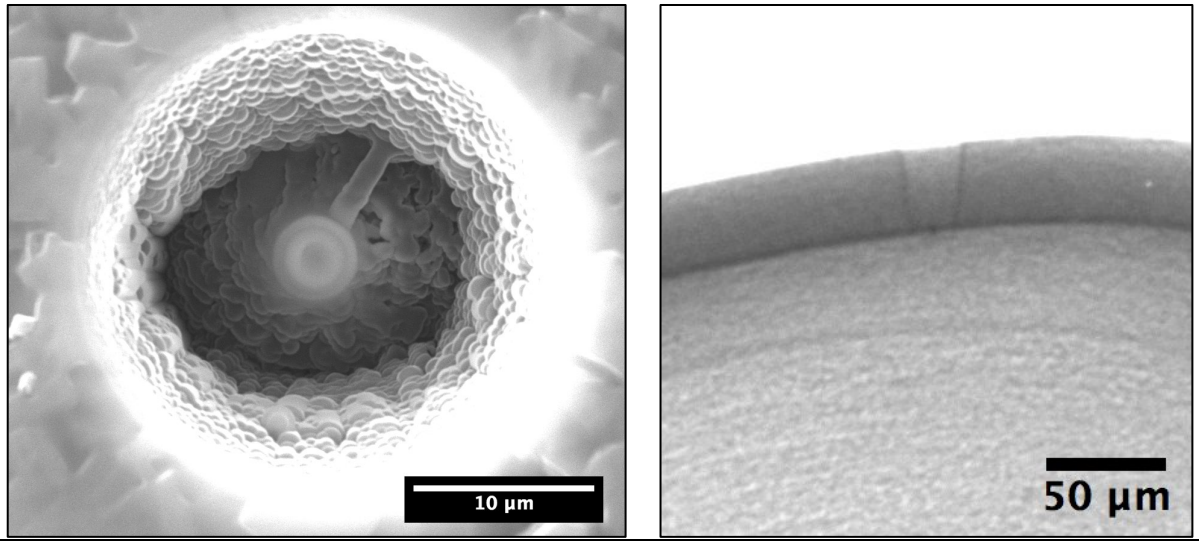

FIB-03

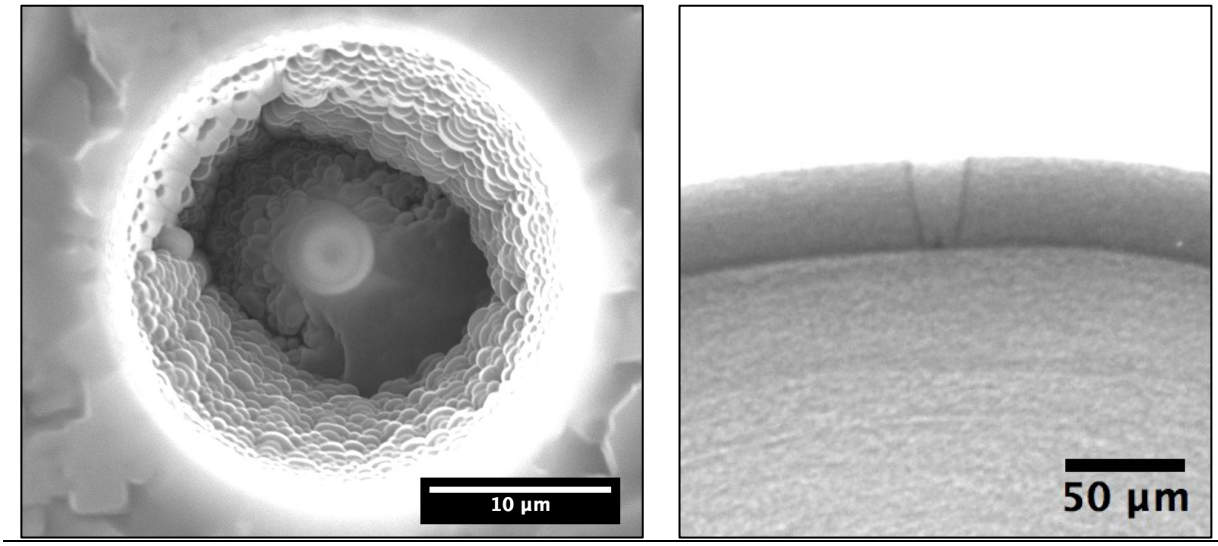

FIB-04

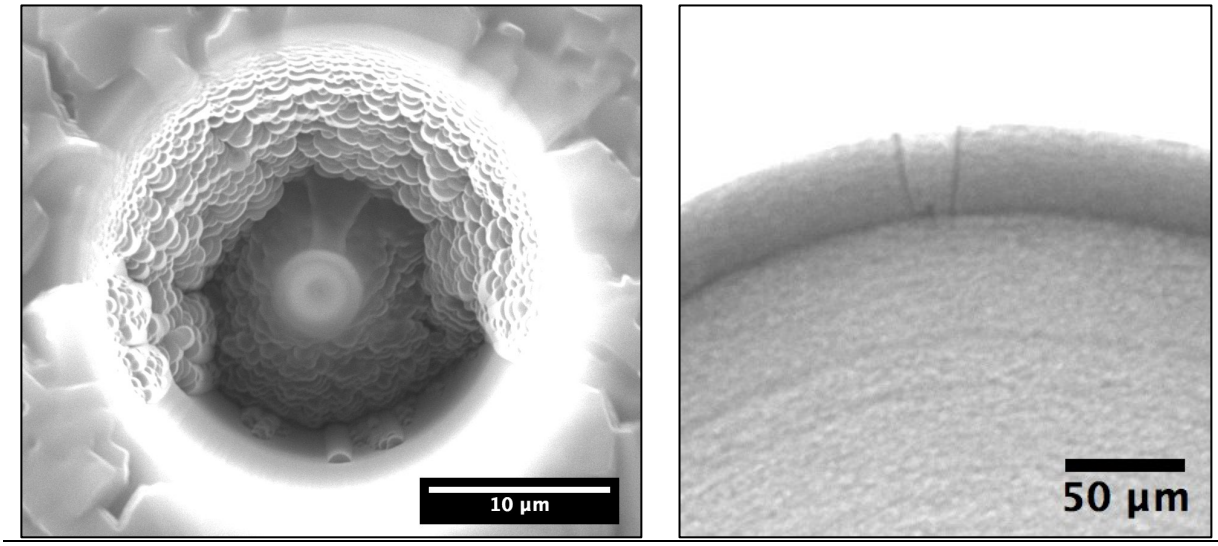

FIB-05

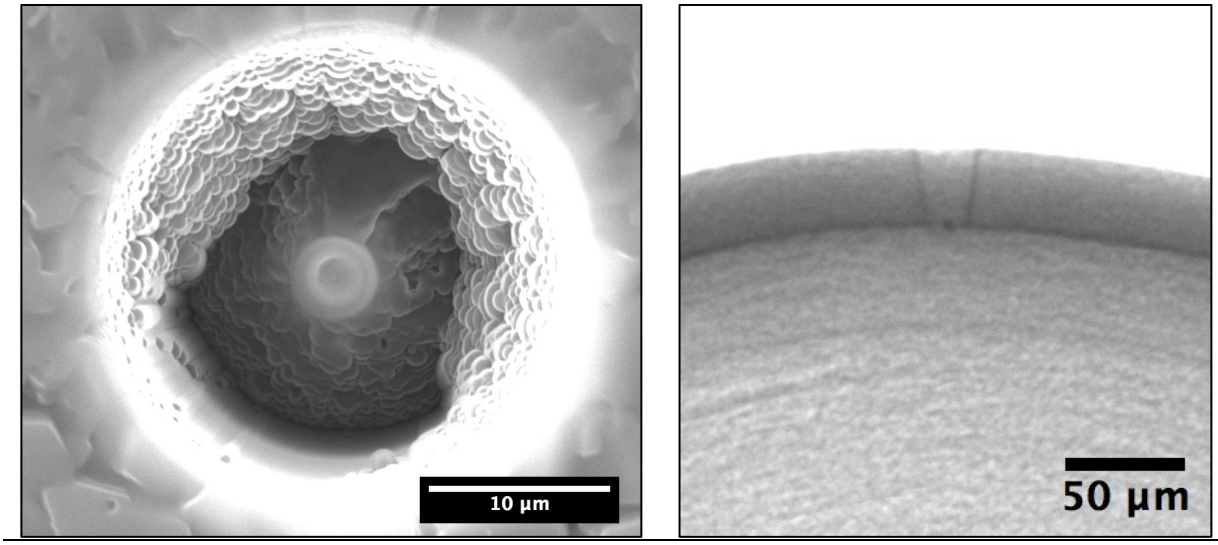

FIB-06

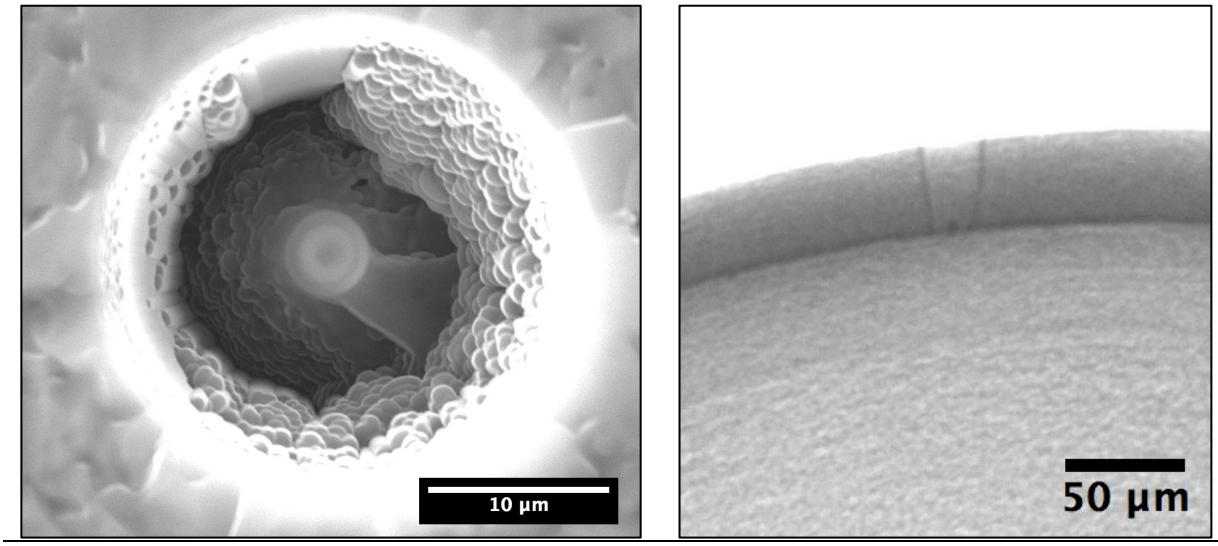

FIB-07

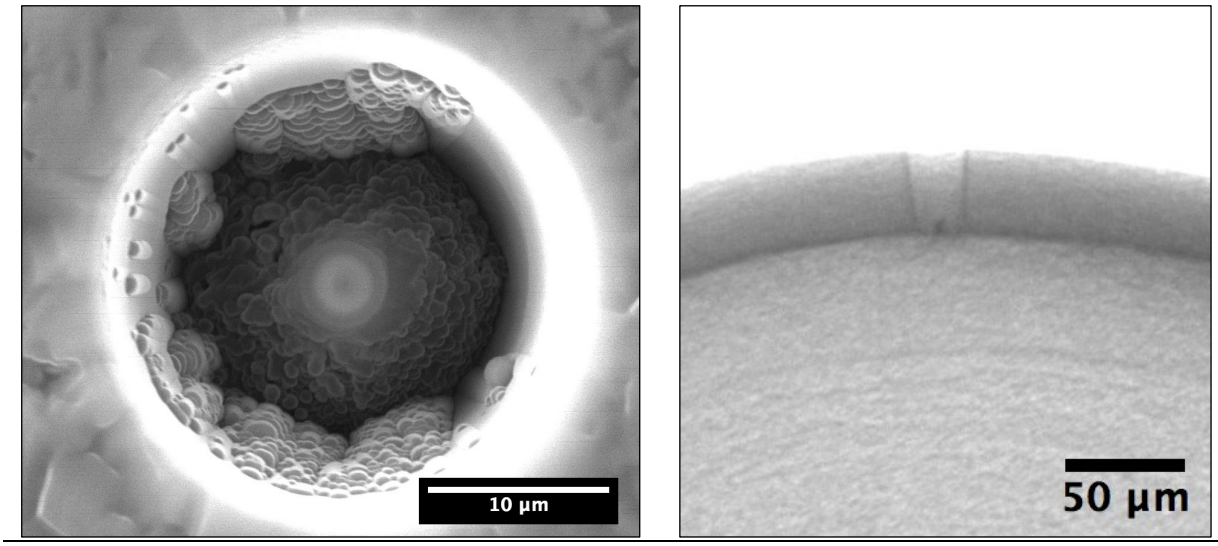

FIB-08

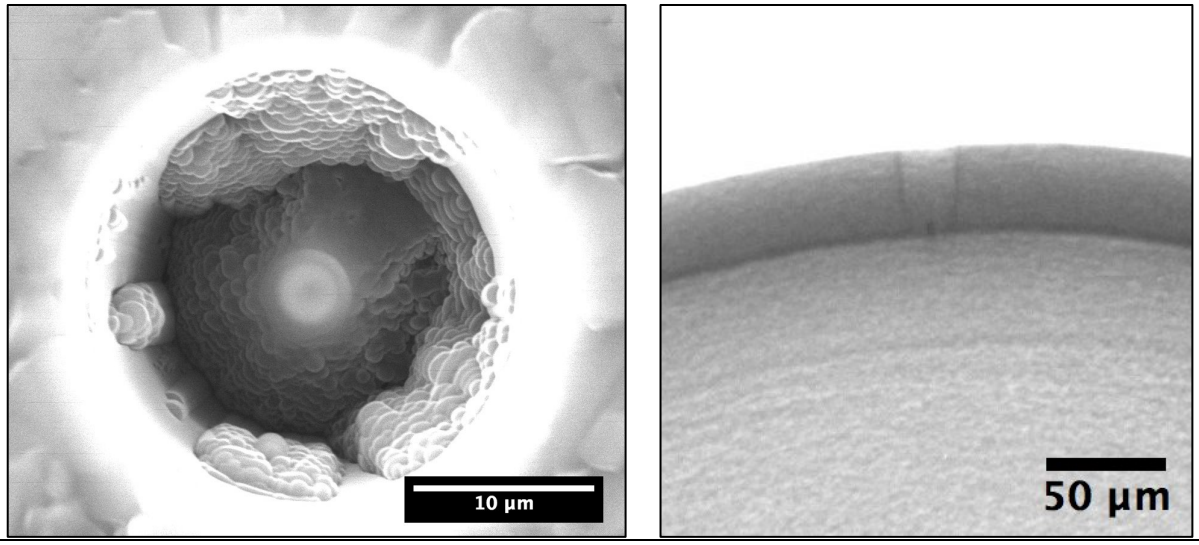

FIB-09

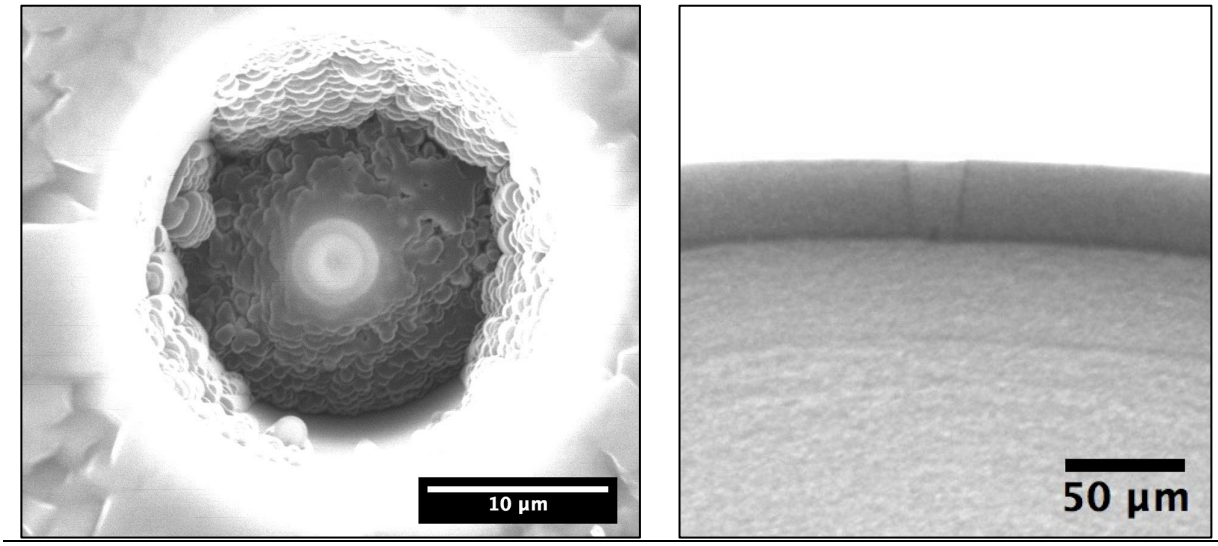

FIB-10

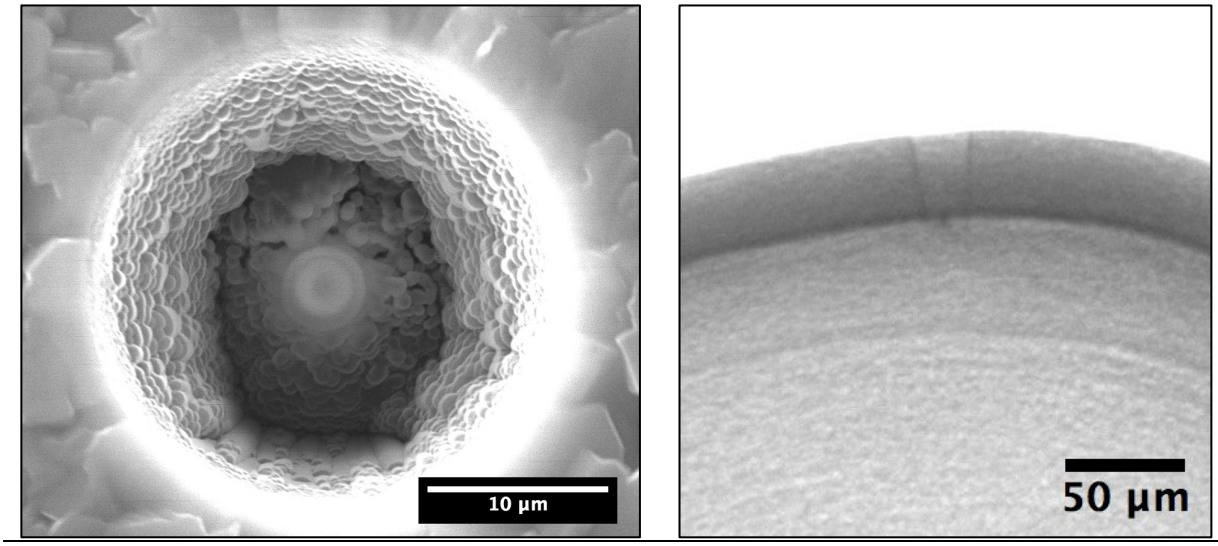

FIB-11

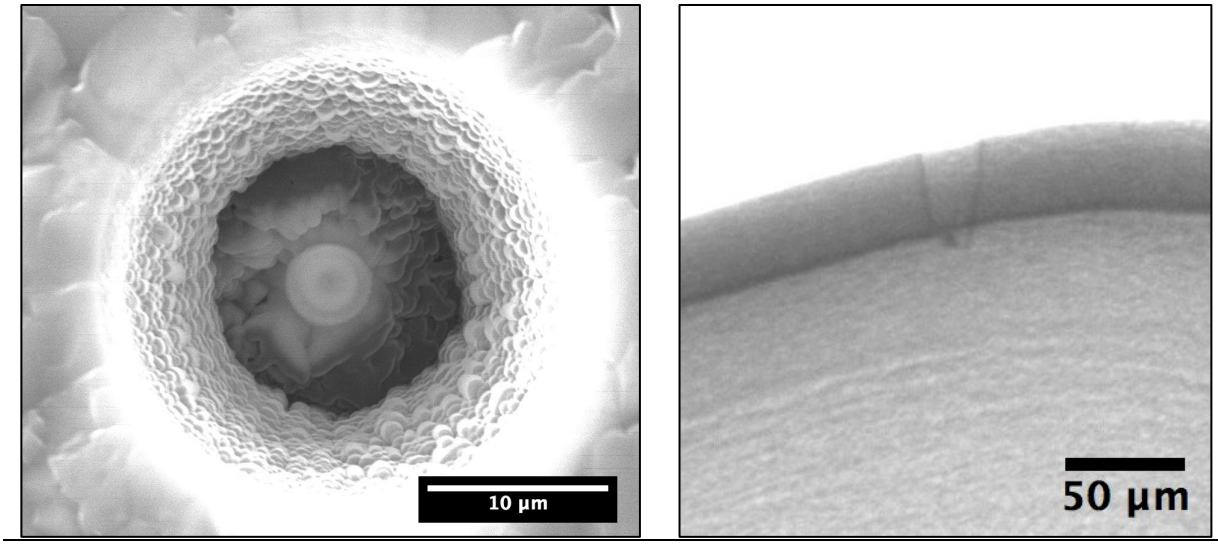

FIB-12

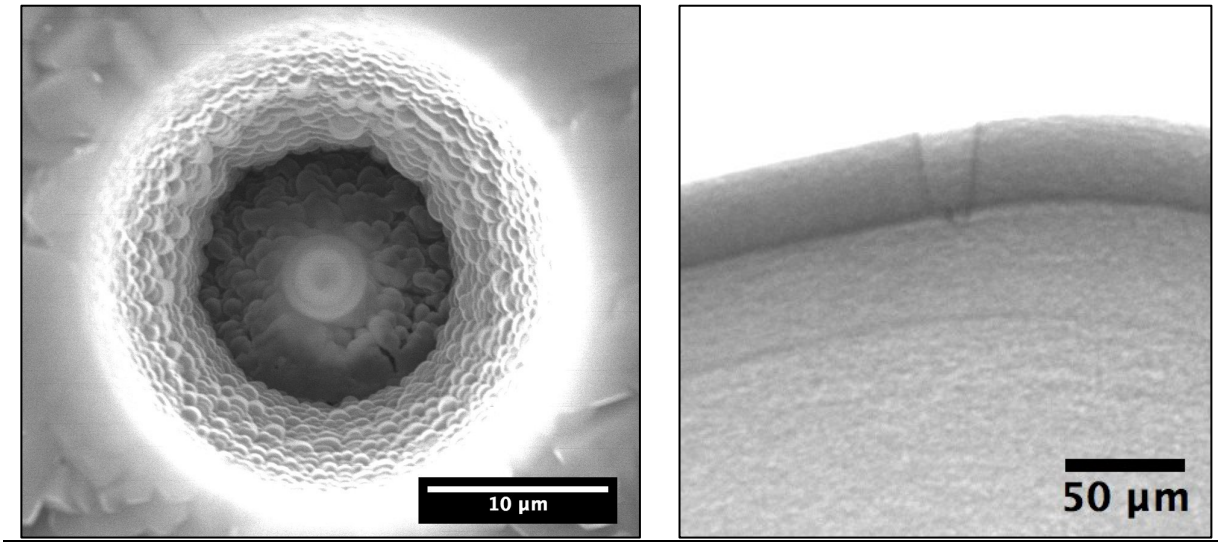

FIB-13

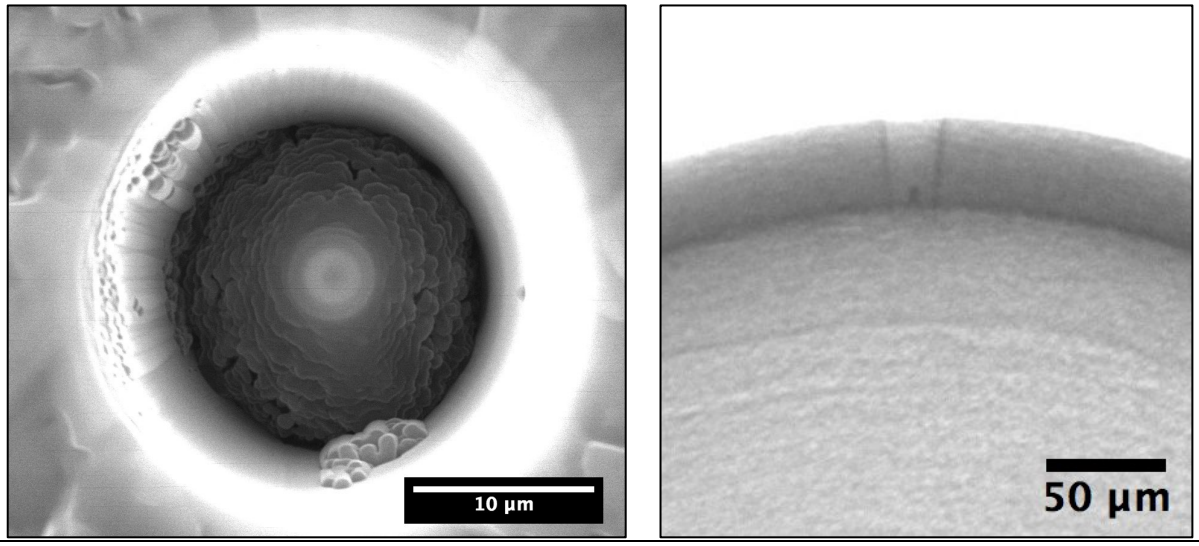

FIB-14

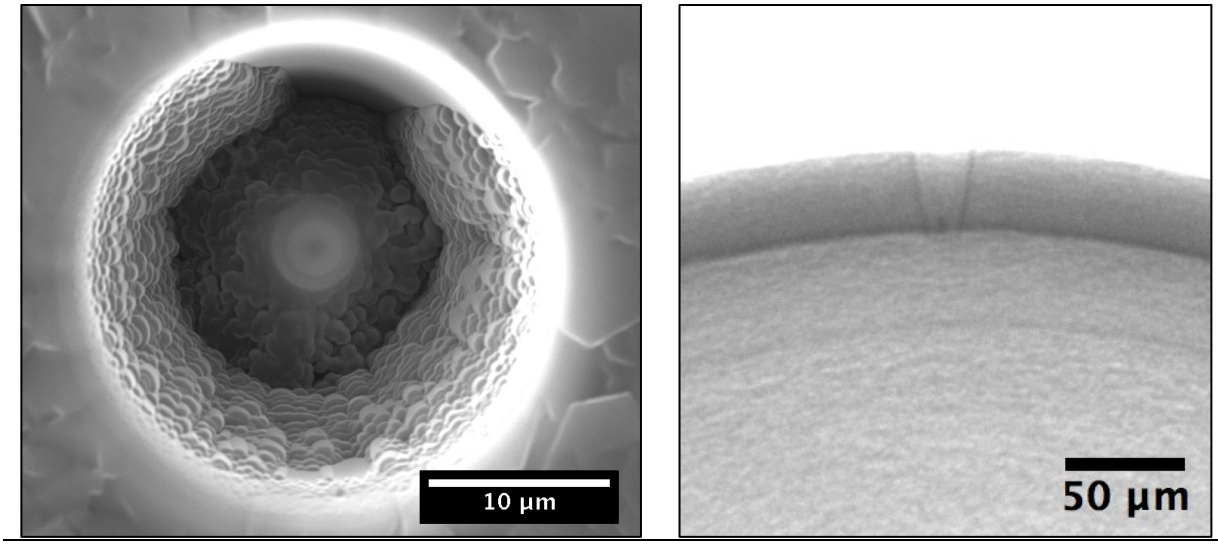

FIB-15

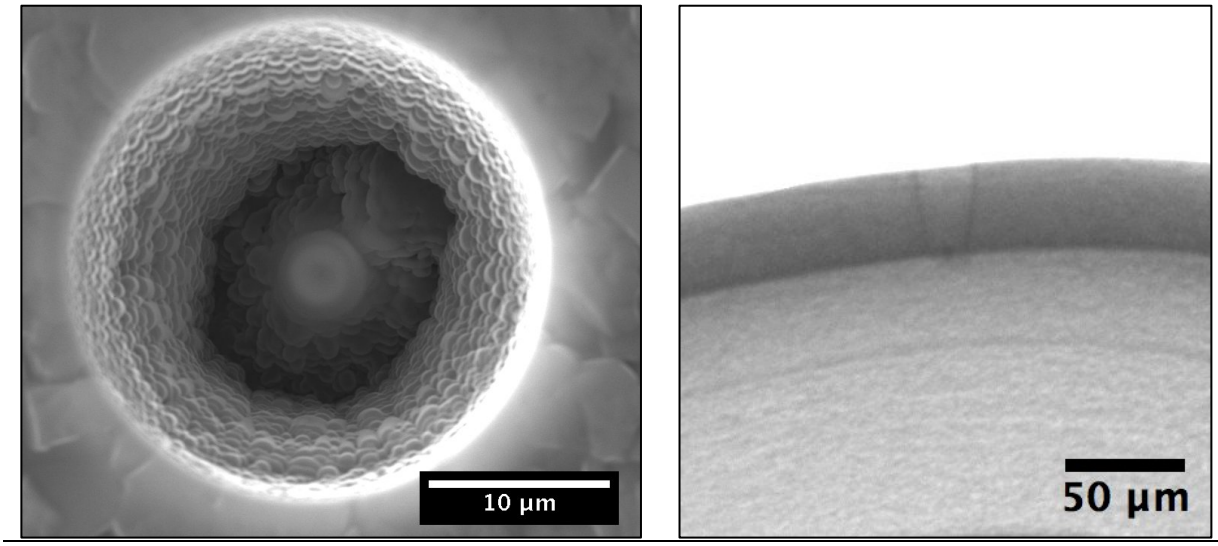

FIB-16

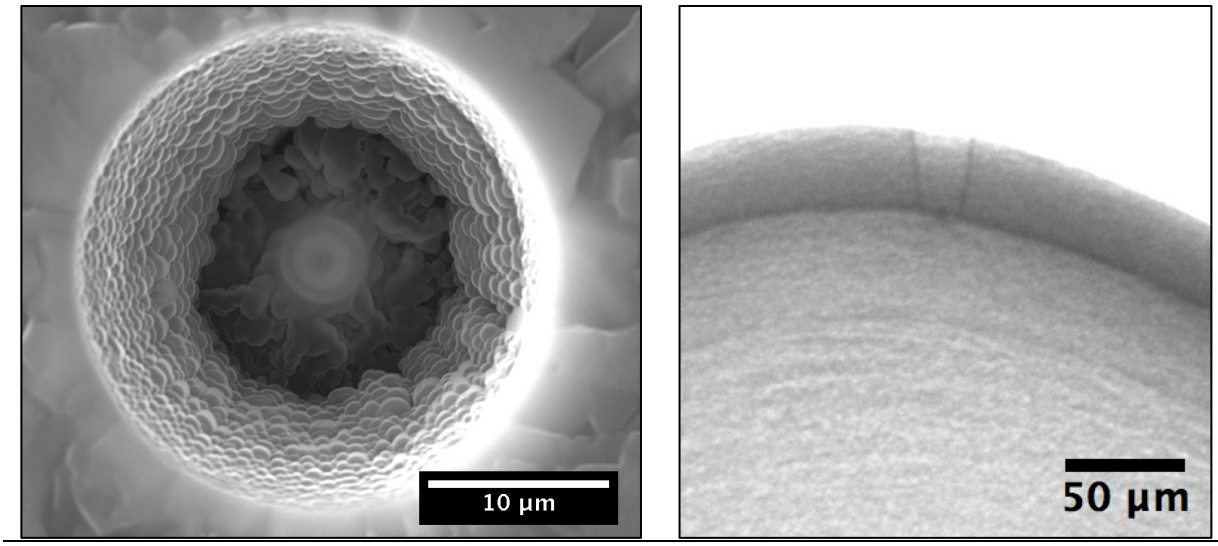

FIB-17

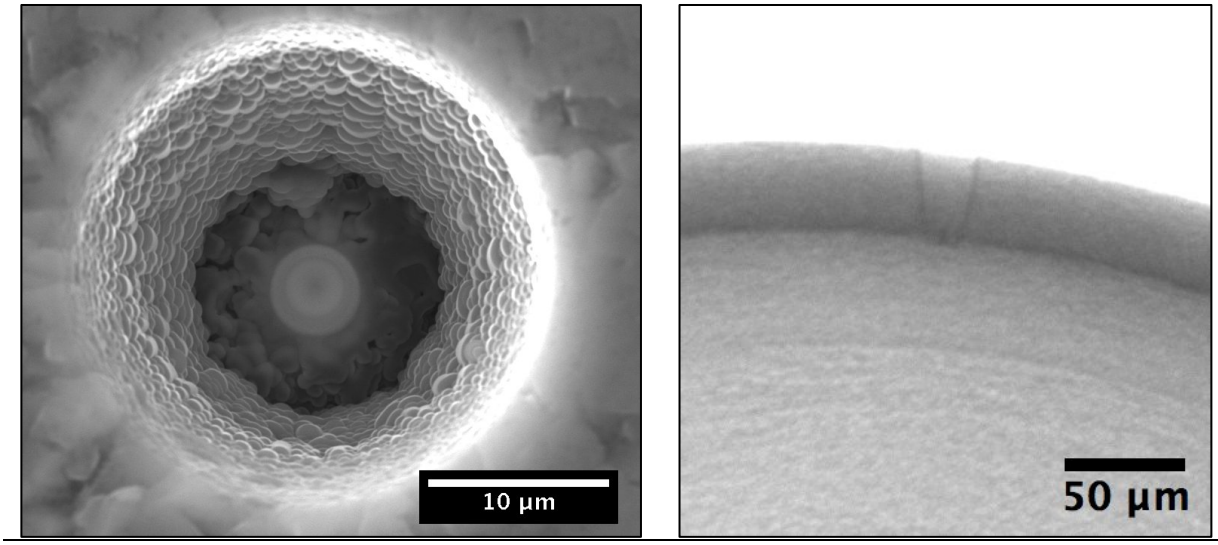

FIB-18

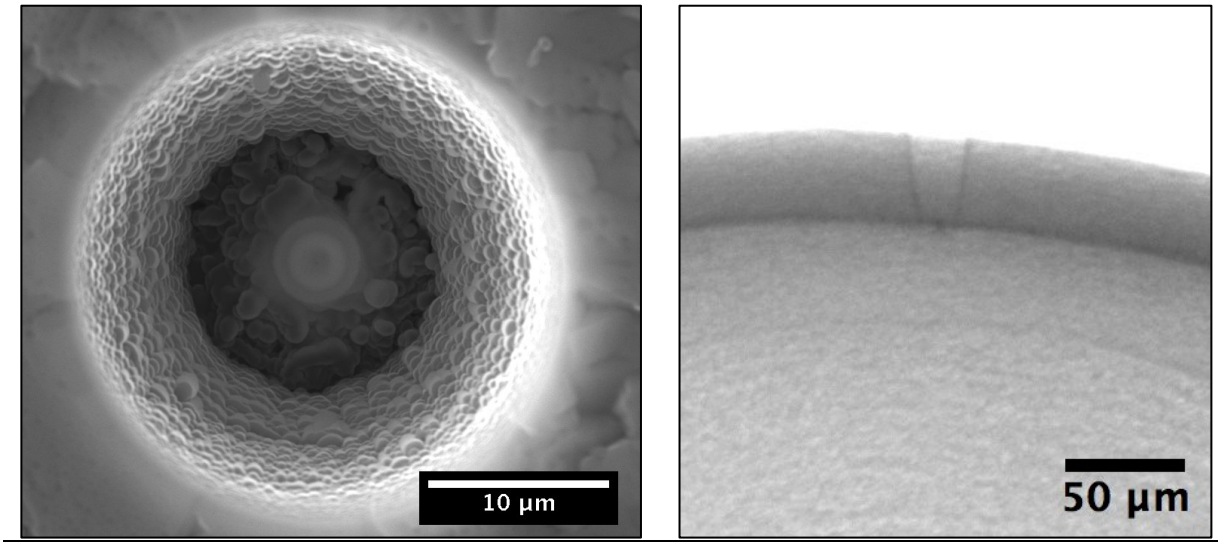

FIB-19

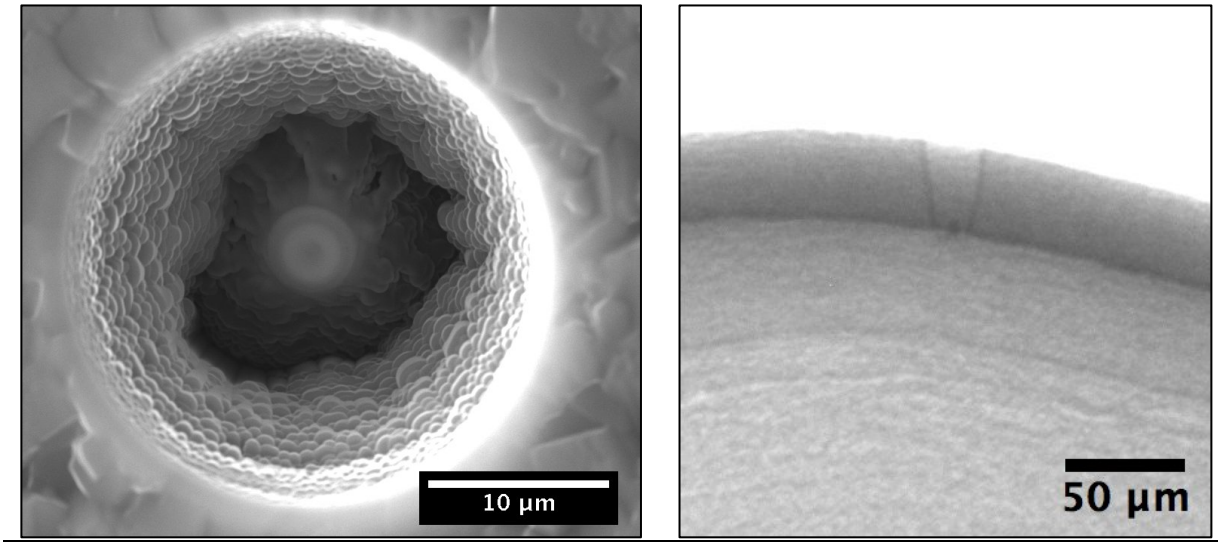

FIB-20

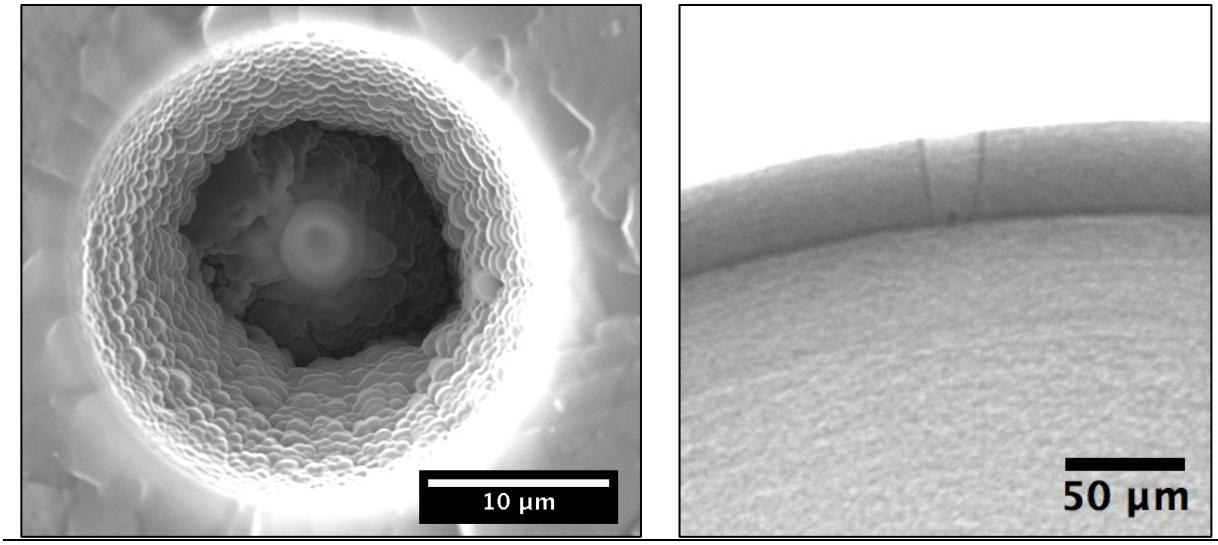

FIB-21

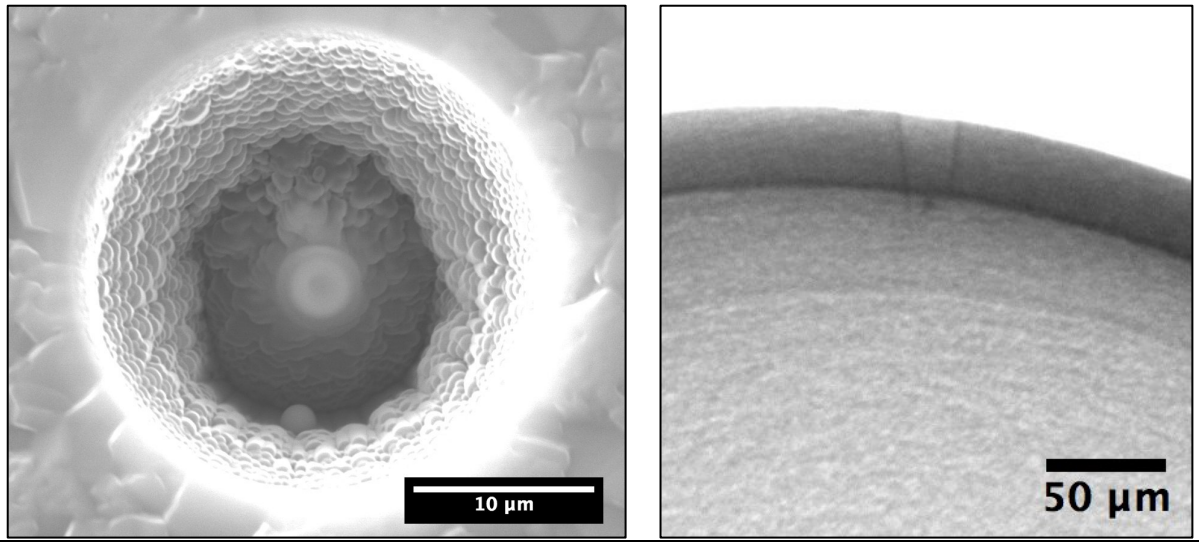

FIB-22

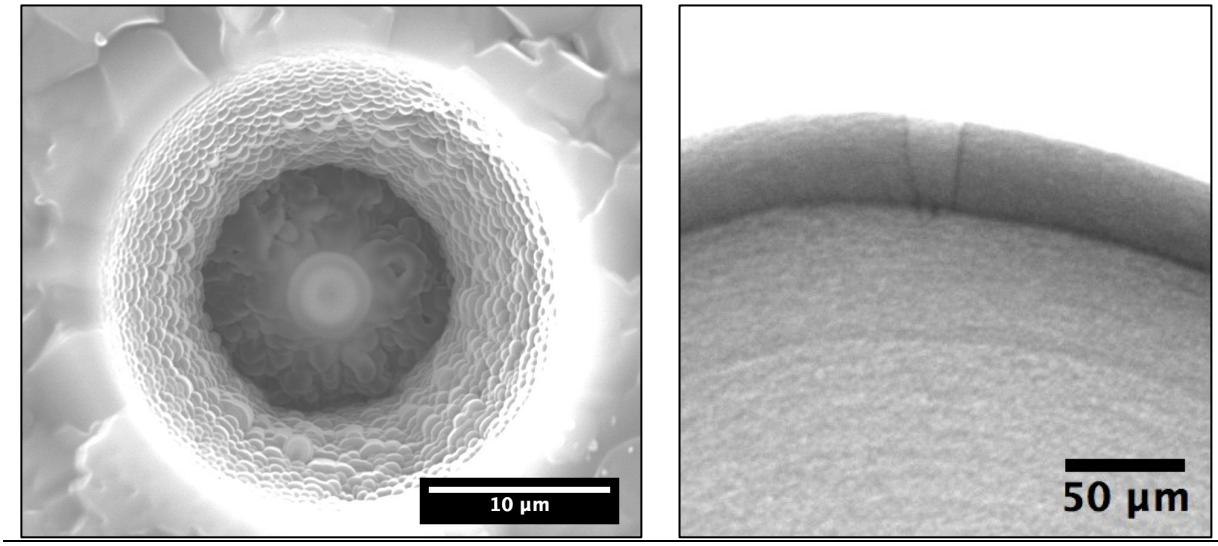

FIB-23

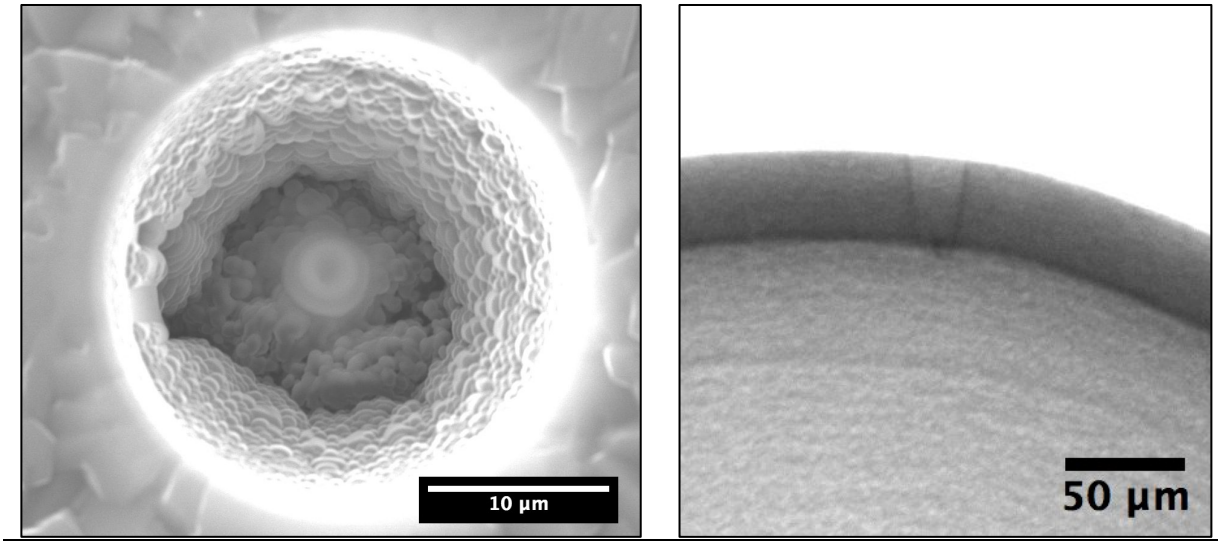

FIB-24

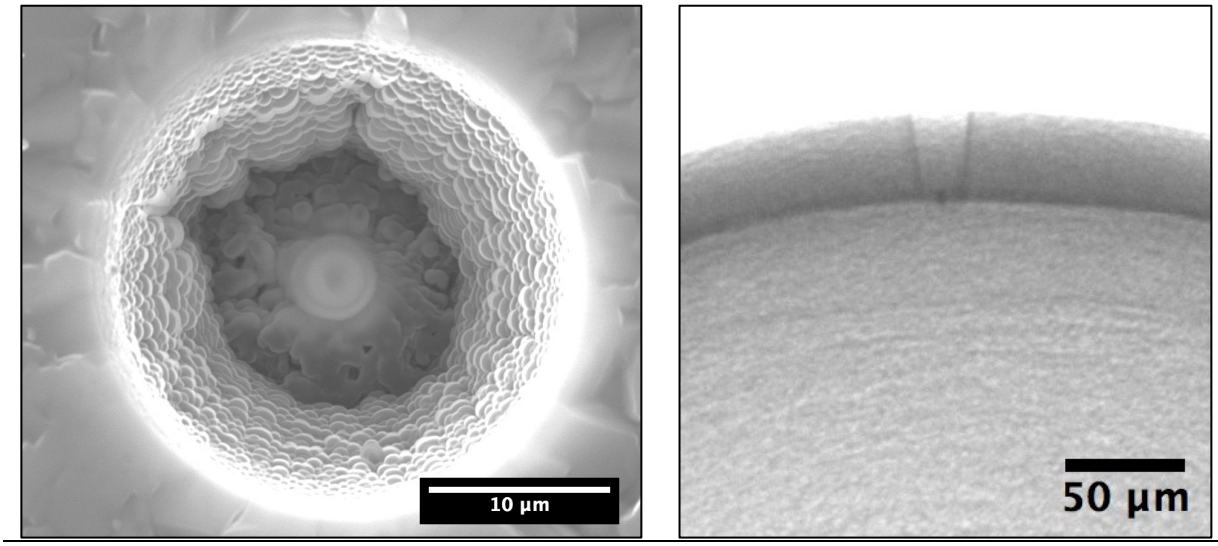

FIB-25

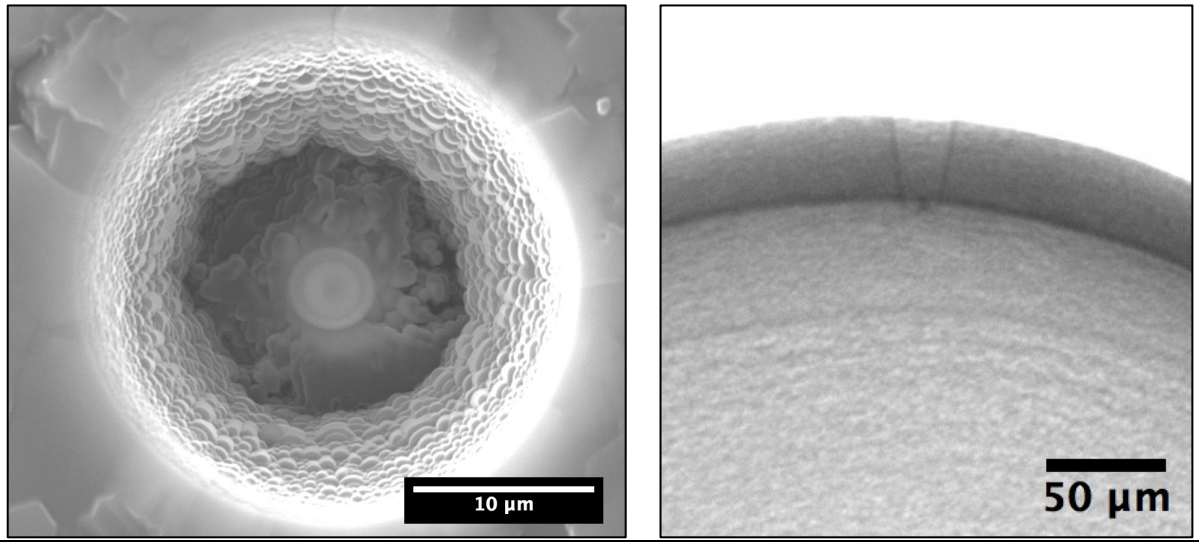

FIB-26

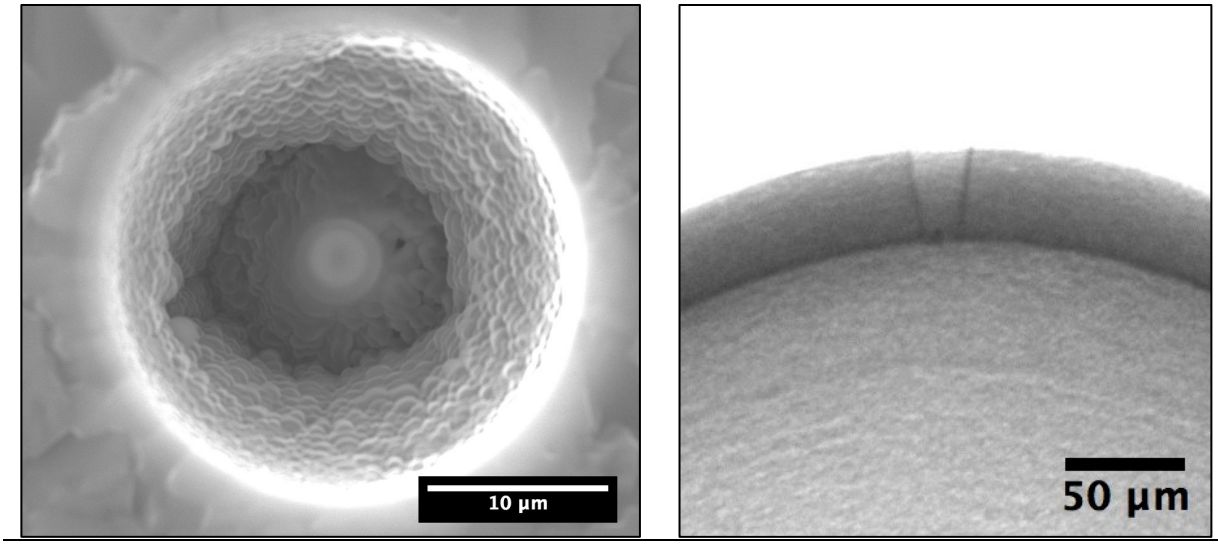

FIB-27

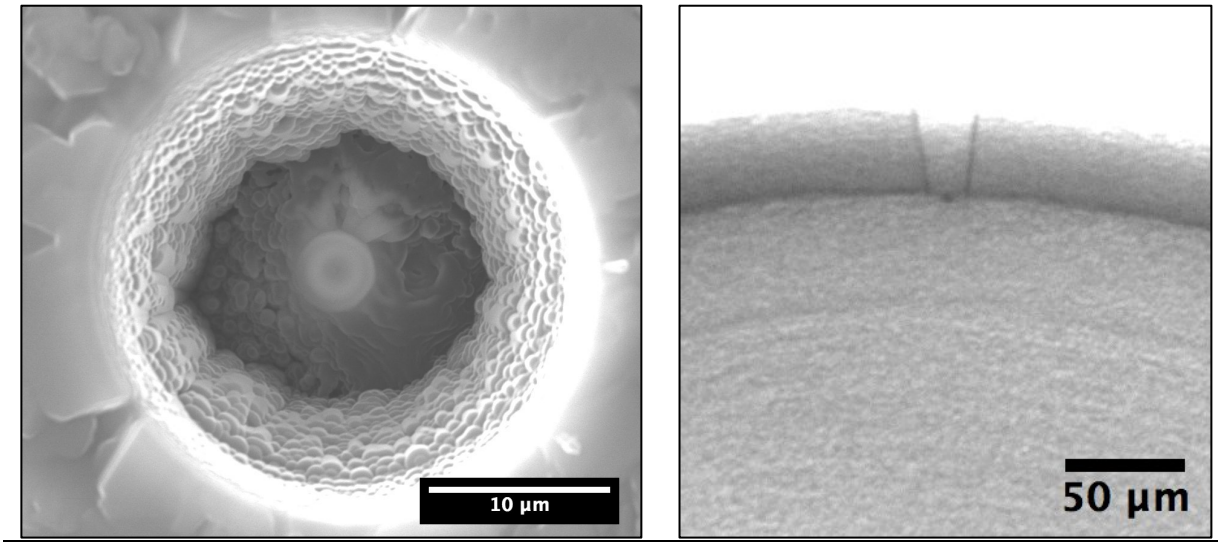

FIB-28